Forschungszentrum Jülich
in der Helmholtz-Gemeinschaft

Modeling Based Process Development of Fed-Batch Bioprocesses: L-Valine Production by *Corynebacterium glutamicum*

Michel Brik Ternbach

Lebenswissenschaften
Life Sciences

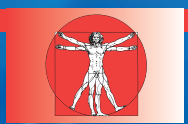

Schriften des Forschungszentrums Jülich
Reihe Lebenswissenschaften/Life Sciences Band/Volume 21

Forschungszentrum Jülich GmbH
Institut für Biotechnologie 2

Modeling Based Process Development of Fed-Batch Bioprocesses: L-Valine Production by *Corynebacterium glutamicum*

Michel Brik Ternbach

Schriften des Forschungszentrums Jülich
Reihe Lebenswissenschaften/Life Sciences Band/Volume 21

ISSN 1433-5549 ISBN 3-89336-413-7

Bibliographic information published by Die Deutsche Bibliothek.
Die Deutsche Bibliothek lists this publication in the Deutsche Nationalbibliografie; detailed bibliographic data are available in the Internet <http://dnb.ddb.de>.

Publisher and Distributor:	Forschungszentrum Jülich GmbH Zentralbibliothek 52425 Jülich Phone +49 (0)2461 61-5368 · Fax +49 (0)2461 61-6103 e-mail: zb-publikation@fz-juelich.de Internet: http://www.fz-juelich.de/zb
Cover Design:	Grafische Medien, Forschungszentrum Jülich GmbH
Printer:	Grafische Medien, Forschungszentrum Jülich GmbH
Copyright:	Forschungszentrum Jülich 2005

Schriften des Forschungszentrums Jülich
Reihe Lebenswissenschaften/Life Sciences Band/Volume 21

D 82 (Diss., Aachen, Univ., 2005)

ISSN 1433-5549
ISBN 3-89336-413-7

Neither this book nor any part of it may be reproduced or transmitted in any form or by any means, electronic or mechanical, including photocopying, microfilming, and recording, or by any information storage and retrieval system, without permission in writing from the publisher.

'Therefore, mathematical modeling does not make sense without defining, before making the model, what its use is and what problem it is intended to help to solve.'

James E. Bailey (1998)

'The ability to ask the right question is more than half the battle of finding the answer.'

Thomas J. Watson

'You will only see it when you understand it.'
(Translated freely from the Dutch: 'Je gaat het pas zien als je het door hebt.')

Johan Cruijff

Contents

1. Introduction

The OECD (the Organisation of Economic Co-operation and Development) defines biotechnology as "the application of scientific and engineering principles to the processing of materials by biological agents." Biotechnology is actually already thousands of years old, when we realize that for instance already ancient Egyptians used yeast for making bear and bread. A major difference between modern biotechnology and those early applications lies in the possibility to precisely identify and change the genes which govern the desired traits.

Nowadays, modern biotechnolgy is applied in many different fields. Biotechnology plays an important role in pharmaceutical industry, the so called 'red' biotechnology (Moore, 2001), for for instance diagnostic kits, production of vaccines, antibodies and other medicines. In food and agriculture, biotechnolgy is used for instance to breed high-yielding crops and reduce the need for insecticides or herbicides ('green' biotechnology, (Enriquez, 2001)). Also in several other industrial processes, enzymes or micro-organisms are used for instance for the production of intermediary products for chemical industries ('white' biotechnology, (Frazzetto, 2003)).

Since several decades, modern biotechnology is a major technology which increased substantially especially in the last decade. In the Ernst & Young Report 2003, more than $41 billion revenues of biotechnolgical companies were mentioned for 2002. Moreover, these figures do not include large pharmaceutical or large agribusiness companies for which biotechnology forms a part of the business.

The competitiveness of biotechnological industries depends strongly on knowledge and innovations (Pownall, 2000). In many cases, such as the introduction of new pharmaceutical products, it is especially important to keep the time to market as short as possible. So it is important to have fast process development procedures.

On the other hand, it can be very important to keep production costs as low as possible and guarantee a good product quality. This can benefit from optimization of the production organism or the process conditions. With modern biotechnological techniques, new organisms or catalysts are developed fast. Due to the strong interaction between the used organism and the optimal process conditions, this even increases the need for proper and fast process development.

It is well accepted that process models can be very useful for process optimization and -control. One of the main reason why this is not used very extensively in industry, is probably the fact that the development of the model itself is often rather difficult and time-consuming (Shimizu, 1996). A survey, published by Bos et al. (1997) indicated the

need for improved methods to determine reaction kinetics within the chemical industry. Starting from this survey, the "EUROKIN" consortium was established in 1998, comprising eleven companies and four universities (Berger et al., 2001). Currently, the consortium is still active in its third two-year programme. One of the main focuses of the consortium is to provide techniques for modeling of reactor systems and the reaction kinetics. Case studies were developed to evaluate commercially available software packages for kinetic modeling with respect to their capabilities of parameter estimation, model discrimination and design of experiments. Also the programs which are presented in the current thesis participated in this evaluation[1].

The aim of the current thesis is to establish a method for development and optimization of fed-batch bioprocesses using kinetic modeling. Opposed to selecting the model only after all experiments are performed, special techniques are suggested to use modeling already for designing the experiments. An important part of the thesis is the practical application of the technique to a relevant example. More specific, the goal is to:

- develop and present a framework for modeling of dynamic bioprocesses. The framework has to allow the simulation of fed-batch experiments. Model parameters have to be estimated from measured data from prior experiments and the accuracy of the estimated parameters needs to be evaluated. Furthermore, the accuracies of the model fits have to be addressed, also enabling the comparison of model fits. Importantly, the framework should also include the possibility to design experiments, based on the available model(s) and prior information. The developed framework will be described in chapter 3.

- Useful experimental design criteria have to be selected and implemented. This includes criteria which aim at discrimination between the competing models, improvement of parameter estimation or optimization of the production process. A strong focus is on the design of experiments for model discrimination. Several such criteria are adjusted for use with dynamic multi-variable processes and compared in a simulativ study, which is shown in chapter 4. Also several criteria are suggested for off-line process optimization.

- Besides the simulativ study, an important aspect of the current work is the practical application of the presented approach to the real relevant case of development of a process for the production of L-valine by a genetically modified strain of *Corynebacterium glutamicum*. This is shown in chapter 5.

[1] The D-optimality criterion was successfully used for selection of experiments for improvement of the parameter estimates. This criterion will be explained in paragraph 2.5.2. The Box and Hill criterion was successfully used for design of experiments to discriminate between competing model structures. This criterion will be explained in paragraph 2.5.1

2. Theory

2.1. Biotechnological Processes

In biotechnological processes, or bioprocesses, biological systems such as bacteria, yeast, fungi, algae or also animal cells, plant cells or isolated enzymes, are used to convert supplied substrates to desired products[1]. This product can be the organism itself or a chemical substance.

2.1.1. Bioreactors

For many applications, it is necessary to run the bioprocesses in well controlled and closed bioreactors. Several types of bioreactors exist to meet the different requirements of different organisms and products. Some of the most common types are the stirred tank, the bubble column, the airlift, and the packed bed (Riet and Tramper, 1991; Williams, 2002).

The stirred tank reactor is usually a cylindrical vessel equipped with a mechanical impeller, baffles and aeration at the bottom of the vessel.

The bubble column on the other hand does not have a mechanical stirrer. Mixing occurs due to the gas flow coming from a sparger at the bottom of the column.

The airlift also uses the gas flow from a sparger at the bottom of the reactor to introduce mixing, but has two interconnected parts instead of one cylinder. The supplied gas rises in one compartment, the riser, and due to the different density caused by the gas, the medium circulates going down in the other compartment, the downcomer, and rising in the riser.

Whereas the other three mentioned reactor types run with fluid systems, the packed bed is filled with solid particles containing the biocatalysts and medium flows past these particles.

2.1.2. Modes of Operation

The bioprocesses can be run in batch, fed-batch, or continuous mode.

[1] Also treatment of waste with (micro)organisms is a bioprocess, but in this case the goal is not so much a desired product but more a loss of undesired substrates.

In a batch process, all substrates are available in the initial medium and none is supplied extra during the process [2]. The process is stopped after the substrate is converted and the whole batch is harvested together.

In a fed-batch process, substrates are fed into the reactor during the process, but the harvesting is still done all at the end of the process. This type of process is used very often since it allows relatively high biomass or product concentrations to be achieved. These may not be achievable in batch because the total amount of needed substrate would be so much that the initial substrate concentration would be strongly inhibiting the process. In continuous processes the high product concentrations would inhibit cell growth. The feeding of the substrates also allows maintaining optimal substrate concentrations which allow faster production processes or avoid unwanted by-products. Also in the current work, fed-batch processes are used. One important advantage is that the dynamics and the many possibilities to influence the process render these processes potentially very information rich. Furthermore, most industrial bioprocesses are operated in batch or fed-batch mode and it is more likely that a proper model describing these processes is achieved, when the model is built with similar systems as the final production system. Especially living cells can act different after adaptation to a stable environment in a steady state of a continuous process, compared to the situation of constant adaptation in a dynamic process (Sonnleitner, 1998; Wirtz, 2002). The sole use of steady state kinetics from continuous systems for describing the dynamic (fed-)batch processes is then less likely to be successful.

In continuous processes, medium is fed continuously and product is harvested continuously. In the most common type of continuous processes with growing cells, medium is fed into the reactor at a constant rate and the suspension is removed at the same rate. This way the culture will run into a steady state where the growth of the organism equals the dilution by the feeding. This type of operation is called a chemostat. There is no feedback control needed[3]. In some other continuous systems, the feedrates are controlled by a feedback controller which regulates a certain measured value at a constant level. For instance in a nutristat, the concentration of a medium component is measured and controlled and in a turbidostat the biomass concentration, measured as the turbidity is kept at a constant level.

A plug-flow reactor provides a special way of running continuous processes. In such a reactor the medium runs through a tube in a laminar way without axial mixing and is harvested continuously at the end of the tube.

[2] Only correction fluids for for instance pH correction or against foam are possibly added during the process.

[3] except maybe for the volume in the reactor, but this is usually done by an outlet at a fixed level

2.2. Modeling

A mathematical model is a collection of mathematical relationships which describe a process. In practically each model, a simplification of the real process is made, but still mathematical models have proven to be very useful in gaining insight in processes (Bailey, 1998; Kitano, 2002), for instance by comparing different models and their ability to describe experimental data (Auer and Thyrion, 2002; Bajpai et al., 1981). Furthermore, models have been successfully uses for optimization or control of processes (Heinzle and Saner, 1991; Hess, 2000; Yip and Marlin, 2004). Different types of models can be distinguished for the different goals and depending on the available information. Some characteristics which are of interest for modeling bioprocesses are mentioned here.

2.2.1. Mechanistic and Black-Box Models

Mathematical models can be classified depending on the type of knowledge the models are based on. When theoretical knowledge about the mechanism is used to describe the process, the models are called mechanistic-, white-box-, or first-principle models. Generally, these models are easily interpretable and can often be extrapolated comparably well. For complex processes they might however prove to be difficult to develop. This type of models can be used very well for gaining insight in the mechanisms behind a process and also for other purposes such as process optimization and -control, these models are readily applicable.

In contrast to the mechanistic white-box models, black box models do not require a thorough understanding of the principles behind the process. These models are empirical models which are based on available data. Some examples of such modeling techniques are polynomes, artificial neural networks (Becker et al., 2002; Zhu et al., 1996) and fuzzy logic models (Filev et al., 1985; Lee et al., 1999). Generally, black-box models which describe the used data reasonably well, can be obtained straightforward. One drawback of black-box models is that those models usually have poor extrapolation properties, meaning they are likely to perform poorly in situations which differ from the ones used for model building.

In addition to the white-box and the black-box models, also combinations of both forms exist. These grey-box-, hybrid- or semi-mechanistic models use black-box substructures within a white-box model to describe some aspects of the process which the white-box part of the model fails to model properly and for which the underlying principles are either unknown or too complex for the desired level of detail. An overview and several examples of the use of hybrid models in biotechnology can be found in Roubos (2002). Examples include combinations of mechanistic models with fuzzy modeling for enzymatic conversions (Babuška et al., 1999) and fermentation processes (Horiuchi et al., 1995). Also examples of hybrid models using artificial neural networks for modeling and optimization of fermentation processes have been reported (Can et al.,

1997; Goncalves et al., 2002; Harada et al., 2002; Schubert et al., 1994).

The current work focuses on the development of mechanistic models and does not include the use of special black-box modeling techniques, although the actual processes which take place inside the cells are not regarded in detail, as also mentioned in the next paragraph.

2.2.2. Macroscopic Modeling

In every model, the real process is simplified. The models can differ in the extent to which details are described.

In modeling fermentation processes, 'macroscopic models' describe the whole bioreactor as one system. These models include equations for the rates of the reactions taking place, as well as for mass transfer and fluxes into and out of the bioreactor. Usually, these models do not describe the actual processes taking place inside the organisms, but use a simplified form which hopefully describes the overall behaviour well enough for process optimization or process control.

A more detailed description of the processes taking place in the organisms, can be found in metabolic network models (Bailey, 1991). Here, the enzymatic conversions in the (relevant) metabolic routes of the cells are modeled. These stoichiometric models can be used to determine the metabolic fluxes through the cell. Therewith, they can provide useful information on the actual metabolism and be helpful for the identification of targets for metabolic engineering[4]. On the other hand, they may prove to be too complicated for optimization of process conditions or for use in process control.

Going even further into detail in the cell, also the regulation of the expression of genes and the activity of enzymes could be added to the models. Many different mechanisms of regulation exist and they are not yet all understood completely. Some examples can be found in Bajpai et al. (1981); Cheng et al. (2000); Covert and Palsson (2002); Elf et al. (2001); Herwig and von Stockar (2002).

In the current work, macroscopic models are used, which can be used for optimization of the process conditions. The detailed description of the intracellular processes is outside the scope of the project.

2.2.3. Structured and Unstructured Models

Models can also be categorized by the way they are structured.

In models of bioprocesses, the term 'unstructured model' is usually used for models which describe the biomass as one (chemical) compound (Fredrickson et al., 1970). In this simplification, balanced growth is assumed. Structured models use compartimentation, for instance introducing intracellular metabolite pools as in Birol et al. (2002);

[4]Metabolic engineering is the technique of developing improved strains of organisms by modifications of the genome of the cell. An introduction into this topic can be found in Nielsen (2001)

Palaiomylitou et al. (2002). Unstructured models can be expected to fail in highly transient situations (Esener et al., 1981).

In the current work, unstructured models were aimed at. However, some slight structuring was implemented by introducing imaginary intracellular pools of some substrates by decoupling the uptake and the use of the compounds. This was necessary due to the characteristics in the measured data and based on information about inhibition of the uptake, as is mentioned in paragraph 5.2.3 on page 104.

2.3. A Model of a Fed-Batch Process

2.3.1. Mass Balance

The macroscopic models of bioprocesses are based on mass balances:

$$accumulation = conversion + transport \tag{2.1}$$

So, assuming ideal mixing[5], we can write for the bioreactor:

$$(\dot{CV}) = rV + \sum_f F_f C_f \tag{2.2}$$

where dots above the symbols denote the time derivatives, r are net conversion rates per unit volume and F are fluxes of feeds into and out of the reactor[6], with concentrations C_f in these feeds.

The total mass of the compounds in the fermentation suspension is balanced, so we have to keep in mind that, besides the concentration of the compounds, also the volume of the suspension has to be regarded. This is especially important for fed-batch fermentations where the volume generally changes significantly during the process. So using

$$(\dot{CV}) = \dot{C}V + \dot{V}C, \tag{2.3}$$

the balance can be rewritten as:

$$\dot{C} = r + \sum_f \frac{F_f C_f}{V} - \sum_f \frac{F_f C}{V}. \tag{2.4}$$

with

$$\dot{V} = \sum_f F_f \tag{2.5}$$

[5] For small scale stirred bioreactors, this assumption is generally valid since mixing times in these systems are well below the time scale at which the process takes place.

[6] The fluxes out of the reactor are negative. Also sampling can be regarded as such a flux out of the reactor.

For batch fermentations, the equations can be simplified since all fluxes are 0[7]. For chemostat fermentations at steady state, all time derivatives are 0 which simplifies the balance to yield:

$$-r = \sum_f \frac{F_f(C_f - C_{ss})}{V} \tag{2.6}$$

which can readily be solved using the steady state concentration C_{ss}.

For fed-batch fermentations, such general simplifications cannot be made. The concentrations can however be simulated over time when the initial concentrations $C(0)$ and the fluxes are known and kinetic equations for the conversion rates as a function of the concentrations are given:

$$C(t) = C(0) + \int_{t=0}^{t} \dot{C} dt \tag{2.7}$$

2.3.2. Kinetics

Now the challenge is to find kinetic descriptions for the conversion rates r as a function of the concentrations for all relevant substances: biomass, substrate(s) and product(s).

One common type of kinetic equations is the Monod kinetics, which is based on the Michaelis-Menten type enzyme kinetics (Michaelis and Menten, 1913):

$$r = \frac{v_{max} C_S C_C}{K_m + C_S} \tag{2.8}$$

where C_S is the concentration of substrate, C_C the catalyst concentration and K_m the Michaelis-Menten constant, which is a binding constant, equal to the concentration needed to achieve an enzyme specific conversion rate[8] of half the maximal specific conversion rate v_{max}. For more detailed explanation of the theoretical background of this equation and similar enzyme kinetic models, see for instance Biselli (1992); Roels (1983).

For biomass growth on one limiting substrate, the Monod kinetics (Monod, 1942) can be written analogously as:

$$r_x = \mu_{max} \frac{C_S C_X}{K_S + C_S} \tag{2.9}$$

$$r_s = -\frac{r_x}{Y_{xs}} \tag{2.10}$$

[7] except for the fluxes for for instance pH control and the flux of samples out of the reactor. The first of which is usually of little importance as long as sufficiently high concentrations of the correction fluids can be used. The last point is usually only of importance in research where many samples are taken and small biorectors are being used. However, since this does not change the concentrations but changes all amounts in an equal way, and since no substrates are added into the system, this can also be neglected.

[8] This is the conversion rate per unit enzyme, for instance in $mmol_{substrate} mmol_{enzyme}^{-1} s^{-1}$

with μ_{max} being the maximal specific growth rate, K_S the Monod-constant, analogous to the Michaelis-Menten constant and Y_{xs} the yield of biomass production on substrate, which is the amount of biomass which is produced from one unit of substrate.

The Monod equation is probably the most often used equation to describe biomass growth. Some alternative equations have also been proposed, amongst which the Blackman equation (Dabes et al., 1973), the equations by Konak (1974) and a logistic equation (used for instance in Bona and Moser (1997)).

Maintenance

Substrate is not only needed for biomass production, but also some energy is needed for the maintenance of the cells. This is usually added as an extra maintenance term in the equations, either as extra substrate uptake:

$$r_s = -\frac{r_x}{Y_{xs}} - m_S C_X \tag{2.11}$$

or as biomass degradation:

$$r_x = \mu_{max} \frac{C_S C_X}{K_S + C_S} - m_S C_X \tag{2.12}$$

with m_S the maintenance coefficient. From a mechanistic point of view, the former can be expected to be more correct as long as substrate is available (Roels, 1983).

Product Formation

In fermentations, besides the biomass also another product is formed from the substrate. This production can be classified into three groups: directly associated to the energy generation of the organism, indirectly coupled to it and a group in which no clear coupling to the energy generation of the cell is apparent (Roels, 1983).

Production of ethanol, acetic acid and many other products are directly associated to the energy generation. In these cases the substrate uptake rate can still be described as in equation 2.11 and the production rate can be given by:

$$r_p = r_x \cdot Y_{px} + m_P C_X. \tag{2.13}$$

where Y_{px} is the ratio between the production of product and biomass of the growth associated part of the production and m_P is the specific production rate without growth (Luedeking and Piret, 1959).

For instance the production of amino acids is regarded to be indirectly coupled to the energy metabolism. Here, a separate contribution of the product formation is added to the substrate conversion:

$$-r_s = \frac{r_x}{Y_{xs}} + \frac{r_p}{Y_{ps}} + m_S C_X \tag{2.14}$$

with Y_{ps} being the yield of product on substrate and r_p the rate of product formation, which can for instance be described by a Monod-type equation:

$$r_p = \pi_{max} \frac{C_S C_X}{K_P + C_S} \tag{2.15}$$

where π_{max} is the maximal specific production rate and K_P a bindings constant analogue to the Monod-constant K_S in equation 2.9.

For the third class, where there is no clear coupling between the energy generation and product formation, one general mechanistic model cannot be given. For instance secondary metabolites such as antibiotics have been categorized in this group.

Multiple Substrates

The prior model equations presume one rate-controlling substrate. This may hold for many cases, but an increasing amount of processes which are controlled by more than one substrate are being reported.

Now let the overall specific growth rate μ be defined by

$$r_x = \mu C_X \tag{2.16}$$

Several macroscopic descriptions of this overall specific growth rate, controlled by multiple substrates, have been reported, such as a multiplicative, additive and non-interactive approach (Neeleman et al., 2001; Roels, 1983).

In the multiplicative case, the overall specific growth rate is calculated by multiplying the fractions of the maximal specific growth rate according to the different substrates, so for n substrates:

$$\mu = \prod_{i=1}^{n} \mu_{S,i} \tag{2.17}$$

where $\mu_{S,i}$ is the specific growth rate supported by substrate i. So for instance using two simple Monod type kinetics for both substrates $S1$ and $S2$, the overall specific growth rate according to the multiplicative approach would be [9,10]

$$\mu = \mu_{max} \frac{C_{S1}}{K_{S1} + C_{S1}} \frac{C_{S2}}{K_{S2} + C_{S2}} \tag{2.18}$$

One major drawback of this multiplicative approach is the fact that moderate limitation by several substrates leads to severe limitation of the overall growth rate, which is unlikely to be the real case.

[9] Only one maximal specific growth rate μ_{max} is used here. When separate maximal growth rates for both substrates are used, these would not be distinguishable mathematically. Furthermore, from a mechanistic point of view, one maximal rate and two processes which limit this is also well interpretable.

[10] The mechanistic theory behind the Michaelis-Menten kinetics for enzyme reactions does not support this multiplication (Biselli, 1992) but for whole cell processes it has often been used successfully.

In the multiplicative approach, all substrates are essential for growth. Tsao and Hanson (1975) have enhanced this multiplicative approach with the addition of not essential substrates C_E which increase the growth rate. For m enhancing substrates and n essential substrates, they proposed the following equation:

$$\mu = \left(1 + \sum_{i=1}^{m} \frac{k_i C_{E,i}}{K_{E,i} + C_{E,i}}\right) \left(\prod_{j=1}^{n} \mu_{max,j} \frac{C_{S,j}}{K_{S,j} + C_{S,j}}\right) \tag{2.19}$$

where k_i are rate constants for the enhancing substrates and $K_{E,i}$ are analogues to the $K_{S,i}$ binding constants.

In the additive approach, the specific growth rates on different substrates are added. The supposed mechanism of this approach can be explained when we assume the cells to be able to take up all substrates parallel and grow on each substrate without the others. So with n substrates, this can be formulated as:

$$\mu = \sum_{i} \mu_{S,i} \tag{2.20}$$

or with 2 substrates and Monod kinetics:

$$\mu = \mu_{max,S1} \frac{C_{S1}}{K_{m1} + C_{S1}} + \mu_{max,S2} \frac{C_{S2}}{K_{m2} + C_{S2}} \tag{2.21}$$

In the non-interactive approach there is always only one rate controlling substrate at a time. However, the limiting substrate can change during the process or differ between experiments. At all time points, the limiting substrate is determined. For two substrates and Monod kinetics this can be described as:

$$\mu = \min \begin{cases} \mu_{S1} = \dfrac{\mu_{max,S1} C_{S1}}{K_{m1} + C_{S1}} \\ \mu_{S2} = \dfrac{\mu_{max,S2} C_{S2}}{K_{m2} + C_{S2}} \end{cases} \tag{2.22}$$

Another option mentioned in literature uses the averaging of the reciprocals of the growth reduction by the different substrates. For n substrates this would give:

$$\mu = \mu_{max} \frac{n}{\sum_{i=1}^{n} \frac{\mu_{max}}{\mu_i}} \tag{2.23}$$

where all specific growth rates μ_i use the same maximal specific rate μ_{max}.

Besides the macroscopic unstructured approaches mentioned here, also structuring has been used to deal with multiple substrates.

Inhibition

Some catalytic conversions are inhibited by certain substances. Based on the principle of reversibility of each chemical process at a molecular level, each product also inhibits its own production.

The catalytic reactions (such as enzymatic reactions) can be inhibited through different mechanisms such as competitive, non-competitive or uncompetitive inhibition.

Competitive inhibition occurs when the inhibitor and the substrate compete for the same active site. This can be mathematically described by the following equation:

$$r = v_{max} \frac{v_{max} \cdot C_S}{K_S \cdot \left(1 + \frac{C_I}{K_I} + \frac{C_S}{K_S}\right)} \tag{2.24}$$

Non-competitive inhibitors bind the catalyst or the catalyst-substrate complex, preventing the conversion. This can be described by:

$$r = v_{max} \frac{v_{max} \cdot C_S}{K_S \cdot \left(1 + \frac{C_I}{K_I} + \frac{C_S}{K_S} + \frac{C_S \cdot C_I}{K_S \cdot K_I}\right)} \tag{2.25}$$

Uncompetitive inhibitors only bind the catalyst-substrate complex but do not inactivate the catalyst before binding of the substrate. This can be described by:

$$r = v_{max} \frac{v_{max} \cdot C_S}{K_S \cdot \left(1 + \frac{C_S}{K_S} + \frac{C_S \cdot C_I}{K_S \cdot K_I}\right)} \tag{2.26}$$

A special case of this form of inhibition is the inhibition of the reaction by excess of substrate:

$$r = v_{max} \frac{v_{max} \cdot C_S}{\left(K_S + C_S + \frac{C_S^2}{K_I}\right)} \tag{2.27}$$

This happens when a second substrate molecule can bind the complex and prevent the conversion.

A more detailed explanation of the shown mechanisms and equations is for instance shown in Biselli (1992). In many enzymatic processes, the real mechanisms are much more complex than the shown simple cases and in complete cells, even much more complex mechanisms take place. These complex regulatory mechanisms are beyond the scope of the current work and are often not completely understood. Several of the shown inhibition kinetics have been used for cellular kinetics. Equation 2.27 for instance corresponds to the well-known Andrews kinetics (Andrews, 1968).

Lag-Times

Directly after inoculation of a batch experiment, an initial adaptation phase with reduced rates often occurs. In macrokinetic models, the underlying mechanisms are not described exactly, but an overall expression can be added to account for this phenomenon in the models. In the current work, the expression by Bergter and Knorre (1972) is used, where the rates are multiplied by a factor according to:

$$r = r_{nolag} \cdot \left(1 - e^{t/t_{lag}}\right), \tag{2.28}$$

depending on the time t and the lag-time t_{lag}.

This is by no means the only reported equation. For other options, see for instance the suggestions by Pirt (1975) or Bona and Moser (1997).

In the current work, a parameter t_{lag} is estimated for each experiment and each model during fitting of the model to the experimental data. In the planning of experiments, the lag-time was not used and an attempt was made to adjust the planning in the initial phase of the experiment, as will be described in paragraph 3.4.1 on page 50.

2.4. Fitting Models to Experimental Data

2.4.1. Parameter Estimation

In some cases, the parameters of models which are based on first-principles might be known a priori, but in many cases, amongst which the current project, they are not. In those cases, the parameter values need to be estimated from experimental data. This parameter estimation, model fitting or regression, consists of searching for a set of model parameters $\boldsymbol{\theta}$ within the allowed parameter space, which minimizes the distance between the measured values y and the model predictions of these values $f(x, \theta)$. Usually the sum of the squared distances are minimized: a least squares optimization. When several different variables are measured or when the measured values come from a wide range, it is likely that the N measured values are not equally accurate. In this case the errors need to be weighted by the corresponding standard deviations giving the maximum likelihood criterion:

$$\hat{\boldsymbol{\theta}} = \arg\min_{\theta} \sum_{i=1}^{N} \frac{(y_i - f(\mathbf{x_i}, \boldsymbol{\theta}))^2}{\sigma^2} \tag{2.29}$$

where $\hat{\boldsymbol{\theta}}$ indicates the estimated parameter set, and σ^2 contains the variances of the measured values. For linear models, the parameters can be estimated explicitly, but for the non-linear models which are used in the current work, a non-linear optimization routine is needed to find the parameters.

The method of least squares is the most commonly used regression method and is also applied in the current study. It is however not the only available option. Several alternative methods have been developed, for instance to reduce the sensitivity of the solution with respect to outliers in the data (Birkes and Dodge, 1993).

2.4.2. Parameter Accuracy

It is of course very important for the use of mathematical models that the used parameter values are correct. When the parameter values are estimated from measured data as mentioned before, the quality of the data determines the achievable accuracy of the estimated parameter. In special cases, some parameters may not be uniquely estimable at all, for instance in the trivial example of fitting a second order polynomial to two measured values only. In other cases, the parameter might be estimable but only with a very poor accuracy, as was for example shown to be the case for Monod type nonlinear models fitted to data from one batch fermentation only (Holmberg, 1982; Nihtilä and Virkkunen, 1977). The accuracy of the estimated parameters can be addressed using the covariance matrix of the parameter estimates.

Assuming the models to be smooth around the measured values and the estimated parameters $\hat{\boldsymbol{\theta}}$ to be close enough to the real parameter values $\boldsymbol{\theta}$, so that the (nonlinear) model can be approximated between the two sets of parameters by a first order Taylor series, we can write:

$$y(t, \mathbf{u}, \boldsymbol{\theta}) \cong f(\mathbf{x}, t, \mathbf{u}, \hat{\boldsymbol{\theta}}) + \sum_{i=1}^{p} (\hat{\theta}_p - \theta_p) \frac{\partial f(\mathbf{x}, t, \mathbf{u}, \boldsymbol{\theta})}{\partial \theta_p} \tag{2.30}$$

Then, the covariance matrix of the parameter estimates $\mathbf{Cov}_\theta$ can be calculated from the measurement variances σ^2 and the first order derivative of the model to the parameters $\frac{\partial y}{\partial \theta}$.

These derivatives form the jacobian matrix with all N measured values in separate rows and all p model parameters in separate columns:

$$\mathbf{J} = \begin{bmatrix} \frac{\partial y_1}{\partial \theta_1} & \cdots & \frac{\partial y_1}{\partial \theta_p} \\ \vdots & \ddots & \vdots \\ \frac{\partial y_N}{\partial \theta_1} & \cdots & \frac{\partial y_N}{\partial \theta_p} \end{bmatrix} \tag{2.31}$$

The calculation of this jacobian matrix, especially for dynamic systems, is addressed in more detail in paragraph 2.4.4 on page 21.

With the measurement variances in an N by N matrix $\mathbf{Cov_m}$, the covariance matrix of the parameter estimates can be calculated as

$$\mathbf{Cov}_\theta = (\mathbf{J}^T \cdot \mathbf{Cov_m}^{-1} \cdot \mathbf{J})^{-1} \tag{2.32}$$

In words: the possible error in the parameter estimates is caused by the possible error in the measured values and depends on how sensitive the predicted values are towards the parameter values.

The covariance matrix of the parameters is a symmetric matrix with the variances of the parameters on the diagonal. When all measurements are independent, all other entries of the matrix are zeros. A very important indication of the accuracy of the parameter estimation is the comparison of the standard deviations of the parameter estimates with the estimated parameter values themselves. These standard deviations are calculated as the square root of the diagonal entries of the covariance matrix.

From the covariance matrix of the parameter estimates, the correlation matrix of the parameter estimates $\mathbf{Cor}_\theta$ can easily be calculated with element i, j of the correlation matrix defined as

$$\mathbf{Cor}_\theta(i,j) = \frac{\mathbf{Cov}_\theta(i,j)}{\sqrt{\mathbf{Cov}_\theta(i,i)\mathbf{Cov}_\theta(j,j)}} \tag{2.33}$$

The elements of this matrix, the correlation coefficients, are values between -1 and 1 where -1 indicates a complete negative correlation, 0 means no correlation was found and 1 indicates complete correlation. Correlation coefficients close to 1 or -1 also indicate that these parameters are not estimable uniquely. In some of these cases, it might be easily possible to simplify the model without much loss of accuracy of the model predictions, or an experiment could be planned aiming at estimating this pair of parameters.

2.4.3. Accuracy of the Fitted Model

After the parameters of a model are estimated, the accuracy of the model fit to the available data needs to be evaluated. A couple of options for this evaluation are mentioned here.

When the measured values have a normal distributed measurement error with zero mean and standard deviation σ, the difference between the predictions by an accurate unbiased model and the measured values is also expected to follow this distribution. The agreement between the distribution of the observed errors and the expected normal distribution can be tested by a chi squared test. A reduced chi squared, $\tilde{\chi}^2$, can be defined as (Taylor, 1982)

$$\tilde{\chi}_i^2 = \frac{1}{d}\sum_{i=1}^{N}\left(\frac{y_i - \hat{y}_i}{\sigma_i}\right)^2. \tag{2.34}$$

where y_i indicates the measured value whereas $\hat{y}_i$ is the corresponding model prediction. The degrees of freedom d is used to scale the chi squared value. This degree of freedom can be calculated as the difference between the amount of estimated model parameters and the amount of measurements N. For good fitting models, $\tilde{\chi}^2$ is expected to be about 1. All models leading to lower values are accepted and models with much higher values do not fit properly. When values of slightly more than 1 are achieved, a more accurate

evaluation can be made by comparing the achieved $\tilde{\chi}^2$ with values from standard chi squared tables. The strict use of this rule might be difficult for dynamic fermentation processes. Often, models are used with success although they probably do not meet the chi squared rule. As also discussed in paragraph 2.2 on page 9, a severe simplification of the complex system has to be made in order to get models which might be suitable for process optimization and control. Furthermore it is often difficult to estimate the real standard deviation of some of the measurements. The real measurement error of dilution steps and the measurement equipment can usually easily be determined. Possible errors by non-homogeneous samples, time delays in the off-line measurements et cetera, may be more difficult to estimate. These errors can cause higher standard deviations and a relatively high amount of outliers. Therefore, the choice of whether to reject a model is usually not done solely based on a little bit too high a $\tilde{\chi}^2$. Still the reduced chi squared value forms a very valuable quantitative measure for the goodness of the fit and can also be used to compare the fit of different models. The weighting by the degree of freedom in the reduced form of the chi squared value provides some favouring of more simple models with less parameters.

By using the reciprocal of $\tilde{\chi}^2$, so that higher values represent better fits, and by subsequent scaling of the values for all m compared models to 1, a measure of the relative goodness of fit of different models can be calculated. So, the measure G_i for model i can be calculated as:

$$G_i = \frac{\frac{1}{\tilde{\chi}_i^2}}{\sum_i^m \frac{1}{\tilde{\chi}_i^2}} \tag{2.35}$$

Another method of comparing the fits of competing models is the Bayes approach of calculating relative model probabilities as mentioned for instance by Box and Hill (1967) or discussed by Stewart et al. (1996, 1998). Assuming a normal distribution of the measurement error, they formulated the probability density function p_i of a model prediction $\hat{y}_{i,n}$ according to model i and measurement n as

$$p_{i,n} = \frac{1}{\sqrt{2\pi(\sigma^2 + \sigma_{i,n}^2)}} \exp\left(-\frac{1}{2(\sigma^2 + \sigma_{i,n}^2)}(y - \hat{y}_{i,n})^2\right) \tag{2.36}$$

where σ^2 is the variance of the measured value and $\sigma_{i,n}^2$ is the variance of the model prediction. This last variance is also called the model variance, which is the term that will be used further in the current work. This model variance is described in more detail in paragraph 2.5.1 on page 26.

Then, the relative probability of model i out of m competing models after n measurements is calculated as

$$P_{i,n} = \frac{P_{i,n-1} \cdot p_{i,n}}{\sum_{i=1}^m P_{i,n-1} \cdot p_{i,n}}. \tag{2.37}$$

When the models stay the same, as is for instance the case in the publication by Box and Hill, the prior probabilities $P_{i,n-1}$ are simply the probabilities which were calculated after the last measurement. However, as soon as a new model is added or when model parameters are re-estimated, which strictly speaking also means that the model is actually changed, the relative probabilities should be re-calculated using all available data. This is also done after each experiment in the current work, so that, when all m models have an equal initial relative probability prior to all measurements, the relative probabilities calculated this way after n measurements is:

$$P_{i,n} = \frac{\prod_{j=1}^{n} p_{i,j}}{\sum_{i=1}^{m} \prod_{j=1}^{n} p_{i,j}}. \tag{2.38}$$

Note that the total sum of the relative model probabilities calculated this way always stays 1.

One other important way of evaluating fitted models is by simply looking at plots of the measured values and the model predictions. This seems trivial but can be important. When working with dynamic experiments, such as batch or fed-batch experiments, where measurements are taken at several time points, the course of the curves through the measured values is very important. See for instance the results in paragraph 5.2.3 on page 104. Unfortunately, this is not taken into account by the quantitative methods of evaluation mentioned above. This is a general problem when one global criterion is used to evaluate the fit, which does not regard local differences. However, by plotting the measured values and the model predictions against the time, this aspect is clearly noticed. It can even be better seen when a residual plot is made over time. In such a residual plot, the difference between the measured values and model predictions is plotted against the time. An optimal fitting model should lead to a horizontal trend around 0 with only (white) noise added to it. When the residuals are weighted by the standard deviation of the measurements, more than 95% of the values is expected to stay between -2 and 2 for a perfect fitting model and normal distributed noise.

2.4.4. Jacobian in dynamic systems

Since the calculation of the jacobian is not trivial, especially for dynamic systems with nonlinear models, this is addressed here in more detail.

As mentioned before (equation 2.31 on page 18), the jacobian matrix consists of the sensitivities of the measured values $\mathbf{y}$ to the parameter values $\boldsymbol{\theta}$:

$$\mathbf{J} = \frac{\partial \mathbf{y}}{\partial \boldsymbol{\theta}} = \begin{bmatrix} \frac{\partial y_1}{\partial \theta_1} & \cdots & \frac{\partial y_1}{\partial \theta_p} \\ \vdots & \ddots & \vdots \\ \frac{\partial y_n}{\partial \theta_1} & \cdots & \frac{\partial y_n}{\partial \theta_p} \end{bmatrix} \tag{2.39}$$

We define the measured or simulated values y as a function of the state variables $\mathbf{x}$, the control variables $\mathbf{u}$, the parameters $\boldsymbol{\theta}$ and, in dynamic systems, the time t. The change in the state variables $\mathbf{x}$ over time is also a function of the state variables itself, the control variables and the time:

$$y = f(\mathbf{x}, t, \mathbf{u}, \boldsymbol{\theta}) \tag{2.40}$$

$$\frac{d\mathbf{x}}{dt} = g(\mathbf{x}, t, \mathbf{u}, \boldsymbol{\theta}) \tag{2.41}$$

For calculation of the parameter sensitivity of the output variable y, we need the parameter sensitivity of the state variables $\mathbf{x}$, $\frac{\partial \mathbf{x}}{\partial \boldsymbol{\theta}}$.

In dynamic systems, the effect of a changed parameter value can propagate over time so we have to use the integral over time here:

$$\frac{\partial x}{\partial \hat{\theta}_p}(\mathbf{x}, t_i, \mathbf{u}, \hat{\boldsymbol{\theta}}) = \frac{\partial x}{\partial \hat{\theta}_p}(\mathbf{x}, 0, \mathbf{u}, \hat{\boldsymbol{\theta}}) + \int_{t=0}^{t_i} \frac{\partial x(\mathbf{x}, t, \mathbf{u}, \hat{\boldsymbol{\theta}})}{\partial \hat{\theta}_p} dt \tag{2.42}$$

With the initial parameter sensitivities being 0, the $\frac{\partial x}{\partial \hat{\theta}_p}(\mathbf{x}, 0, \mathbf{u}, \hat{\boldsymbol{\theta}})$ can be omitted.

For solving the integral of equation 2.42, we use Schwarz' rule:

$$\frac{d}{dt}\left(\frac{\partial x}{\partial \hat{\theta}_p}\right) = \frac{\partial}{\partial \hat{\theta}_p}\left(\frac{dx}{dt}\right) \tag{2.43}$$

which, combined with equation 2.41, yields:

$$\frac{d}{dt}\left(\frac{\partial x}{\partial \hat{\theta}_p}\right) = \frac{\partial (g(\mathbf{x}, t, \mathbf{u}, \boldsymbol{\theta}))}{\partial \hat{\theta}_p} \tag{2.44}$$

It is important to remember that we are working with partial differential equations here. So, besides the fact that the function g is directly depending on the parameters, it is also depending on the state variables $\mathbf{x}$ which on their turn also depend on the parameters. Therefore, we have to use the chain rule:

$$\frac{\partial (g(\mathbf{x}, t, \mathbf{u}, \boldsymbol{\theta}))}{\partial \hat{\theta}_p} = \frac{\partial g(\mathbf{x}, t, \mathbf{u}, \boldsymbol{\theta})}{\partial \hat{\theta}_p} + \frac{\partial g(\mathbf{x}, t, \mathbf{u}, \boldsymbol{\theta})}{\partial \mathbf{x}} \cdot \frac{\partial \mathbf{x}}{\partial \hat{\theta}_p} \tag{2.45}$$

After combining 2.45 with equation 2.42, this yields:

$$\frac{\partial x_i}{\partial \hat{\theta}_p}(t_i, \mathbf{u}, \hat{\boldsymbol{\theta}}) = \int_{t=0}^{t_i} \left(\frac{\partial g(x_i, t_i, \mathbf{u}, \boldsymbol{\theta})}{\partial \hat{\theta}_p} + \frac{\partial g(x_i, t_i, \mathbf{u}, \boldsymbol{\theta})}{\partial \mathbf{x}} \cdot \frac{\partial \mathbf{x}}{\partial \hat{\theta}_p} \right) dt \tag{2.46}$$

So, with the direct derivative functions of g to $\hat{\theta}_p$ and to $\mathbf{x}$, the parameter sensitivities of the state variables can be simulated over time. Note that $\mathbf{x}$ contains the whole set

of state variables here. Equation 2.46 can also be written with the explicit summation over all n state variables:

$$\frac{\partial x_i}{\partial \theta_p}(t_i, \mathbf{u}, \boldsymbol{\theta}) = \int_{t=0}^{t_i} \left(\frac{\partial f(x_i, t_i, \mathbf{u}, \boldsymbol{\theta})}{\partial \theta_p} + \sum_{j=1}^{n} \frac{\partial f(x_i, t_i, \mathbf{u}, \boldsymbol{\theta})}{\partial x_j} \cdot \frac{\partial x_j}{\partial \theta_p} \right) dt \tag{2.47}$$

When the measured output variables $\mathbf{y}$ are the same as (a selection of) the state variables $\mathbf{x}$, the parameter sensitivity of the measured variables equals of course the parameter sensitivities of the corresponding state variables. This is for instance the case in the used models for describing the L-valine production in the current work. However, in the general case where the measured variables are a function of the state variables as in equation 2.40 on the preceding page, the parameter sensitivity of the output variables is determined in an analogue way yielding:

$$\frac{\partial y_i}{\partial \theta_p}(x, t_i, u, \theta) = \int_{t=0}^{t_i} \left(\frac{\partial g(x, t_i, u, \theta)}{\partial \theta_p} + \sum_{j=1}^{n} \frac{\partial g(x, t_i, u, \theta)}{\partial x_j} \cdot \frac{\partial x_j}{\partial \theta_p} \right) \tag{2.48}$$

where the parameter sensitivity of the state variables ($\frac{\partial x_j}{\partial \theta_p}$) can be calculated from equation 2.47.

By including the derivative functions in the model, the parameter sensitivities can be simulated together with the rest of the model. The jacobians were calculated this way for instance in the design of experiments for improvement of parameter estimation (Munack, 1989; Versyck et al., 1997). In the current work it is used for the calculation of model discriminating functionals, which are discussed in paragraph 2.5.1 on page 26, for the simulative study in chapter 4. Noteworthy, care had to be taken not to get problems with numeric inaccuracies of the simulations, especially when differences between the sensitivities were needed. Determining the model discriminating design criteria like this, a minimal relative accuracy of 10^{-8} was used in the current work.

The parameter sensitivities show how much the predicted value would change when a model parameter would be slightly different. Another way of calculating these values, which is intuitively very easy to understand, is by *'finite difference approximation'*, where the model is re-simulated using slightly changed parameter values and the achieved change in the response is regarded (Degenring et al., 2004; Turányi, 1990):

$$\frac{\partial y_i}{\partial \theta_p} = \frac{(y(t_i, u, (\theta + d\theta))) - (y(t_i, u, \theta))}{d\theta} \tag{2.49}$$

where $d\theta$ contains a small change in the value of parameter p.

An advantage of this simple, but less elegant method is the fact that the derivatives of the model equations to all state variables and to all parameter values do not need to be

build in the model. An obvious pitfall, on the other hand, is that this method only produces proper results when the change of the parameter values is in an appropriate range. When the applied difference would be too small, no effect of the changed parameter value will be found. And even if an effect would be found, the risk of numerical inaccuracies having much influence is rather high. On the other hand, large changes in the parameter values can give strongly erroneous results when the model cannot be approximated by a first order Taylor series any more in the used range. These problems seem very likely to occur, especially in multivariable and dynamic systems, where the parameters can have very different influences on the different state variables and in different phases of the simulations. To diminish the risk of getting wrong results due to too small or too large changes in the parameter values, it can be checked whether similar results are obtained using a small increase and a small decrease in the parameter values:

$$\frac{\partial y_i}{\partial \theta_p} = \frac{(y(t_i, u, (\theta + d\theta))) - (y(t_i, u, \theta))}{d\theta} = \frac{(y(t_i, u, \theta)) - (y(t_i, u, (\theta - d\theta)))}{d\theta} \tag{2.50}$$

When the two values differ too much, the parameter can be changed with a different amount. When used with care, this method should produce the same results as the more analytical method mentioned above. Just as with the former, it might be necessary to use rather tight bounds on the accuracy of the simulation itself. As an example, figure 2.1 on the next page shows the parameter sensitivities simulated over time, calculated using both methods, for a Monod-type model with substrate and product inhibitions in a batch experiment and the maximal specific growth rate as the investigated parameter. The results of the two methods differed less than 0.1% for all values.

One drawback of the finite differentiation method is the intensive calculation time for multiple simulations. Even if the parameters are directly changed with an appropriate amount for all state variables during the whole simulation, the models need to be re-simulated twice for each parameter value. This method was used in the current work on several occasions for calculation of the covariance matrix of the estimated parameter values, which has to be done only once for each model. For the design of experiments, this was not the method of choice, since the parameter sensitivities need to be recalculated very many times during the optimization process. As an example let us regard a relatively simple model with 9 parameters and 3 state variables as mentioned in the simulative study in paragraph 4.2 on page 63. The calculation of all parameter sensitivities for a simulated batch experiment with 36 measured values in 20 hours, the finite differentiation method took 2.2 seconds using 98 simulations, whereas the other method took 0.30 seconds on a personal computer with a pentiumIII 700 MHz processor. One simulation of the model used in the method of finite differentiation takes much less time (about 0.022 s) than for the other method, because the simulation of all parameter sensitivities in the other method makes the model much larger. The effect of the larger amount of simulations needed for the method of finite differentiation is, however, much stronger.

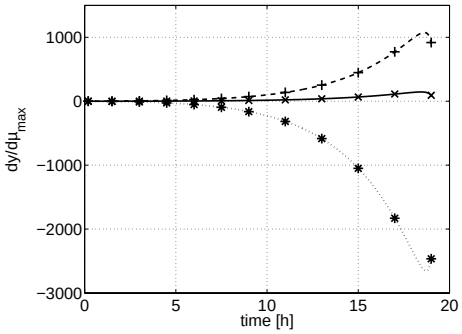

FIGURE 2.1.: Jacobian calculated in two ways. Parameter sensitivities are shown for the concentrations of biomass $[OD_{600}h]$, substrate $[gh/L]$ and product $[mMh]$ depending on the maximal specific growth rate (μ_{max}). Lines are calculated using explicit simulation of the sensitivities in the model and the markers by re-simulation with changed parameter values. Solid lines and $\times$ show the sensitivities of the simulated biomass concentrations, dotted lines and $*$ of substrate concentrations and dashed lines and $+$ of product concentrations.

2.5. Experimental Design

Every experiment takes time, money and other resources. Therefore it is very important to limit the number of experiments and get much relevant information from each experiment. Experimental design stands for techniques which help to plan informative experiments. Many different approaches have been developed, depending for instance on the type of information needed and the kind of information available.

The experimental designs can first be divided in two groups which will be called 'statistical experimental design' and 'model based experimental design' here. The term 'model based experimental designs' is used here for designs which use predictions of a mathematical model in order to determine how an experiment should be performed, whereas with 'statistical experimental designs', techniques are meant, which do not explicitly need these model predictions.

In the current work, model based designs are investigated and used and some of this type of designs will be discussed in more detail in the following paragraphs.

Examples of statistical experimental designs are for example factorial designs such as 2-level full factorial designs, where two values are chosen for each variable and all combinations of these variable values are used. Many different statistical designs have been used, depending for instance on the type of effects, influential factors and combi-

nations, the researcher is looking for. An overview of different statistical experimental designs can be found in textbooks such as Bandemer and Bellmann (1994) or the review by Draper and Pukelsheim (1996).

Two different types of model based experimental design techniques are explained and used here, depending on the goal of the designed experiment. First of all, model discriminating designs are used for planning of experiments, in order to determine which of several competing models describe the phenomena best. Second, there are experimental design criteria, which are used for planning experiments in order to improve the parameter estimation[11].

2.5.1. Experimental Design for Model Discrimination

The development of design criteria for discriminating between rival models already dates back to the sixties, when, amongst others, Hunter and Reiner suggested a criterion which consists of maximizing the difference between expected measurements y_1 and y_2, according to two competing models (Hunter and Reiner, 1965):

$$\xi^* = \arg\max_{\xi}(\hat{y}_1 - \hat{y}_2)^2 \tag{2.51}$$

where ξ describes an experiment and the asterisk denotes the optimized values.

For more than two rival models, either a summation over the model pairs or a maximization of the minimal distance between two models were suggested (Cooney and McDonald, 1995; Espie and Macchietto, 1989).

These approaches did not yet take into account the accuracy of the measurements. However, an expected difference between two accurately measurable values is of course more informative than the same difference between inaccurate values, so it was suggested to weight the differences by the estimated variances in the measurements. Especially when a number of different state variables are measured and also for experiments with large differences between the measured values, as is usually the case for dynamic experiments, this is very important since the accuracy of the different measured variables can differ strongly. For the multivariable and dynamic experiments, also the summation over all expected measured values has to be introduced:

$$\arg\max_{\xi}\sum_{k=1}^{N}\sum_{i=1}^{m-1}\sum_{j=i+1}^{m}((\hat{y}_{i,k} - \hat{y}_{j,k})\sigma_k^{-2}(\hat{y}_{i,k} - \hat{y}_{j,k})) \tag{2.52}$$

where N is the total amount of measurements, including all state variables and all measurement times. $\hat{y}_{i,k}$ is the expected measured value k according to model i. σ_k is the

[11] This is also sometimes called 'optimal experimental designs', but this term has been used in different ways and can be confusing. Model discriminating designs or statistical designs are also 'optimal' in a sense and therefore the description 'designs for parameter estimation' or 'parameter estimation design' will be used here.

expected variance of the difference between the model expectations for measurement k, which is calculated as the sum of the measurement variances of these expected measurements for model i and j (Taylor, 1982).

In matrix notation this can be written as:

$$\arg\max_{\xi} \sum_{i=1}^{m-1} \sum_{j=i+1}^{m} ([\hat{\mathbf{y}}_i - \hat{\mathbf{y}}_j]^T \boldsymbol{\Sigma}_{ij}^{-1} [\hat{\mathbf{y}}_i - \hat{\mathbf{y}}_j]) \tag{2.53}$$

where $\mathbf{y}_i$ is a $[N \times 1]$ column vector containing the N expected measured values according to model i:

$$\mathbf{y_i} = \begin{bmatrix} y_{i,1} \\ \vdots \\ y_{i,N} \end{bmatrix}. \tag{2.54}$$

$\boldsymbol{\Sigma}_{ij}$ is a symmetric quadratic matrix of size $[N \times N]$, consisting of the sum of the measurement (co)variance matrices according to model i, $\boldsymbol{\Sigma}_i$ and j, $\boldsymbol{\Sigma}_j$:

$$\boldsymbol{\Sigma}_{ij} = \boldsymbol{\Sigma}_i + \boldsymbol{\Sigma}_j \tag{2.55}$$

with $\boldsymbol{\Sigma}_\mathbf{i}$ defined as:

$$\boldsymbol{\Sigma}_\mathbf{i} = \begin{bmatrix} \sigma_{i,1}^2 & \sigma_{i,12} & \cdots & \sigma_{i,1N} \\ \sigma_{i,12} & \sigma_{i,2}^2 & \cdots & \sigma_{i,2N} \\ \vdots & \vdots & \ddots & \cdots \\ \sigma_{i,1N} & \sigma_{i,2N} & \cdots & \sigma_{i,N}^2 \end{bmatrix} \tag{2.56}$$

where $\sigma_{i,1}^2$ is the measurement variance of measurement 1 as expected by model i and $\sigma_{i,12}$ is the measurement covariance of expected value 1 and 2 according to that model.

In the summation in equation 2.52, it is assumed that the measurements are independent, which means that $\boldsymbol{\Sigma}$ only contains non-zero values in its diagonal and all covariances are zero.

For the dynamic case, instead of the summation over all N measured values, also the integration over the experiment time was suggested. However, since we use a limited amount of discrete off-line measurements in the current work, the discrete description is shown here.

Besides the measurement error, it was also argued that the variance in the expected response should be taken into account. This variance originates from the fact that the simulated values are based on a model which has inaccurate parameter estimates. With somewhat different parameter values, which might still allow a proper fit to prior data, the expected values will change. With the sensitivity of the expected values towards the parameters in jacobian matrix $\mathbf{J}$ of size $[N \times P]$, this model variance $\mathbf{W}$ (size $[N \times N]$) can be calculated as:

$$\mathbf{W} = \mathbf{J} \cdot \mathbf{Cov}_\theta \cdot \mathbf{J}^T \tag{2.57}$$

The used jacobian matrix of the expected values can be calculated as explained in paragraph 2.4.4 on page 21, containing the parameter sensitivities of the expected measured values in separate rows and the sensitivities towards all parameters in separate columns. The $[P \times P]$ covariance matrix of the parameters, $\mathbf{Cov}_\theta$, can be calculated from prior data according to equation 2.32 on page 18. Note that the covariance matrix of the parameter estimates is calculated using the parameter sensitivities of all prior measured data, whereas the sensitivities $\mathbf{J}$ in equation 2.57 are the sensitivities of the expected new measurements.

The impact of the use of the model variance can be expected to be much stronger for dynamic experiments than for static ones. The sensitivity of the expected response towards the estimated model parameters can get rather strong in these experiments. Furthermore, the parameter sensitivities can have strongly differing values during the experiment, due to the fact that the influence of the parameters can propagate over time. The impact of the model variance will increase, when the parameters are less well estimable, i.e. when the covariance matrix of the parameter estimates has higher values.

Many different model discriminating design criteria have been suggested in literature, which all contain structures which are similar to the basic structure of equation 2.52 on page 26 (Burke et al., 1997; Hill, 1978). Many of them also use the model variance. Many of these approaches use a statistical test in which the expected difference between the model predictions is compared to the estimated variance of this difference (Atkinson and Fedorov, 1975; Buzzi-Ferraris et al., 1984; Chen and Asprey, 2003), or calculation of probability density functions (Box and Hill, 1967; Hsiang and Reilly, 1974; Reilly, 1970). Some of the suggested criteria were developed for special situations such as discrimination between nested models (Pukelsheim and Rosenberger, 1993), (nested) polynomes (Dette and Roder, 1997) or autoregressive models (Uosaki and Hatanaka, 1988). A selection of criteria which might be applied to discrimination of dynamic nonlinear models will be discussed here in more detail.

Box and Hill

The model discriminating experimental design approach of Box and Hill (1967) has been widely used with and without several adjustments.

They based their criterion on Shannons information theory (Shannon, 1948) using the concept of system entropy, which can be defined as:

$$-\sum_{i=1}^{m} P_i \ln P_i \tag{2.58}$$

for m models, with relative probability P_i of model i and a total sum of all probabilities of 1. These relative probabilities can be addressed as shown in equation 2.37 on page 20.

This entropy is maximal when all models have an equal probability and decreases when larger differences between the models are detected. The expected change in this entropy should thus be maximized and this change R can be formulated as

$$R = \sum P_{i,n-1} \int p_i \ln \frac{p_i}{\sum P_{i,n-1} p_i} dy_n \tag{2.59}$$

where p_i is the probability density function of the expected new measurement y_n according to model i.

Box and Hill have used the maximization of a maximal expected value for R, as the criterion for a model discriminating design. They formulated their criterion for the univariate static case with constant measurement variance σ^2 as:

$$\arg\max_{\xi} \frac{1}{2} \sum_{i=1}^{m} \sum_{j=i+1}^{m} P_{i,n-1} P_{j,n-1} \left(\frac{(\sigma_i^{*2} - \sigma_j^{*2})^2}{(\sigma^2 + \sigma_i^{*2})(\sigma^2 + \sigma_j^{*2})} + [\hat{y}_i - \hat{y}_j]^2 * \left(\frac{1}{\sigma^2 + \sigma_i^{*2}} + \frac{1}{\sigma^2 + \sigma_j^{*2}} \right) \right) \tag{2.60}$$

The peculiar use of the *upper bound* on the expected value for R has been criticized by several statisticians (Meeter et al., 1970). Reilly suggested a method to estimate the expected value for R instead (Reilly, 1970).

The use of this maximal value is also the cause for the use of the differences in expected model variances in the numerator of the first part of the criterion. Especially in dynamic experiments and in models with poor parameter estimates, the model variances can take extreme values which can change very fast. This happens, for instance, in situations of sudden changes such as a depletion of substrate. Therefore it is very likely that, in these cases, the differences in the expected measured values play no significant role any more, but the criterion reduces to the maximization of the differences in the model variances, which is intuitively strange. Several examples where basically only the differences in the model variances determine the criterion, were also found in the simulative study in chapter 4.

The calculation of the model variances with the requirement that the model can be approximated by a linearized form, provides another source of problems (Bajramovic and Reilly, 1977). Hsiang and Reilly have suggested a method to avoid this, however requiring the use of a series of discrete parameter sets (Hsiang and Reilly, 1971).

The original criterion from Box and Hill was formulated for one variable and a constant measurement variance. One option to enhance this criterion for several measured variables and several measurements in the dynamic experiments, is the summation over all measured values, assuming all measurements to be independent:

$$\arg\max_{\xi} \sum_{i=1}^{m} \sum_{j=i+1}^{m} \sum_{k=1}^{N} P_{i,n-1} P_{j,n-1} \left(\frac{(\sigma_{i,k}^{*2} - \sigma_{j,k}^{*2})^2}{(\sigma_{i,k}^2 + \sigma_{i,k}^{*2})(\sigma_{j,k}^2 + \sigma_{j,k}^{*2})} + [\hat{y}_{i,k} - \hat{y}_{j,k}]^2 * \left(\frac{1}{\sigma_{i,k}^2 + \sigma_{i,k}^{*2}} + \frac{1}{\sigma_{j,k}^2 + \sigma_{j,k}^{*2}} \right) \right) \quad (2.61)$$

where $P_{i,n-1}$ still is the probability of model i before experiment ξ, $\sigma_{i,k}^2$ is the estimated variance of the expected measurement k according to model i, which might be different from the corresponding variance of the measurement according to model j: $\sigma_{j,k}^2$. $\sigma_{i,k}^{*2}$ is the model variance of the expected value of measurement k according to model i (Pritchar and Bacon, 1974).

One problem, which was encountered in the use of the criterion of Box and Hill for the dynamic bioprocesses in the current project, was an extreme exaggeration of the differences in the relative model probabilities. This seems to be caused by sensitivity towards outliers. The exaggeration especially occurred with increasing amounts of measured values and a clear lack of fit in all models, which is not an unusual situation in macroscopic modeling of bioprocesses. An alternative option is the calculation of relative goodness of fit as stated in equation 2.35 on page 20 instead of the relative probability, which tends to result in much more moderate differences.

Despite the mentioned problems and criticism, the criterion by Box and Hill has been used successfully in several cases, for instance in heterogeneous catalysis (Froment, 1975; Froment and Mezaki, 1970) or in continuous fermentations (Takors et al., 1997).

Buzzi-Ferraris and Forzatti

Buzzi-Ferraris and Forzatti (1983); Buzzi-Ferraris et al. (1990, 1984) suggested an intuitively appealing discriminating design criterion which is based on the statistical chance that a difference between two model predictions could also be explained by the variance of the predictions (both by measurement inaccuracy and inaccurate parameter estimates). They suggested maximizing the ratio between the expected differences in the model predictions and the total variance of this difference, which was build up from the measurement variance and the model variances.

$$\arg\max_{\xi} \sum_{i=1}^{m-1} \sum_{j=i+1}^{m} [\hat{\mathbf{y}}_i - \hat{\mathbf{y}}_j]^T \mathbf{V}_{ij}^{-1} \times ([\hat{\mathbf{y}}_i - \hat{\mathbf{y}}_j] + \mathrm{trace}[2\boldsymbol{\Sigma}\mathbf{V}_{ij}^{-1}]) \quad (2.62)$$

where the variance matrix $\mathbf{V}_{ij}$ consists of two times the measurement variance matrix $\boldsymbol{\Sigma}$ and the model variances of model i and j:

$$\mathbf{V}_{ij} = 2\boldsymbol{\Sigma} + \mathbf{W}_i + \mathbf{W}_j \quad (2.63)$$

The model variances $\mathbf{W}$ are also explained in equation 2.57 on page 28.

Buzzi-Ferraris and Forzatti published their criterion with a model independent variance matrix $\mathbf{\Sigma}$. In the current work, the terms $2\mathbf{\Sigma}$ in equation 2.62 and 2.63 have been replaced with $\mathbf{\Sigma_i} + \mathbf{\Sigma_j}$, the sum of the estimated measurement variances of the expected values according to model i and j, which allows a different measurement variance at different values.

Buzzi-Ferraris and Forzatti suggested the addition over all model pairs as shown in equation 2.62 and did not use of the weights of the importance of the model pairs as done for instance by Box and Hill. Instead, they stated that all models which passed the chi-squared adequacy test based on all prior data, should be regarded with equal probability and all other models should simply not be regarded. When models which did not pass the test before, pass the test after addition of new data, the model could be reintroduced for the construction of the next experiment.

Buzzi-Ferraris and Forzatti also suggested to stop the procedure when it would fail to design experiments which give higher values for the criterion than the amount of new expected measurements, claiming that the experiment is not expected to be informative. Such a criterion seems appealing, but is somewhat problematic in the suggested form for the use in multiresponse experiments since it actually suggests that the average of the expected responses should be informative. It could however very well be, that many measurements and many variables are not informative, having practically equal responses according to both models, whereas only a few expected measurements are expected to differ significantly. In this case the experiment would be rejected, although the same experiment would be accepted when only these relevant measurements would be planned. One other option could therefore be to accept only experiments which expect at least one measurement to be informative.

Chen and Asprey

Based on the criterion by Buzzi-Ferraris and Forzatti, Chen and Asprey recently published a similar criterion for dynamic experiments and multiresponse nonlinear situations with discrete sampling (Chen and Asprey, 2003):

$$\arg\max_{\xi} \sum_{i=1}^{n_{sp}} [\hat{\mathbf{y}}_i - \hat{\mathbf{y}}_j]^T \mathbf{S}_{ij}^{-1} [\hat{\mathbf{y}}_i - \hat{\mathbf{y}}_j] \tag{2.64}$$

using an addition over all suggested sampling points n_{sp}. So, all sampling points are regarded independent, also with respect to the model variance which is caused by the parameter estimates, which seems strange. The $[n_v \times 1]$ vectors of expected measurements $\mathbf{y}$ contain the n_v different measured variables at one sampling time, and all these variables were suggested to be dependent. Also the $[n_v \times n_v]$ matrix with variances, S_{ij}, contains the covariances at one sample time only. Note that this criterion is equal to a criterion

with all measured values in one vector and a corresponding bigger covariance matrix, when all covariances between two measured values which are taken at different sampling times, are zero.

The weighting by $\mathbf{V}_{ij}$ has been replaced by the very similar $\mathbf{S}_{ij}$, which however contains the measurement variance only once:

$$\mathbf{S}_{ij} = \mathbf{\Sigma} + \mathbf{W}_i + \mathbf{W}_j \tag{2.65}$$

They suggested to estimate the experimental variance from prior data and did not include the possibility of having different expected measurement variances based on different model predictions.

Furthermore, they used their criterion only for one model pair at a time and suggested to use it on the two best fitting models in one of their examples.

Based on the suggestion of Buzzi-Ferraris and Forzatti, also Chen and Asprey suggested not to perform any experiments which give rise to criteria smaller than the amount of measurements, being all measured variables at all sampling times together. This has been discussed above for the criterion of Buzzi-Ferraris and Forzatti. An example of an experiment which would not pass this criterion, but which would be accepted when only some of the measurements are taken, is shown in the simulative study in chapter 4.

The criterion by Chen and Asprey has been used in a simulative comparison in the current work with the adjustment that the criterion was added over all model pairs, just like suggested by Buzzi-Ferraris and Forzatti, and with the measurement variance of the expected measurements being the average between the ones estimated for the 2 models.

Discriminating Design Criteria for Dynamic Experiments Without Model Variances

The calculation of model variances and the parameter sensitivities which are needed for this, is a rather difficult task for dynamic experiments, as is also pointed out in paragraph 2.4.4 on page 21. Furthermore, the model variances can take extreme values when used in dynamic systems and with models with poor parameter estimates. Besides the problems this may cause in the calculation of the experimental designs, also the fact that a large part of the calculation time is used for the calculation of the model variances, is an important disadvantage of these design criteria. For example, calculation of the criterion of equation 2.51, which does not use the model variance, for a simple Monod-type model with 3 measured variables and 9 model parameters and a simple batch experiment of 20 hours duration with 12 samples, took approximately 0.08 s. Calculation of the criteria with model variances, such as equation 2.61 and 2.62, on the other hand, took about 0.8 s in the same situation on a personal computer with a PentiumIII 700MHz processor!

In this respect, it should also be mentioned that it can already be difficult and time-consuming to include all derivatives of the differential equations towards the parameters and the state variables in the models, which is needed for calculation of the model

variance. This is especially so when the models get more complex. In a more automated model building, this might however be done automatically using symbolic mathematical tools.

Clear examples of criteria which do not use a model variance are the criterion by Hunter and Reiner (equation 2.51) or the similar criterion with weighting by the measurement variances (equation 2.53).

Based on these criteria, some extensions are presented here, in an attempt to improve the criteria for the use in dynamic multivariable experiments.

The first extension is introduced to consider the variance in the timing of the sampling, which can highly influence the measured values. Regard, for instance, the expected measured values of one variable according to two competing models, shown in figure 2.2. The values change very fast in the final part of the curves, but not exactly at the same time. This temporarily causes relatively large differences, especially when compared to the low values of the expected measurements themselves, although the curves stay close to each other. This is a situation which can easily occur when using

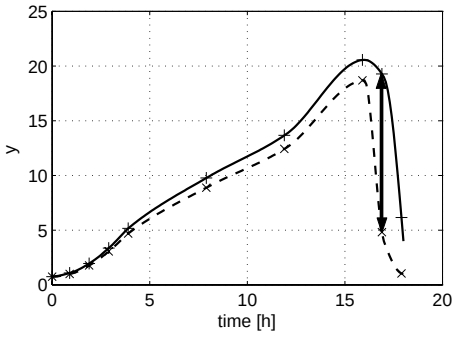

FIGURE 2.2.: Expected responses of two competing models (one shown as a solid line with + and one dashed with ×) for a designed dynamic experiment. Due to the fast changes in the measured values in the final part of the experiment, the differences between the models are relatively high, also when the curves are close to each other.

criteria like 2.53 to design dynamic experiments. However, such situations are not likely to be very informative for discrimination between the two models. In many cases, the model variances get relatively high in these situations. Therefore, such less informative situations can be avoided by criteria which are weighted by the model variance, such as the criteria by Buzzi-Ferraris and Forzatti or Chen and Asprey, shown in the preceding two paragraphs. One other way to account for this problem is by introducing a part of the measurement variance which is based on the variances in the measurement time,

which can be estimated using:

$$\boldsymbol{\sigma}_{i,t} = s_t \frac{d\mathbf{y}_i}{dt} \tag{2.66}$$

where $\boldsymbol{\sigma}_{i,t}$ is the standard deviation of the expected measurements $\mathbf{y}_i$, according to model i, caused by the variance in the measurement time point which is described using a standard deviation s_t and the time derivative of the estimated response $\frac{d\mathbf{y}_t}{dt}$. This time derivative is already needed for the simulations of the models and is therefore available without much extra computational effort. The standard deviation of the timing is dependent on the way of sampling and handling of the samples and can be estimated from timing of a series of measurements in practice. In the current work, a standard deviation of 10 minutes was used.

When all measured values are assumed to be independent, the corresponding squared values of equation 2.66 can be used in the diagonal of a larger timing dependent covariance matrix of all measurements. However, when a sample is taken somewhat delayed, this will count for all state variables measured in this sample, so this part of the measurement error is assumed to be correlated amongst measured values taken from the same sample, but not between values from different samples. For one sample with all measured values in an $[n_v \times 1]$ column vector $\mathbf{y}_i(s)$ and the corresponding timing dependent part of the standard deviation $\boldsymbol{\sigma}_{i,t}(s)$ in a column vector of the same size, the $[n_v \times n_v]$ covariance matrix $\boldsymbol{\Sigma}_{i,t}(s)$ caused by the timing error could be calculated as:

$$\boldsymbol{\Sigma}_{i,t}(s) = \boldsymbol{\sigma}_{i,t}(s) \cdot \boldsymbol{\sigma}_{i,t}(s)^T \tag{2.67}$$

For experiments with more than one sample, the covariance matrices for each sample can be used as parts of the total timing dependent covariance matrix with the covariances between measured values from different samples being 0, assuming no correlation between the errors in the timing of the different samples. So, when we use the column vector of all $N = n_v \cdot n_s$ expected measurements with first all n_v measured variables from the first sample $\mathbf{y}_i(1)$, then all from the second sample $\mathbf{y}_i(2)$, etc:

$$\mathbf{y}_i = \begin{bmatrix} \mathbf{y}_i(1) \\ \vdots \\ \mathbf{y}_i(n_s) \end{bmatrix} \tag{2.68}$$

we can use the covariance matrix of the measurement error caused by the timing errors as:

$$\boldsymbol{\Sigma}_{i,t} = \begin{bmatrix} [\boldsymbol{\Sigma}_{i,t}(1)] & 0 & \dots & 0 \\ 0 & [\boldsymbol{\Sigma}_{i,t}(2)] & 0 & \vdots \\ \vdots & 0 & \ddots & 0 \\ 0 & \cdots & 0 & [\boldsymbol{\Sigma}_{i,t}(n_s)] \end{bmatrix} \tag{2.69}$$

The squared brackets are added around the timing dependent covariance matrix of the values from the first sample $\mathbf{\Sigma}_{i,t}(1)$ to the last of n_s samples $\mathbf{\Sigma}_{i,t}(n_s)$, to emphasize the fact that these are $[n_v \times n_v]$ matrices taken from equation 2.67 and not just scalars.

Now, this matrix can simply be added to the corresponding covariance matrix $\mathbf{\Sigma}_{i,m}$, caused by measurement errors such as dilution inaccuracy or the accuracy of the used analytic equipment

$$\mathbf{\Sigma}_i = \mathbf{\Sigma}_{i,m} + \mathbf{\Sigma}_{i,t} \tag{2.70}$$

and used in the criterion formulated in equation 2.53 and 2.55.

Obviously, when the measurement variance would be determined from replication of complete experiments, this part of the measurement error, caused by timing of the sampling, would be included in the measurement variance. This would, however, not be the case when the measurement variance would be determined solely based on the accuracy of the analytical methods or repeated measurement from one sample.

Another adaptation of the simple criterion of 2.53 on page 27 comes from the idea that, in dynamic experiments, besides the difference between the expected values, also the difference between the expected shapes of the curves is likely to improve the discrimination between models. To elucidate this idea, regard the curves in figure 2.3. The fact that the two curves have clearly different shapes is expected to provide a better discrimination than when both curves would stay horizontal, although this would result in the same distance between measured points.

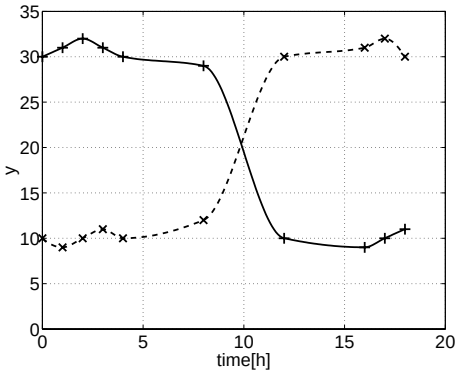

FIGURE 2.3.: Expected responses of two competing models (one with a solid line and + and the other as dashed line with ×) for a designed dynamic experiment. It is hypothesized that the different shapes of the two curves around 10 hours makes a good discrimination more likely than when both curves would have stayed on a constant distance.

One option to account for this, which is suggested and tested here, is by regarding the changes in the expected values between subsequent discrete measurements by extending the design criterion to:

$$\arg\max_{\xi} \sum_{i=1}^{m-1} \sum_{j=i+1}^{m} ([\hat{\mathbf{y}}_i - \hat{\mathbf{y}}_j]^T \boldsymbol{\Sigma}_{ij}^{-1} [\hat{\mathbf{y}}_i - \hat{\mathbf{y}}_j]) + ([\hat{\boldsymbol{\Delta}\mathbf{y}}_i - \hat{\boldsymbol{\Delta}\mathbf{y}}_j]^T \boldsymbol{\Sigma}_{\Delta ij}^{-1} [\hat{\boldsymbol{\Delta}\mathbf{y}}_i - \hat{\boldsymbol{\Delta}\mathbf{y}}_j]) \quad (2.71)$$

where $\boldsymbol{\Delta}\hat{\mathbf{y}}_i$ is a column vector of length $(N - n_v)$ containing the differences between all subsequent expected measurements according to model i:

$$\hat{\boldsymbol{\Delta}\mathbf{y}}_i = \begin{bmatrix} \hat{\mathbf{y}}_i(2) - \hat{\mathbf{y}}_i(1) \\ \vdots \\ \hat{\mathbf{y}}_i(n_s) - \hat{\mathbf{y}}_i(n_s - 1) \end{bmatrix} \quad (2.72)$$

and $\boldsymbol{\Sigma}_{\Delta ij}$ is a square $[N - n_v \times N - n_v]$ covariance matrix which is used to weight this added part of the criterion, which can be calculated as:

$$\boldsymbol{\Sigma}_{\Delta ij} = \boldsymbol{\Sigma}_{ij}(1 : n_s - 1) + \boldsymbol{\Sigma}_{ij}(2 : n_s) \quad (2.73)$$

where $\boldsymbol{\Sigma}_{ij}(1 : n_s - 1)$ denotes the covariance matrix containing measurement errors and timing errors, as mentioned before, but using only samples 1 to $n_s - 1$, so disregarding the final sample. Analogous, the first sample is omitted in $\boldsymbol{\Sigma}_{ij}(2 : n_s)$. This way, the squared difference $\hat{\mathbf{y}}_i(2) - \hat{\mathbf{y}}_i(1)$ is weighted by the expected variance of this difference, consisting of the addition of the variances of both subsequent measurements. The covariance matrices $\boldsymbol{\Sigma}_{ij}(1 : n_s - 1)$ and $\boldsymbol{\Sigma}_{ij}(2 : n_s)$ can be estimated as the covariance matrix due to real measurement errors and due to the variance in sampling times as mentioned above.

2.5.2. Experimental Design for Parameter Estimation

As mentioned in paragraph 2.4.2 on page 18, the accuracy of the parameter estimation depends on the quality of the data. Experimental design techniques for parameter estimation aim at designing experiments in order to get good quality of the data for parameter estimation.

Also the covariance matrix of the estimated parameter as a measure for the accuracy of the parameter estimation was already introduced in paragraph 2.4.2. A parameter estimating design will try to minimize the expected values in this covariance matrix.

It is common practice to work with the inverse of the covariance matrix of the parameter estimates: the informationmatrix $\mathbf{M}$ [12]:

$$\mathbf{M} = \mathbf{Cov}_{\theta}^{-1} = \mathbf{J}^T \cdot \mathbf{Cov}_{m}^{-1} \cdot \mathbf{J} \quad (2.74)$$

[12] Analogue to the Fisher informationmatrix. This matrix originates from the communication theory of Shannon (Shannon, 1948).

For the current theoretical explanations, it may be more convenient to work with the covariance matrix. In practice, however, one might want to avoid the need for calculation of the inverse of a matrix.

The determinant of $\mathbf{M}$ is always zero or positive. If the determinant of $\mathbf{M}$ is zero, not all parameters can be estimated. This happens, for instance, when the amount of measurements is less then the amount of parameters. This would lead to a jacobian $\mathbf{J}$ with a lower rank than the amount of parameters. Another characteristic of $\mathbf{M}$, which is mentioned here because it may be helpful in understanding the algorithms, is the additive character:

$$\mathbf{M}(\xi_{1+2}) = \mathbf{M}(\xi_1) + \mathbf{M}(\xi_2) \tag{2.75}$$

assuming both experiments to be independent, with ξ indicating an experiment, $\mathbf{M}(\xi_1)$, the information matrix according to experiment 1, $M(\xi_2)$, the information matrix according to experiment 2 and $M(\xi_{1+2})$, the information matrix when the measurements of both experiments are regarded together (still being independent from each other).

More detailed mathematical information on the information matrix or the covariance matrix can also be found in textbooks such as Bandemer and Bellmann (1994).

In order to understand the experimental design criteria for parameter estimation, it can be very helpful to try to visualize the meaning of the covariance matrix of the parameters.

Assuming normally distributed measurement errors, the probability density function for a set of parameters $\boldsymbol{\theta}$ close to the estimated parameters $\hat{\boldsymbol{\theta}}$ can be formulated as

$$p(\boldsymbol{\theta}) = (2\pi)^{-r/2}(\det \mathbf{Cov}_{\hat{\theta}})^{-1/2} \exp\left(-\frac{1}{2}(\hat{\boldsymbol{\theta}} - \boldsymbol{\theta})^T \mathbf{Cov}_{\hat{\theta}}^{-1}(\hat{\boldsymbol{\theta}} - \boldsymbol{\theta})\right). \tag{2.76}$$

with r being the number of parameters. This probability density function is constant when

$$(\hat{\boldsymbol{\theta}} - \boldsymbol{\theta})^T \mathbf{Cov}_{\hat{\theta}}^{-1}(\hat{\boldsymbol{\theta}} - \boldsymbol{\theta}) = constant \tag{2.77}$$

This function 2.77 describes the surface of an r-dimensional ellipsoid with the parameter sets inside this ellipsoid all having a higher probability than the sets outside. For the simple case with only two parameters ($r = 2$), the ellipsoid becomes an ellipse which can easily be visualized as in figure 2.4.

The more accurate the parameter estimates are, the smaller this ellipsoid will be. Several criteria have been suggested which aim at minimizing different aspects of the size of the ellipsoid of which some will be mentioned here. More details can also be found in reviews and textbooks such as Atkinson (1982); Bandemer and Bellmann (1994); Walter and Pronzato (1990).

An often used criterion for parameter estimating experimental designs is to aim at the minimization of the expected volume inside the ellipsoid. Except for a constant factor, this volume equals $\sqrt{\det \mathbf{Cov}_{\hat{\theta}}}$. Experimental designs which aim at minimizing this are

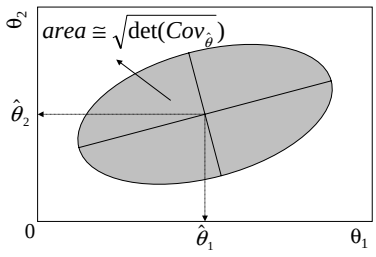

FIGURE 2.4.: Confidence ellipse of the parameter estimates for 2 parameters. The area inside the ellipse corresponds to the square root of the covariance matrix of the parameter estimates, which is used in a D-optimal design.

called D-optimal designs:

$$\xi^* = \arg\min_{\xi}(\det(\mathbf{Cov}_{\hat{\theta}})) = \arg\min_{\xi}(\frac{1}{\det(\mathbf{M}_{\hat{\theta}})}) \tag{2.78}$$

Besides this D-optimal design criterion, several other criteria have been suggested based on the covariance matrix of the parameters. A design is called A-optimal when the trace of the covariance matrix is minimized, which corresponds to the minimization of the average length of the axes of the ellipsoid:

$$\arg\min_{\xi}(trace(\mathbf{Cov}_{\hat{\theta}})) = \arg\min_{\xi}(trace(\mathbf{M}_{\hat{\theta}}^{-1})) \tag{2.79}$$

The E-optimal design on the other hand aims at the minimization of the largest axis of the ellipsoid by minimization of the largest eigenvalue of the covariance matrix $\lambda_{max}(\mathbf{Cov}_{\hat{\theta}})$:

$$\arg\min_{\xi}(\lambda_{max}(\mathbf{Cov}_{\hat{\theta}})) = \arg\min_{\xi}(\lambda_{max}(\mathbf{M}_{\hat{\theta}}^{-1})) \tag{2.80}$$

Munack (1989) suggested to minimize the ratio between the longest and the shortest axis of the ellipsoid: the modified E-criterion or the Λ optimality criterion:

$$\arg\min_{\xi}(\frac{\lambda_{max}(\mathbf{Cov}_{\hat{\theta}})}{\lambda_{min}(\mathbf{Cov}_{\hat{\theta}})}) = \arg\min_{\xi}(\frac{\lambda_{max}(\mathbf{M}_{\hat{\theta}}^{-1})}{\lambda_{min}(\mathbf{M}_{\hat{\theta}}^{-1})}) \tag{2.81}$$

This criterion was introduced, because an ellipsoid which is long in one direction means a set of parameter is not uniquely estimable, since a linear combination of the parameters will be accepted. Baltes et al. (1994) extended the Λ optimality criterion in an attempt to avoid extreme fast changing experimental conditions, which would deteriorate the

validity of the unstructured kinetic models. Berkholz wanted to avoid experiments which performed very poor as a production experiment and extended the Λ optimality criterion accordingly (Berkholz et al., 2000). The fact that the modified E-criterion regards the shape of the ellipsoid rather than the volume, can result in larger confidence intervals of the parameter estimates after the designed experiment than, for instance, using the D-optimal or E-optimal designs (Faller et al., 2003).

When the estimation of just one parameter or a certain set of parameters should be improved, the C-optimal design can be used, where the vector $\mathbf{c}$ is used to select and possibly weight the parameters.

$$\arg\min_{\xi}(\mathbf{c}^T(\mathbf{Cov}_{\hat{\theta}})\mathbf{c}) = \arg\min_{\xi}(\mathbf{c}^T(\mathbf{M}_{\hat{\theta}}^{-1})\mathbf{c}) \tag{2.82}$$

Besides the designs which use the covariance of the parameter directly, also design criteria have been suggested which regard the variance of the expected measured values of the new experiment (the model-variance, see also paragraph 2.5.1 and equation 2.57 on page 28), such as the G-optimality criterion which aims at minimizing the maximal expected variance of the expected measurements:

$$\arg\min_{\xi}\max(\mathbf{j}^T(\mathbf{Cov}_{\hat{\theta}})\mathbf{j}) \tag{2.83}$$

where $\mathbf{j}$ is a column vector of parameter sensitivities of the new measurement.

Lee (1987) suggested to combine several of the mentioned criteria, optimizing one criterion with the constraint of reaching a minimal quality with respect to another criterion.

For the current work the D-optimality criterion (equation 2.78) was chosen and implemented in the programs.

2.5.3. Experimental Design for Model Discrimination and Parameter Estimation

Experiments which are optimal for discrimination between competing models are not necessarily useful for the improvement of the parameter estimation and vice versa.

To reach the final useful model, both problems, model discrimination and parameter estimation, need to be solved. Both problems are interconnected: the model discriminating designs are based on model predictions which can be very inaccurate when the parameters are poorly estimated, but one model structure needs to be selected for the use of a parameter estimating design.

One option, which is also suggested in the current work, is to use two separate different design criteria and design each experiment for either of the two purposes. First a model needs to be selected using a discriminating design criterion and as soon as one model is selected, its parameter can be estimated better after following experiments which are

designed using a parameter estimation criterion (Chen and Asprey, 2003; Froment, 1975; Montepiedra and Yeh, 1998).

However, also some suggestions were made to use one criterion for the dual problem (Fedorov and Khabarov, 1986; Ford et al., 1989; Froment, 1975). Although they will not be explained in detail here, some are mentioned shortly. For instance, Hill et al. (1968) used a weighted combination of both criteria. Borth (1975) later published an entropy criterion adapted from the model discriminating criterion from Box and Hill. Spezzaferri (1988) used a multiplicative combination of two criteria and Pronzato (2000) suggested the use of a penalty function for poor parameter estimation in a model discriminating design criterion.

2.6. Optimization of Bioprocesses

Bioprocesses are optimized at different stages: strain development, development of the production process and optimization of the industrial plant, which are, however, closely interconnected (Roubos, 2002). Optimal process conditions, for instance, depend strongly on the used strain.

Using modern genetic techniques, strain improvement and improvement of process conditions and the medium are more and more parallel processes. In the current work, however, the used strain, the type of bioreactor and to a large extent also the used media are assumed to be selected already. Nevertheless, suggestions for strain improvement may very well come from identification of limitations during improvement of the process conditions or the medium using the techniques presented in the current work.

In order to optimize a process, first a performance function is needed. In industrial processes, this can be a rather complex function depending on many interconnected steps in the process (Yuan et al., 1997). Optimization of the biological reactions is usually of high importance. The overall yield of product on substrate, the total volumetric productivity, the purity of the product or the quality of a complex product are some of the common criteria to be optimized with respect to the biological process (Heinzle and Saner, 1991).

Two strategies of process optimization can be distinguished: model based optimization and empirical optimization. In the latter case, search techniques such as simplex methods, gradient searches, or genetic algorithms can be used with sequential experiments in order to improve the process. For instance, WeusterBotz et al. (1997) have used a genetic algorithm to optimize the trace element composition for cultivation of a *Corynebacterium glutamicum* strain. The review by Schügerl (2001) contains other examples of the use of empirical optimization strategies for optimization of bioprocesses.

For more complex processes with many control parameters, as is usually the case for optimization of trajectories in fed-batch processes, such search techniques may prove to get very laborious and converge slowly. When a proper process model is available,

the optimal settings of the control parameters can be calculated off-line without further experiments. In some relatively simple cases, this may be possible analytically. For more complex systems with many state variables and control parameters, this becomes complicated or even impossible, so numerical techniques have to be used.

The calculated optimal trajectories can then be applied in the process directly (feed-forward control), as is also done in the example by Lee et al. (1997) and in the current work in paragraph 5.2.6. Since the process model, the initial conditions and the controlled variables all include inaccuracies, it is, however much, better to include feedback control based on online measured values. This measured variable can be simply the variable which was intended to be controlled, such as the pH or temperature, or an online measurable substrate concentration. Or, if this variable is not measurable online, it may be possible to control a derived variable instead. Biomass growth can, for instance, be monitored by measurement of the oxygen consumption rate and carbon dioxide production rate (Golobic et al., 2000).

The availability of a model which can be used for model based optimization may also allow for the use of model based predictive control. Here, the prediction of the model is calculated regularly online and the optimal control is calculated, using this prediction, for a limited time. The basic concepts and an overview of model predictive control can be found in Garcia et al. (1989); Henson (1998). Preuss et al. (2000) applied model predictive control for the glucose feed for the growth of yeast in a fed-batch culture. Another example is the optimization of ethanol production by *Zymomonas mobilis* by Hodge and Karim (2002).

2.7. L-valine Production in Corynebacterium glutamicum

In the current project, the aim is to produce L-valine using a genetic modified strain of *C. glutamicum*.

The gram positive, nonmotile, non spore forming bacterium *C. glutamicum* is generally regarded as safe (GRAS). It has already been isolated in 1957 in a screening for L-glutamate producing bacteria in soil by Kinoshita and co-workers (Kinoshita et al., 1957) and it is nowadays widely used for the fermentative production of natural amino acids such as L-glutamic acid and L-lysine(Burkovski, 2003a; Hermann, 2003). Due to its industrial importance and its GRAS status, it has been investigated very intensively, which resulted amongst other things in the complete sequencing of its genome in several strains (Degussa, Kyowa Hakko Kogyo, BASF (Ikeda and Nakagawa, 2003; Kalinowski et al., 2003)). Besides the investigation of the genome, also the transcriptome[13] (Hayashi et al., 2002; Krömer et al., 2004; Muffler et al., 2002; Wendisch, 2003),

[13]The investigation of the transcriptome indicates the investigation of the gene expression.

proteome[14] (Hermann et al., 2001) and the metabolome[15] (Chassagnole et al., 2003; Drysch et al., 2003; Park et al., 1997; Sahm et al., 2000; Vallino and Stephanopoulos, 1993; Varela et al., 2003; Wittmann and Heinzle, 2001) are thoroughly investigated. This also resulted in the availability of many tools for genetic modifications of *C. glutamicum* (Nampoothiri and Pandey, 1998).

C. glutamicum needs biotin for growth, which was an important characteristic because the glutamate production was triggered by biotin limitation in wild-type strains (Shiio et al., 1962). Nowadays, with modern biotechnological techniques, also other growth limitations and other mechanisms are available to achieve overproduction of amino acids (Kimura, 2002), as is also the case in the organism which is used in the current study.

Another characteristic of *C. glutamicum*, which may be of importance for its use, is the complex cell envelope containing mycolic acids (Bayan et al., 2003; Christensen et al., 1999), which are typical for *Corynebacteriaceae*, *Mycobacteriaceae*, *Nocardiaceae* and a few small other families (Glazer and Nikaido, 1995). These mycolic acids form an extra hydrophobic barrier which probably causes the low permeability of the cell wall for hydrophilic compounds (Jarlier and Nikaido, 1990). Hydrophilic compounds therefore have to pass the cell wall through a channel (Costa-Riu et al., 2003a,b).

L-Valine is a natural proteinogenic amino acid and it is one of the essential amino acids for humans. Together with leucine and alanine, it forms the pyruvate family of amino acids. Furthermore, it is a branched chain amino acid just like leucine and isoleucine. It is a fairly hydrophobic ($log_p = 1.64$), neutral amino acid (pI=5.96), which makes it likely that it may be able to pass the cell membranes relatively good through passive diffusion (Krämer, 1994). The structure of L-valine is shown in figure 2.5.

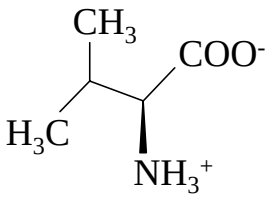

FIGURE 2.5.: L-Valine

The annual production of L-valine is about 1000 tons, which is among the smaller amounts for natural proteinogenic amino acids (Drauz et al., 2003; Eggeling et al., 2001; Leyval et al., 2003). It is mainly being used in infusion fluids and special dietary nutrition. However, also beneficial effects of addition of L-valine to pig- and chicken feed were reported (Boyd et al., 2000; Harms and Russell, 2001; Kidd et al., 2000).

L-Valine is currently being produced by isolation from protein hydrolysates, in fermentative processes or by enzymatic resolution of N-acetyl-D,L-valine

[14]The proteome indicates the proteins which are present in the cells.
[15]The intracellular concentration of metabolites: intermediates and products of metabolic pathways.

(Bodalo-Santoyo et al., 1999). The fermentative production of L-valine is performed using either α-aminobutyric acid-resistant mutants of *Serratia marcescens* or coryneform bacteria such as *Corynebacterium* or *Brevibacterium* (Drauz et al., 2003). *Brevibacterium* strains are actually nowadays regarded as a subspecies of *Corynebacterium*, since both organisms could not be distinguished at the rRNA level (Liebl et al., 1991). Besides these two groups of bacteria, also several other L-valine accumulating micro-organisms have been reported (Chatterjee and Chatterjee, 1982; Chattopadhyay and Banerjee, 1978; Mandal and Majumdar, 1973). The fermentative production of up to 10 g/L L-valine by *C. glutamicum* was already published in the sixties (Nakayama et al., 1961) and already in 1977, almost 40 g/L was reported, produced by a *Brevibacterium lactofermentum* using limited oxygen supply (Akashi et al., 1977). *Brevibacterium lactofermentum* AJ12341 is reported to produce 39 g/L L-valine at 28 % yield (Drauz et al., 2003).

Although the total yearly production volume is not very large, it is expected to grow steadily (Hermann, 2003) and there is a strong interest in further improvement of the fermentative production processes, as is also illustrated by the European research project VALPAN: 'construction of *C. glutamicum* strains producing either L-valine or D-pantothenic acid - a rational approach using genome research', which took place from February 2001 until March 2004 (Puhler and Tauch, 2003). The strain which is used in the current work, was also used in the VALPAN project.

In the natural production of L-valine, two molecules of pyruvate are used to produce one molecule L-valine. This metabolic pathway is described in more detail in paragraph 5.1.1 on page 87, where also the genetic modifications of the used strain are mentioned.

3. Dynamic Modeling Framework

In this chapter, some remarks are made on the developed and used programs for modeling of dynamic processes using special experimental design techniques. The programming was done in Matlab, using Simulink for dynamic simulations. Most programs were written as functions. Their use and the ideas behind them are explained here and in more detail in the documentation in the program code.

3.1. The Modeling Procedure

A schematic flowsheet of the suggested modeling procedure with experimental designs is shown in figure 3.1.

Since we need the parameter estimates and their accuracies in order to use the experimental design techniques, the first data are taken from intuitively planned preliminary experiments. A first set of simple models is based on these data and available information on the biological system and the model parameters of these models are estimated by fitting the models to the data from these intuitively planned experiments. Enough data have to be gathered and the used models have to be relatively simple, so all model parameters can be estimated.

After this initialization, the model based approach is started. First, an iterative approach for model discrimination using experimental designs is performed, resulting in one selected model. The parameters of this selected model may still be partly poorly estimable from the available data. In a subsequent iterative process, the parameter estimation can then be improved, using special experimental designs for this purpose. The resulting model can be used for optimization and control of the final process.

The different steps in the modeling procedure are explained in more detail in the following paragraphs.

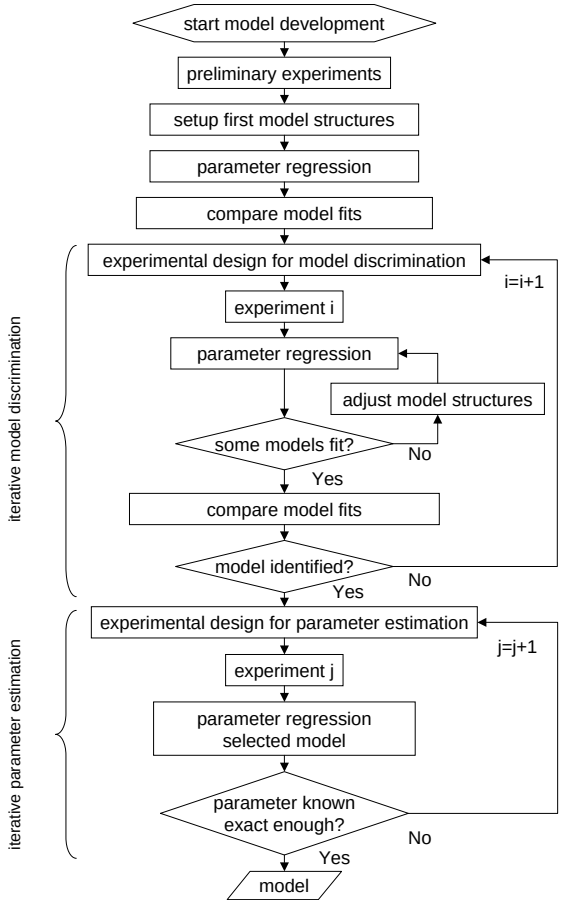

FIGURE 3.1.: Schematic flowsheet of the modeling procedure using experimental design techniques.

3.2. Parameter Estimation

After each experiment, be it intuitively planned or designed for model discrimination or parameter estimation, the parameters of the models are re-estimated using all available (prior and new) data.

It turned out to be very important to limit the allowed parameter space as much as possible, especially when the models are large and nonlinear. Many of the parameters in the kinetic models are directly correlated to characteristic values which are calculable from measured values, such as the yields and the specific rates of growth, consumption and production. With the calculated values from available measured data, tight bounds on parameters can be set.

Within this limited parameter space, the parameters are estimated by a non-linear least squares technique using the maximum likelihood criterion explained in paragraph 2.4.1 on page 17.

The standard deviation of the measurements are calculated in the same way as suggested by Wiechert (Takors et al., 1997; Wiechert, 1990):

$$\sigma_y = y \cdot \sigma_{y,rel,min} \cdot \left(1 + \frac{1}{(\frac{y}{lb_y})^2 + \frac{y}{lb_y}} \right) \tag{3.1}$$

using a constant minimal relative error of $\sigma_{y,rel,min}$ and an increasing relative error at decreasing measured values y due to the introduced lower accuracy bound on the measurement, lb_y.

First a global minimization within the allowed parameter space is performed using a genetic algorithm[1]. The resulting set of parameters is then optimized further locally using a bounded nonlinear least squares routine[2].

The used genetic algorithm also allows (but does not necessarily need) the suggestion of parameter values by the user, which may save a lot of calculation time before reaching convergence. The user supplied suggestion can for instance be the set of parameter values which was estimated before, based on prior data in the prior iterative loop. The differential evolution program which is used for optimization of design parameters (see paragraphs 3.3.1 and 3.3.2 on page 49) does not foresee this user supplied initial guess and is therefore not used here. With slight adjustments, the parameter estimation program has also been used without the global search or with re-estimation of only a selection of the parameters.

[1] The used freeware Matlab algorithm is implemented by and available from MathWorks (www.mathworks.com) and based on the algorithm described by Goldberg (1989).

[2] The function lsqnonlin, taken from the Matlab optimization toolbox, uses an algorithm which is based on Coleman and Li (1996).

3.3. Designing Experiments

3.3.1. Model Discriminating Design

Five model discriminating design criteria, adjusted for the dynamic multivariable experiments, were implemented in the Matlab programs. See also paragraph 2.5.1 on page 26 for more information on the used criteria. The criterion by **Box and Hill** (equation 2.61 on page 30) was implemented using a summation over all measured variables and all time points, assuming all measurements to be independent. The criterion by **Buzzi-Ferraris and Forzatti** (equation 2.62) was used with the matrix of model variances including covariances, but independent measurements with respect to the measurement variance matrix, which therefore contained non-zero values only in its diagonal. The criterion by **Chen and Asprey** (equation 2.64 on page 31) was adapted for the use with more than two models by a summation over all model pairs, although it was originally used only for the two closest competitors among the models. Besides these three design criteria which use the model variance, two criteria were implemented without this variance of the model prediction. First the criterion by **Hunter and Reiner**, weighted by the expected measurement variances (equation 2.53 on page 27) was implemented, assuming all measurements to be independent. Finally, also a similar criterion was used, but with the use of a time dependent measurement variance and including an extension regarding the shape of the curve, as shown in equation 2.71 on page 36.

These five criteria were all used in a simulative study, as mentioned in chapter 4 on page 61, and two of them have been applied during the process development of the L-valine production process. The first model discriminating design during this process development (paragraph 5.2.3 on page 104) was realized using the adjusted Box and Hill criterion and the second model discriminating design (paragraph 5.2.5 on page 113) was proposed using the criterion without the model variance with the extensions mentioned above.

The design parameters for a new experiment (see paragraph 3.4.1 on page 50) are first searched for in a bounded parameter space using the global optimization algorithm 'differential evolution'[3], which is thought to be more efficient than the genetic algorithm used for parameter estimation. After the global search, the parameters are further optimized locally using a simplex algorithm[4], starting from the results of the global optimization. Since the used simplex algorithm works in an unlimited parameter space, the parameters are converted from the limited to the unlimited space by

$$\theta_{unlim} = 0.5 \ln \left(\frac{\theta_{lim} - lb_\theta}{ub_\theta - \theta_{lim}} \right) \tag{3.2}$$

[3]This freeware function was programmed by Rainer Storn and more information is available at www.icsi.berkeley.edu/ storn/code.html.

[4]The function 'fminsearch' from the Matlab optimization toolbox was used

and back by

$$\theta_{lim} = lb_\theta + (ub_\theta - lb_\theta)\left(\frac{e^{\theta_{unlim}}}{e^{\theta_{unlim}} + e^{-\theta_{unlim}}}\right), \tag{3.3}$$

where the real parameter θ_{lim}, being limited between lower bound lb_θ and upper bound ub_θ, is projected to the unlimited parameter value θ_{unlim}.

The fitted models are evaluated by visually judging the plots of the concentrations over time and the scaled residuals (the difference between measured- and simulated values, weighted by the standard deviation of the measured values) over time. Furthermore, the models are evaluated by calculating reduced chi squared values, as described in paragraph 2.4.3 on page 19.

Especially during the initial phase of the model development, the available data might not be enough to describe all important features of the process properly, resulting in oversimplified models. Therefore, it is not unlikely that none of these models fit satisfactory after a new designed experiment. In such a case, the model structures need to be adjusted.

The model discrimination procedure is iterative. If several of the resulting models fit satisfactory, a new model discriminating experiment can be designed. When only one model is accepted, or when the remaining models do not predict significantly different results in the relevant range, the model discrimination is stopped. If needed, additional experiments can then be planned in order to improve the parameter estimates of the selected model.

3.3.2. Design for Parameter Estimation

The implemented design criterion for designing experiments to improve the estimation of the model parameters, is the D-optimality criterion, which is explained in paragraph 2.5.2 on page 36.

The optimization of the design parameters for the new experiment (see paragraph 3.4.1) is performed similar to the model discriminating design as described in the previous paragraph. First a global optimization is performed in a bounded parameter space using the differential evolution algorithm, followed by local optimization using a simplex algorithm starting from the values supplied by the global search.

Also the parameter estimating experimental design strategy is iterative. After each experiment, the model parameters are re-estimated and the parameter estimation is evaluated. This evaluation is done by calculating the covariance matrix of the parameter as described in paragraph 2.4.2 on page 18. The square root of the diagonal of this covariance matrix, e.g. the standard deviations of the parameter estimates, is compared to the estimated parameter values. Furthermore, a correlation matrix is calculated from the covariance matrix according to equation 2.33 on page 19, in order to see whether the model parameters are strongly correlated.

3.3.3. Design an Optimized Production Process

The offline calculation of an optimized production process can be performed very similar to the calculation of experiments which are optimized for model discrimination or parameter estimation, instead of production.

In the current work, the total volumetric productivity was used as a criterion to be maximized in the optimal production process. This criterion is also mentioned in paragraph 3.4.3 on page 59.

Again, a local optimization by a simplex algorithm is performed, starting from the results of a bounded global search using the differential evolution algorithm.

3.4. Application: L-Valine Production Process Development

Several details of the presented modeling procedure are specific for the modeled process and the constraints on the system. In the current section, some remarks are made considering the application of the experimental design techniques for modeling and optimization of the L-valine production by *C. glutamicum*. First of all, the description of the designed experiments and its constraints are listed. Furthermore, some remarks are made on the use of the actual measured data in the modeling procedure.

3.4.1. Designed Experiments

A designed fed-batch experiment will normally consist of parameters which describe the initial conditions and the time-variant feedrates. Furthermore, user-supplied limits on the parameter values and constraints on the course of the fermentation can be involved. For very small scale or with special equipment where the number of samples which can be taken is limited, also the measurement time points may be optimized.

For modeling of the L-valine production process, the experiments were planned using the following constraints:

- The maximal fermentation time was fixed to 48 hours. This was expected to be sufficient and practicable. The proposed experiments do not necessarily have to last the complete 48 hours. If better discriminating information would be expected with shorter experiments, because of practical limitations on the experiments stated underneath, these shorter experiments will be proposed. The optimized production experiments in paragraph 5.2.6 on page 117 and appendix G on page 173 were, for instance, shorter than the maximal allowed time. Also when final planned experiments use the maximal duration, the way of dealing with this is still important during in the optimization procedure.

- The feed was described as periods of 6 hours duration with a constant feed rate.

The feed trajectory described this way was easily performed with the used equipment by manual adjustment of the feed rates.

- The feed rates were planned between the bounds of 0 to 0.1 L/h. This maximal value lies well within the range which is possible using the Dosimat system mentioned in paragraph 5.1.3 on page 95, with a 5 mL burette. In the second model discriminating experiment (see paragraph 5.2.5) and the production experiment (paragraph 5.2.6 on page 116), the minimal feed of glucose was 0.003 L/h, which is the minimal pumping rate of the used system, so that this Dosimat did not need to be shut down any more. This limit was not used for the other two feeds or in the other experiments. Designed feed rates which are below the minimal pumping rate in these situations, were rounded mathematically so either no feed or the minimal rate was used. Some rounding of the designed rates was also needed for higher feed rates. This rounding did not change the expected results significantly.

- No feed was used in the first 6 hours of the fermentation. This also has a practical reason because it allows the user to time the start of the feed profiles better. The profile is started at the suggested initial cell density, but inoculated with a little less. Depending on the real initial cell density and possibly also a lag-time, the user can adjust the timing of the feed.

- The initial cell density was fixed to an OD_{600} of 1. In the practical performance of the fermentation, the bioreactor is inoculated with a slightly smaller amount of cells and the timing of the designed experiment is then started when an OD_{600} of 1 is reached, as was also mentioned above. Note that the designed experiment has a fixed initial biomass density of OD_{600} 1, but during later fitting of the models to the new data from the experiment, the real measured data are used, with the lower initial biomass concentration, delayed start of the feeds, and so on.

- The initial concentration of glucose was designed within the bounds of 15 to 50 g/L (83 to 278 mM) .

- The initial concentrations of L-isoleucine and pantothenic acid were designed between the bounds of 0.5 to 5 mM of L-isoleucine and 0.5 to 5 μM pantothenic acid. In the first model discriminating design (see paragraph 5.2.3 on page 104), the ratio between the two compounds was fixed to 1.1 mM : 1 μM. In the optimized production experiment, the maximal initial concentration of L-isoleucine and pantothenic acid were increased to 10 mM and 10 μM respectively.

- The expected concentration of glucose was limited within $1 \cdot 10^{-6}$ to 278 mM at all sampling times for model discriminating experiment I. For the planning of later experiments (model discriminating experiment II and the optimized production experiment, the lower bound was increased to 0.56 mM. Effects which occur

during and after starvation are not expected to be beneficial and the models do not need to describe these processes properly, which is why the lower limit on the glucose concentration is used. The upper bound on the glucose concentration was included because in preliminary experiments, a strong indication of growth inhibition by higher glucose concentrations was found (data not shown).

As soon as the predicted glucose concentration at a measured point is outside these bounds according to any of the competing models, this measurement and all following measurements are discarded before calculating the criterion. This is only checked at the measured points. In the used criteria, all points are discarded after the first time any of the models predicts values outside the bounds. When using more than 2 competing models, it could also be evaluated for each set of 2 models. All designed experiments in the L-valine production process development (except for the optimized production experiment) had the user supplied maximal allowed duration. Apparently, the problems of too high or too low concentrations could be avoided.

- The initial volume in the bioreactor was fixed. The used starting volumes were 2.0 L for the initial batch, 1.85 L in model discriminating experiment I, 1.75 L in the intuitively planned experiment for discrimination between L-isoleucine and pantothenic acid and model discriminating experiment II and 1.65 L in the optimized production experiment. The initial volume consists of a fixed volume of 50 mL for the inoculum and the remaining volume of fresh production medium.

- The sampling times were fixed to be every 1.5 hours with some pre-chosen longer breaks. Also because of obvious practical reasons, the times at which the feed rates are changed, coincide with the measurement times. When needed to avoid too small a suspension volume, samples can be skipped in the designed experiments as is also explained at the next point.

- The volume in the bioreactor is simulated using the fixed initial volume, the suggested feedrates and fixed sampling volumes of 25 mL per sample, including the sample itself and the flushing of the sampling port (see also paragraph 3.4.2 on page 54). The volume is limited between 1.5 and 2.1 liter, which are practical limitations of the used bioreactor. As soon as the simulated volume exceeds the allowed upper bound, the experiment is stopped, so this and all following measurements are discarded before calculating the criterion. When the expected volume becomes too small, on the other hand, the samples which cause the volume to drop below its lower bound are not taken, which allows following samples still to be taken when the volume at that time is high enough. Again, the way these bounds are implemented was of importance during the optimization, but for the final experiments with the L-valine production system, the optimization routine found experimental designs which avoided these problems.

- Retrospective, the calculation of the volume during the performed experiments also includes the measured addition of ammonia for pH control. This is however not part of the experimental design. Based on prior experiments, an attempt was made to estimate the needed addition of ammonia and its effect on the volume and therewith on the concentrations and dilution rates, also in the experimental design. For model discriminating experiment I, the expected ammonia addition was estimated as the expected growth rate multiplied by $2.95 \cdot 10^{-4}$, based mainly on data of the preliminary batch experiment. For the second model discriminating experiment and the optimized production experiment, the ammonia addition was estimated as the expected glucose uptake rate multiplied by $1.67 \cdot 10^{-3}$. The compensation was of limited importance for the L-valine production process, where the total addition of ammonia was always less than about 6% m/m over the entire experiments.

  This assumption and simplification of the needed amount of ammonia was based on data from prior experiments. It seems likely that the needed amount of base is correlated directly to the use of glucose and/or the growth or production rates. The mentioned simple correlation was found to be very satisfactory for this purpose. This correlation may also be very useful for online process monitoring and control, since the needed addition of ammonia is a variable which is easily accessible by on-line measurement.

- During the design of the second model discriminating experiment and the production experiment, some compensation was used for the density differences between the feeds and the culture suspension. The density of the broth was taken to be 1.03 kg/L as measured at the end of several experiments. The density of the glucose feed was assumed to be 1.10 and of the isoleucine feed and the pantothenic acid feed 1.003 and 1.000 respectively.

  Since the mass has to be balanced, the loss of mass through the gas phase is also of interest. Retrospective, this is calculated using the measured concentrations of O_2 and CO_2 in the outgoing gas flow (see also paragraph 3.4.2 on the following page). In an attempt to include this also already in the design of the experiments, the used density of the glucose feed was with 1.10 kg/L somewhat lower than its theoretical density of 1.17 kg/L[5].

  The density differences were accounted for by using slightly adjusted feed concentrations during the design and feed with slightly adjusted feed rates. For instance:

[5] From a theoretical point of view, it would be better to include the production of CO_2 in the models, which would however dramatically increase the complexity of the models and the amount of model parameters. Also coupling of the CO_2 production to the glucose uptake instead of the glucose feed makes more sense. The advantage of the chosen coupling to the feed rate is the fact that the volume of the suspension can now be calculated independent of the kinetic models, therewith saving calculation time during the optimization of the experimental design.

the concentration of the glucose feed was 500 g/L but the design is made, assuming it to be $\frac{1.03}{1.10} * 500 = 468\ g/L$. The actually used feed rate compensates for this by using a slightly adjusted rate in such a way that the same amount of glucose is added as in the simulation. So in this case the feed rate is calculated as $used\ feedrate = \frac{1.03}{1.10} * designed\ feedrate$.

These compensations resulted in adjustment of the feed rates with at the most 6.8% in the L-valine process.

The designed experiment in the first case of the simulative study of chapter 4 on page 61 was designed using similar constraints and a similar description of the fed-batch experiments.

3.4.2. Preparation of Measured Data

After each experiment, the actual measured values and actual performed feed rates need to be prepared for use in the Matlab programs. The measured values of the concentrations of biomass, glucose and L-valine were used as they were measured, without further smoothing. Besides these direct measured values, also the dilution rates were used as input data in the dynamic models.

For calculation of the dilution rates, the volume in the bioreactor needs to be known or estimated. A mass balance of the content of the bioreactor is used for this:

$$M_r(t) = V(t) * \delta_r = V(0) * \delta_r + \sum_f \int_{t=0}^{t} \frac{\mathbf{d}M}{\mathbf{d}t}_f \mathbf{d}t \tag{3.4}$$

The density δ_r of the reactor content was assumed to be constant, measured at the end of the experiments and found to be about 1.03 kg/L. All mass flows into and out of the reactor are depicted together as $\sum_f \int_{t=0}^{t} \frac{\mathbf{d}M}{\mathbf{d}t}_f \mathbf{d}t$ and consist of the feeds of medium compounds and regulating substances (NH_3), the flow of samples out of the reactor and loss of mass through the aeration.

The used feeds of **glucose**, **isoleucine** and **pantothenic acid** are set and controlled during the experiment. The change of mass by these feeds are calculated for instance for the glucose feed as

$$\frac{\mathbf{d}M}{\mathbf{d}t}_{glcfeed} = F_{glcfeed} * \delta_{glcfeed} \tag{3.5}$$

Note that the densities of the feeds, such as $\delta_{glcfeed}$ are usually different from the density in the reactor δ_r and from each other. For the current project, the glucose feed contained 500 g/L glucose, which is known to have a density of about 1.17 kg/L (at room temperature and 1 atm.). The densities of the isoleucine feed and the feed of pantothenic acid were assumed to be 1.003 and 1.000 kg/L respectively.

The addition of **ammonia** for pH control was measured over time by placing the supply flask on a balance. From the online logged data from this balance, the rate of the addition of mass into the reactor can be calculated straightforward.

The loss of volume by **sampling** was measured by measuring the volume withdrawn during flushing of the sampling port and the sample itself, using a small measurement cylinder. Again, the assumed constant density of the culture broth of 1.03 kg/L was used to convert this loss of volume to a loss of mass.

Regarding the loss of mass through the **gas phase**, only the loss by CO_2 production and O_2 consumption was regarded, which can be calculated from:

$$\frac{\mathbf{d}M}{\mathbf{d}t}_{CO_2} = \big((F_{g,out} * ([CO_2]_{out} + [O_2]_{out}) - (F_{g,in} * ([CO_2]_{in} + [O_2]_{in})\big) * MV_g \quad (3.6)$$

where the subscripts $_{out}$ and $_{in}$ indicate the outgoing and incoming flows respectively. The incoming gas flow $F_{g,in}$ is set and controlled by a mass-flow controller and the incoming concentrations of CO_2 and O_2 in the air are taken to be 0.033% v/v and 20.9% v/v respectively. The outgoing concentrations of CO_2 and O_2 are measured (see paragraph 5.1.4 on page 97) and logged online. The molar volume of the gas MV_g is taken to be 24.0 $L.mol^{-1}$ for ideal gas at room temperature.

Due to the production or consumption of gaseous components, the incoming and outgoing gas flows are not necessarily equal. Assuming that O_2 and CO_2 are the only gaseous compounds which were consumed or produced in significant amounts, a balance over the remaining gas (mainly over N_2) allows the estimation of the outgoing gas flow according to[6]:

$$F_{g,out} = F_{g,in} * \frac{100 - [CO_2]_{in} - [O_2]_{in}}{100 - [CO_2]_{out} - [O_2]_{out}} \quad (3.7)$$

This way the volume and mass in the reactor are estimated over time using the set flow rates and measured concentrations of CO_2 and O_2, the weight of the NH_3 supply and the estimated loss of mass by sampling. The dilution rates are then calculated from the feed rates and the estimated volume on a mass basis:

$$D_{feed}(t) = \frac{\frac{dM}{dt}_{feed}(t)}{M_r(t)} \quad (3.8)$$

The dilution rates by feed of glucose, L-isoleucine, pantothenic acid and by addition of ammonia during the course of the experiment were used as input in the Simulink models for estimation of model parameters. In the models, the data between saved points were interpolated. At least all points just before and after each sample and directly before and after each manual change in a feed rate were supplied as input in the models.

[6] which is easily understood, when we realize that $F_{N_2,in} = F_{N_2,out}$ and thus $F_{g,in} * (100 - [CO_2]_{in} - [O_2]_{in}) = F_{g,out} * (100 - [CO_2]_{out} - [O_2]_{out})$.

For design of experiments, the dilution rates are estimated in a similar way, based on the suggested feed rates. However, the addition of NH_3 and the loss of mass through sampling and CO_2 in the gas flow, are not yet available as measured values during the calculation of the design. See also paragraph 3.4.1.

3.4.3. Calculation of other Characteristic Values

It can be crucial for proper estimation of the model parameters to limit the parameter space in which the parameters are sought. In the used mechanistic type of models, several parameters can be directly coupled to certain characteristic values such as yields and specific rates. Therefore, these values are calculated from the measured data before the parameter estimation of the models is performed and several parameter bounds are set accordingly.

Besides the bounds on the parameter values, the characteristics which are mentioned here can also be very helpful in suggesting mechanisms and corresponding model structures. As a trivial example: when the specific growth rate declines at higher product concentrations, this could be explained by growth inhibition by the product.

The characteristic values were calculated from measured data of biomass, glucose, L-valine, L-isoleucine and CO_2. The third substrate, pantothenic acid, was not included since its concentrations were not measurable and also for L-isoleucine the measured concentrations were only available during parts of the fermentations, as long as concentrations were high enough[7].

The calculation of some characteristic values is addressed in the following paragraphs in more detail.

Rates

The growth rate and the rates of product formation and substrate uptake were calculated from the measured values of OD_{600} and the concentrations of L-valine and glucose respectively. Since the rates calculated this way are very sensitive to measurement errors, the measured values were first smoothed. The smoothing was performed by a spline, resulting in the same amount of measurements at the same time points as the raw measured values.

The rates were calculated as average rates between two measured points[8]. Dealing with dynamic experiments, we must compensate for the dilution and addition by feeds in order to obtain the conversion rates by the organism, which we are interested in. For

[7] Regarding the required dilution of at least 50 times as mentioned in appendix D on page 151, concentrations below about 0.5 mM cannot be measured properly.

[8] i.e. assuming a constant rate between two time points. For biomass growth, one might consider assuming exponential growth between two points instead. These two ways of calculation are identical for infinitely small time between two measurements.

instance, the glucose ($S1$) uptake rate r_{S1} in the period between the measured time points $t1$ and $t2$, can be calculated as:

$$r_{S1}(t_{avg}) = \frac{C_{S1}(t1) - C_{S1}(t2) + \sum_f \int_{t=t1}^{t2} (D_f(t) \cdot (C_{S1}(t) - C_{S1f}))\, dt}{t2 - t1} \tag{3.9}$$

where t_{avg} is the average of measurement times $t1$ and $t2$. Besides the change in the glucose concentration C_{S1}, the effect of the feeds f is compensated for by including the dilution $D_f(t)$ between the two measured points. The concentration C_{S1f} in the feeds is 0 for all feeds except for the glucose feed in this case, which contained 500 g/L glucose during development of the L-valine production process.

Having only measured glucose concentrations at the timepoints $t1$ and $t2$ and not between them, the integral of the dilution effects over the time period between two (off-line) measured points was calculated using a constant glucose concentration between two measurements, calculated as the average of the two measured values, so we can write:

$$\int_{t=t1}^{t2} (D_f(t) \cdot (C_{S1}(t) - C_{S1f}))\, dt \simeq Di_f(t1 : t2) \cdot \left(\frac{C_{S1}(t1) + C_{S1}(t2)}{2} - C_{S1f} \right) \tag{3.10}$$

Where $Di_f(t1 : t2)$ denotes the integral dilution by feed f between the two measurement timepoints $t1$ and $t2$ (so as $[g.g^{-1}.period^{-1}]$, whereas the dilution D_f is a momentary rate in $[g.g^{-1}.h^{-1}]$). This integral dilution was estimated first between each pair of subsequential *on-line* logged time points, followed by a summation of the values over the period of interest. So with $n + 1$ logged time points in the period between $t1$ and $t2$, which form n small time periods tp, the dilution $Di_f(t1 : t2)$ can be estimated using

$$Di_f(t1 : t2) \simeq \sum_{tp=1}^{n} D_f(tp) \cdot \Delta t(tp). \tag{3.11}$$

The dilution D_f can be calculated over each short time period tp according to equation 3.8. This momentary rate is multiplied by the duration $\Delta t(tp)$ of the period tp to yield the integral dilution over the short period. This duration of the small periods between 2 online logged points was about 5 minutes in the used system.

Using equation 3.9 to 3.11, the substrate uptake rate can be calculated between all measured points from measured and known data. The rates of biomass growth and product formation were calculated in an analogous way.

Specific Rates

The biomass specific rates, or simply the specific rates, are the rates per amount of biomass. These are calculated by dividing the rates by the estimated biomass concentration at that time. Again the biomass concentration was estimated as the average between two

subsequent measured concentrations. So the specific glucose uptake rate σ_{S1} between time point $t1$ and $t2$ is for instance calculated as

$$\sigma_{S1}(t_{avg}) = \frac{r_{S1}(t_{avg})}{C_X(t_{avg})} = \frac{r_{S1}(t_{avg})}{(C_X(t1) + C_X(t2))/2} \tag{3.12}$$

Again, the measured values were smoothed by a spline before use. The specific growth rate μ and the specific L-valine production rate π are calculated in an analogous manner.

Yields

The yields of biomass on glucose and L-valine on glucose were calculated over each period between two measured points from the changes in concentrations and the feed fluxes over these periods. This corresponds to the calculation by regarding the rates of production and substrate uptake, so for instance for the yield of biomass on glucose, Y_{xs1}, over the period between $t1$ and $t2$:

$$Y_{xs1}(t_{avg}) = \frac{r_X(t_{avg})}{r_{S1}(t_{avg})} \tag{3.13}$$

with the rates calculated according to equation 3.9, although, of course, the division by the time is not necessary.

C-Balance

All products which are produced in substantial amounts give insight in the possible intracellular mechanisms and potential rate controlling steps. Elemental balances can be very useful to check whether all substantial products are detected and to check whether the relative production rates of the different (by-)products change in different situations.

Here, the amount of carbon is balanced over the whole bioreactor content and the conversions inside the bioreactor are regarded in an integral carbon-balance.

Since the carbon itself is not converted, the amount of carbon in the reactor is balanced using only the initial conditions and the fluxes into and out of the bioreactor as $accumulation = flux_{in} - flux_{out}$:

$$\begin{aligned} &\textstyle\sum_s \big(C_{cs}(t)V_r(t) - C_{cs}(0)V_0(t)\big) + \sum_p \big(C_{cp}(t)V_r(t) - C_{cp}(0)V_0(t)\big) = \\ &\textstyle\sum_f \int_{t=0}^{t} F_f(t)C_{cf}dt - \sum_m V_m C_{cm} - \int_{t=0}^{t} \big((F_{g,out}(t)[CO_2]_{out}(t)) - (F_{g,in}(t)[CO_2]_{in}(t))dt\big), \end{aligned} \tag{3.14}$$

using a summation over s substrates and p products with carbon concentration $C_{cs}(t)$ and $C_{cp}(t)$ respectively, in the reactor content with volume $V_r(t)$ at time t. For the L-valine production system, the substrates glucose and L-isoleucine were regarded and the regarded products included biomass, L-valine and other measured amino acids and organic acids as mentioned in paragraph 5.1.4 on page 99. Pantothenic acid could not be measured and would not contribute significantly due to its low concentrations. The sum

over f feeds include the feeds of glucose and of L-isoleucine with their known constant carbon concentrations C_{cf}. The amount of carbon which is removed from the system by sampling, is included as the sum over all m measurements until time t with sample volume V_m and carbon concentrations C_{cm}. This concentration is estimated from the concentrations of all measured compounds. The total amount of produced CO_2 is included as an integral over time and has also been addressed partly in paragraph 3.4.2 on page 54. Note that all concentrations in equation 3.14 are carbon concentrations, so in $[C - mole.L^{-1}]$, which can readily be calculated from measured concentrations and elemental composition of the compounds. This stoichiometry is simply known for all regarded compounds except for the biomass. For the biomass, the measured concentrations as OD_{600} are converted to biomass dry weight by multiplication with 0.25, according to the measurements of both characteristics as mentioned in appendix B on page 139. The amount of carbon per gram dry biomass is assumed to be 0.5 g/g, taken from the values measured for a similar strain of *C. glutamicum* by Kelle (1996).

When all relevant products would be accounted for, equation 3.14 should hold. When important products are unknown, the fraction $C - bal$ of the carbon balance which is accounted for, is calculated by rewriting the equation:

$$C - bal = \frac{\int_{t=0}^{t}((F_{g,out}(t)[CO_2]_{out}(t)) - (F_{g,in}(t)[CO_2]_{in}(t))dt) + \sum_p C_{cp}(t)V_r(t)}{-\sum_s C_{cs}(t)V_r(t) + \sum_i C_{ci}(0)V(0) + \sum_f \int_{t=0}^{t} F_f(t)C_{cf}dt - \sum_m V_m C_{cm}}. \tag{3.15}$$

Besides the degree to which the total carbon balance is closed, also the fractions of the carbon fluxes into the different products is of interest. These values can be calculated analogue to equation 3.15, after omitting all other products from the enumerator.

Total Volumetric Productivity

The total volumetric productivity is used as the optimization criterion for process optimization of the L-valine production process. This characteristic value is also sometimes called the space-time-yield and it consists of the amount of product which can be produced per unit volume of suspension and time, calculated over the total process time.

Here, it is calculated as the increase in concentration of L-valine from the start of the experiment up to each time-point, divided by the time:

$$TVP(t) = \frac{(C_{val}(t) - C_{val}(0))}{t}. \tag{3.16}$$

In the optimization of the process, the time-dependent total volumetric productivity $TVP(t)$, is calculated for each measurement time point and the highest value is taken. The optimized process is stopped at the corresponding time-point.

4. Simulative Comparison of Model Discriminating Design Criteria

In the simulative study, presented in the current chapter, several different model discriminating design criteria are compared using the programs mentioned in chapter 3. The five compared criteria were adapted for use with dynamic multivariable experiments and are based on the criteria of Box and Hill (BH), Buzzi-Ferraris and Forzatti (BF), Chen and Asprey (CA), Hunter and Reiner (HR), and a **n**ew criterion for **d**ynamic systems without use of model variances (ND). The criteria are explained in more detail in paragraph 2.5.1 on page 26.

4.1. Setup

The general setup of the simulative study is shown in figure 4.1.

The initial situation of the study consists of one or more suggested experiments and corresponding simulated data to which several models are fitted. All competing models fit properly to the data at this stage. The relative goodness of fit of the competing models in this initial situation is calculated for use in the design criteria BH and ND.

At this point, an experiment is designed to discriminate between the competing models, according to each of the five different model discriminating design criteria.

Then, data are generated by simulation of these planned experiments using one of the competing models. In order to account for the fact that the model parameters might not be correct, which is addressed in the criteria using the model variance, several alternative sets of model parameters are generated by adding normally distributed white noise to the original preliminary data and re-estimation of the model parameters using this alternative set of initial data. These alternative sets of model parameters are used to generate several sets of measured data with the designed experiment. To all sets of data, several sets of white noise are added, resulting in a larger series of data sets. In the current study, 10 sets of alternative model parameters are used for the generation of data and to each of these data sets, 10 sets of white noise are added, yielding 100 sets of data for re-estimation of the model parameters and comparison of the posterior models.

All competing models are fitted to each new data set, also including the prior data. The reduced chi-squared values are then calculated as described in paragraph 2.4.3 on page 19.

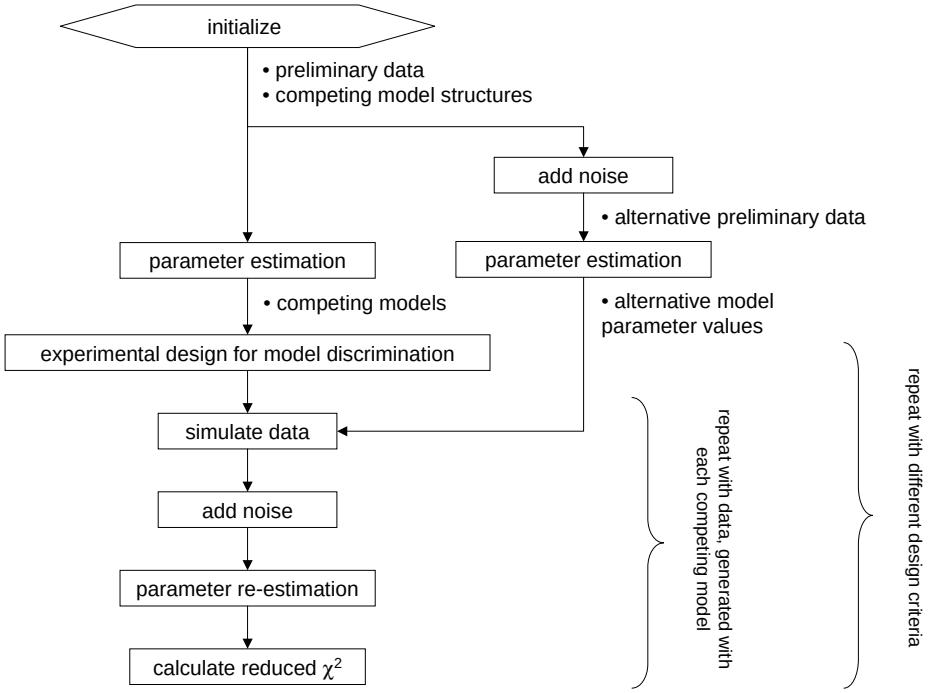

FIGURE 4.1.: General description of the simulative study to compare model discriminating design criteria

The model structure which is used for generating the data, should fit very well to the data, resulting in a reduced chi-squared value of about one[1]. The ratio between the reduced chi-squared value of the competing models and the 'true' model is taken as a measure of the performance of the discriminating criteria. The higher the values for the competing 'not true' models are, the better the models were detected as the 'false' model, e.g. the better the discriminating experiment performed.

The procedure was performed with each of the competing models as the 'true' model

[1]The fitted model can even get closer to the measured values than would be expected based on the measurement variance, which would lead to values below one. On the other hand, the extra variance in the measurements which is introduced here by the alternative sets of model parameters can lead to a worse fit and corresponding values of more than one.

which is used for generating the data.

The study was performed with two different simulative examples, which are mentioned in more detail in the following two sections. From a model discrimination point of view, a major difference between the two examples lies in the fact that the preliminary data only allow poor parameter estimation in the first example, whereas in the second example, a more satisfactory parameter estimation is already possible at that stage.

4.2. First Case: Fermentation

The first case for the simulative study is a fermentation process, very similar to the real L-valine production process which is described in chapter 5. However, the simulative example is somewhat simpler: only one feed is added and only one substrate is used to produce biomass and another product. The concentrations of substrate, biomass and product are used as measured state variables.

4.2.1. Prior Situation

The initial situation consists of a simple batch experiment. Two competing model structures were used (depicted Ferm1 and Ferm2), each based on Monod-type kinetics, having nine model parameters each and differing only in the way the product inhibition was modeled. The differential equations for modeling of the fed-batch system are similar to the equations mentioned in paragraph 2.3, and the kinetic equations are as follows:

Model Ferm1:

$$r_X = \frac{\mu_{max} \cdot C_{S1} \cdot C_X}{K_m + C_{S1} + \frac{C_S^2}{Ki_S}} \cdot \frac{Ki_P}{C_P + Ki_P} \tag{4.1}$$

$$r_P = r_X \cdot Y_{PX} + C_X \cdot m_P \tag{4.2}$$

$$r_S = -\frac{r_X}{Y_{XS}} - \frac{r_P}{Y_{PS}} - C_X \cdot m_S \tag{4.3}$$

where the used symbols have the same meaning as in paragraph 2.3 and listed in appendix A on page 133 and onwards.

Model Ferm2 is similar to Ferm1, but with competitive- instead of non-competitive inhibition of the growth by the product, so equation 4.1 is changed to:

$$r_X = \frac{\mu_{max} \cdot C_{S1} \cdot C_X}{K_m \cdot \left(1 + \frac{C_P}{Ki_P}\right) + C_{S1} + \frac{C_S^2}{Ki_S}} \tag{4.4}$$

The used batch data without noise are shown in figure 4.2, together with the fitted curves of the two competing models.

The model parameters after fitting the model to the data of the batch experiment without noise, are shown in table 4.1, together with estimated standard deviations.

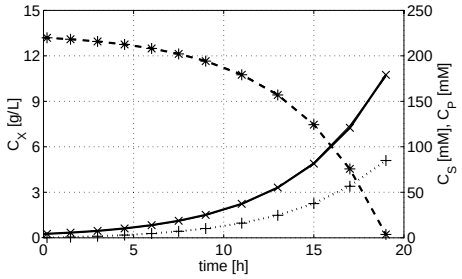

FIGURE 4.2.: Fit of the competing models to the preliminary batch experiment. Markers show the 'measured' values whereas lines are the simulated values of the fitted models. Biomass (C_X) is shown in solid lines and $\times$ as g/L. Dashed lines and $*$ indicate substrate (C_S) concentrations in mM and product (C_P) concentrations are shown as dotted lines and $+$ in mM. The graph actually has separate lines for the best (with thick lines) and worst (thin lines) of the 2 models, but the slight differences are barely visible.

These standard deviations were calculated according to equation 3.1 on page 47, using (arbitrarily chosen) relative standard deviations of 5% for all state variables and lower bounds on the measurement accuracies of 0.025 g/L, 5 mM and 1 mM for biomass (C_X), substrate (C_S) and product (C_P) respectively.

TABLE 4.1.: Model Parameters of the Competing Fermentation Models Before the Model Discriminating Experiment.

	Ferm1		**Ferm2**		
Parameter	Value	σ	Value	σ	Unit
μ_{max}	0.35	0.83	0.22	23	h^{-1}
K_m	2.0	26	4.8	$2.8 \cdot 10^4$	mM
m_s	0.10	$1.8 \cdot 10^5$	2.0	$1.3 \cdot 10^5$	$mmol.g^{-1}.h^{-1}$
Y_{PX}	3.0	22	3.9	15	$mmol.g^{-1}$
m_P	1.0	4.3	8.4	3.1	$mmol.g^{-1}.h^{-1}$
Y_{XS}	0.1	$5.5 \cdot 10^3$	4.7	$1.4 \cdot 10^5$	$g.mmol^{-1}$
Y_{PS}	0.80	$1.2 \cdot 10^5$	9.8	$1.5 \cdot 10^5$	$mmol.mmol^{-1}$
Ki_P	150	482	267	$5.2 \cdot 10^6$	mM
Ki_S	300	$1.6 \cdot 10^3$	1950	$1.9 \cdot 10^5$	mM

Clearly, the parameters are not yet properly estimable. This is however a realistic situation in the initial phase of fermentative process development and this is also the case for the development of the L-valine production process in the current work.

The same standard deviations of the measured values were used to add normally distributed noise with mean 0 to the data and re-estimate the parameters as shown in the setup before.

4.2.2. Designed Experiments

A fed-batch experiment was planned, similar to the experiments used for the development of the L-valine production process as mentioned in paragraph 3.4.1 on page 50. A maximal duration of 48 hours was used and the feed of a solution of 3.9 M substrate was described as periods of constant feed rates of six hours duration, with the first period without feed. The sampling times were fixed to every 1.5 hours with a longer period without sampling between 13.5 and 19.5 and between 37.5 and 43.5 hours. The initial volume was set to be 1.7 L and with the designed feed and the samples of 25 mL, the suspension volume was limited between 1.5 and 2.5 liter throughout the experiment in a similar matter as mentioned in paragraph 3.4.1. The initial biomass concentration was fixed at 0.25 g/L and the initial product concentration was kept fixed at 0.05 mM. Throughout the experiment, the substrate concentration was bound between 0.01 and 277 mM, again in a similar matter as described in paragraph 3.4.1.

The designed experiment consists of the parameters describing the feedrate over time and of the initial concentration of substrate. The initial substrate concentration was bound between 55 and 222 mM. The feedrates were bound between 0 and 0.1 L/h.

The experiment was designed according to the 5 different design criteria which will be discussed in the following paragraphs.

Box and Hill (BH)

The designed experiment according to the BH criterion is shown in figure 4.3, illustrated by the expected concentrations according to the competing models.

The Box and Hill criterion consists of a part which has the difference in the expected concentrations as its driving force and a part which is driven by the difference between the variances of the expected concentrations (model variances). In the current designed experiment, the model variances had by far the larger influence: only $3.4 \cdot 10^{-5}\%$ of the criterion was accounted for by the part which is driven by the differences in the expected concentrations!

The BH criterion is calculated as a summation over all measured values. The criterion for each state variable and each measured point is shown in figure 4.2.2. This figure clearly shows, that the criterion is practically completely accounted for by only a few substrate measurements. The criterion is especially high in a region where the expected substrate concentrations, shown in figure 4.3(b), differ much and where especially the concentration according to model Ferm2 gets high. The maximal contribution is found at the point where the concentration decreases rapidly to very low values according to

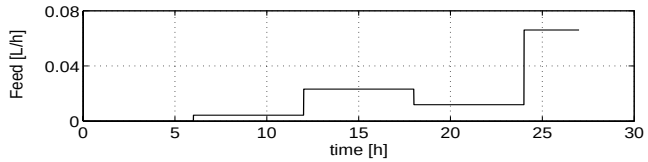

(a) Feedrate in L/h of a 3889 mM substrate solution.

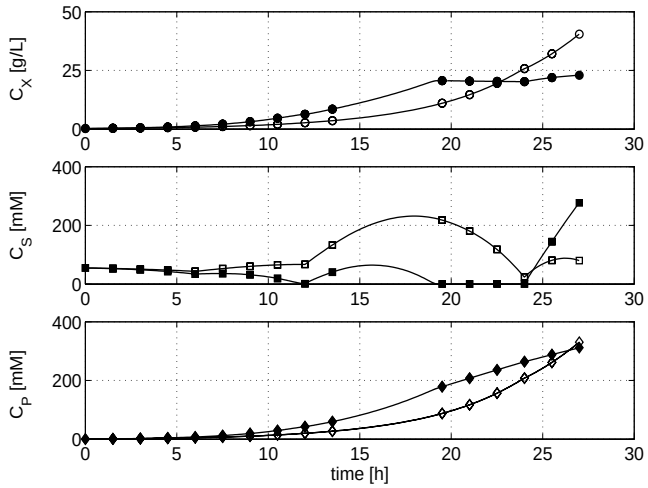

(b) Expected concentrations of biomass (C_X), substrate (C_S) and product (C_P) according to model Ferm1 with closed markers and according to Ferm2 with open markers.

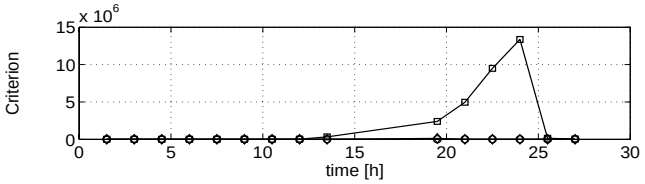

(c) Contribution of the suggested measurements to the BH criterion. ○: biomass; □: substrate; ◊: product. Lines are a visual aid.

FIGURE 4.3.: Designed experiment according to the BH criterion. Initial substrate concentration: 55 mM.

Ferm2, whereas the substrate concentrations according to Ferm1 were already very low for a long time. In such a situation it can be expected that the model variance is very high for model Ferm2 and rather low for Ferm1, which might explain the suggested experiment.

The fact that the experiment lasts shorter than the maximal allowed time, is caused by the bounds on the expected results, as mentioned before. This limited experiment provided a better discriminating experiment according to the used criterion, than experiments which would last longer. It is noteworthy that none of the experiments which were suggested by the other criteria, including the longer lasting experiments, would lead to a better value for the current criterion.

Buzzi-Ferraris and Forzatti (BF)

The designed experiment according to the BF criterion is shown in figure 4.4, illustrated by the expected concentrations according to the competing models.

Again, the suggested experiment was shorter than the maximal duration. The same remarks as stated for the experiment according to the BH criterion hold here, including the fact that all other suggested experiments result in lower values for the BF criterion than the suggested experiment.

The criterion was with $5.9 \cdot 10^5$ by far high enough to exceed the amount of responses (here 63), which was suggested by Buzzi-Ferraris and Forzatti as a limit.

Chen and Asprey (CA)

The designed experiment according to the CA criterion is shown in figure 4.5, illustrated by the expected concentrations according to the competing models.

Since all measurements at different time-points are regarded to be independent, also with respect to the model variance, the criterion consists of a summation over all time-points and can readily be shown over time as is done here in figure 4.5(c), showing that basically only the last measurement determines the criterion (98.67% of the criterion is accounted for by the final measurement point).

The optimized criterion is with 15.34 too small according to the limit which was suggested in the original paper by Chen and Asprey, who suggested not to perform the experiment when the criterion would not exceed the amount of measured values, which are 39 in the suggested experiment. However, if we would only measure the state variables at the final time-point in this experiment, the criterion would be 15.15 and exceed the 3 measured values easily, which is a clear example of the problem with the limit as suggested by Chen and Asprey.

Once again, the suggested experiment was shorter than the maximal duration. None of the experiments, suggested by the other design criteria, would give a better value of the CA criterion.

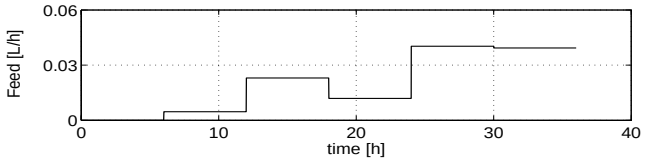

(a) Feedrate in L/h of a 3889 mM substrate solution.

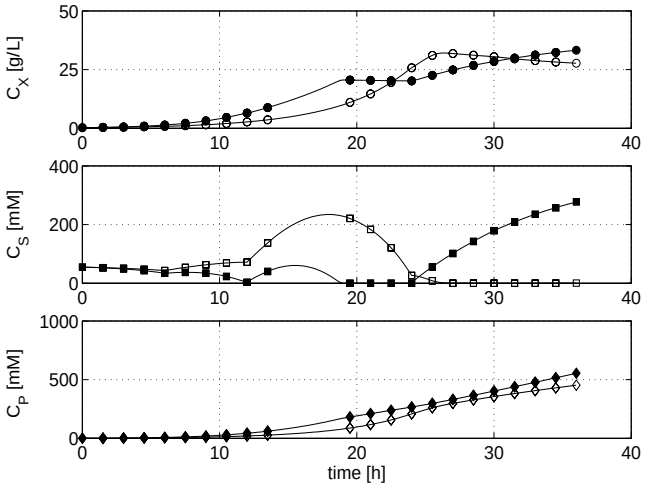

(b) Expected concentrations of biomass (C_X), substrate (C_S) and product (C_P) according to model Ferm1 with closed markers and according to Ferm2 with open markers.

FIGURE 4.4.: Designed experiment according to the BF criterion. Initial substrate concentration: 55 mM.

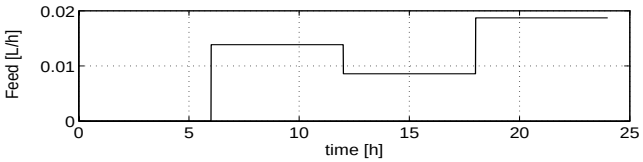

(a) Feedrate in L/h of a 3889 mM substrate solution.

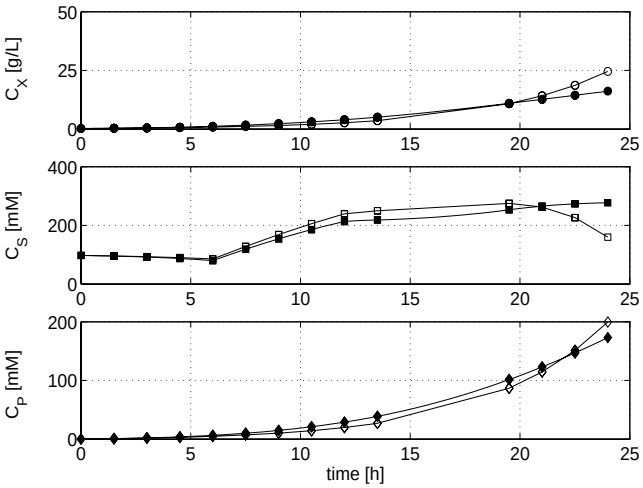

(b) Expected concentrations of biomass (C_X), substrate (C_S) and product (C_P) according to model Ferm1 with closed markers and according to Ferm2 with open markers.

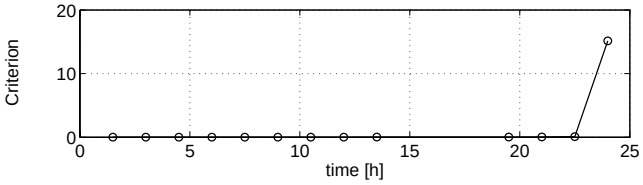

(c) Contribution of the suggested measurements to the CA criterion. Markers show the values, lines are a visual aid.

FIGURE 4.5.: Designed experiment according to the CA criterion. Initial substrate concentration: 97.6 mM.

Hunter and Reiner (HR)

The designed experiment according to the HR criterion is shown in figure 4.6, illustrated by the expected concentrations according to the competing models.

This simple criterion consists of a summation over all measured points, so it can readily be discriminated between the influences of the different state variables and the different time-points, as shown in figure 4.6(c). The majority (79%) of the criterion is driven by the differences in substrate concentrations, whereas 11% and 10% are accounted for by biomass and product, respectively. High values occur when one of the models predicts low values whereas the other model predicts appreciable concentrations.

Just like in the experiments which are planned using the BH and BF criteria, periods are created with very low expected glucose concentrations according to one of the criteria and appreciable concentrations according to the other criterion. Both according to the BH and HR criteria, this contributes the most to the discriminating power of the experiment.

New Simple Criterion for Dynamic Experiments (ND)

The designed experiment according the ND criterion is shown in figure 4.7.

This criterion consists of an addition of two parts: one being driven directly by the expected differences in the measured state variables, the other added to regard the shape of the curves. The different influences of these two parts are shown in figure 4.7(c), showing that the part regarding the shape of the curves has a limited influence (about 3.7% of the total criterion), so this part has, at the most, only some fine-tuning effects in the current example.

Furthermore, the criterion regards all measurements at different measurement time-points to be independent, so the contribution of each time-point can be shown separately, as is also done in the same figure (4.7(c)). It seems likely that here, again, the expected differences in the substrate concentrations play a major role, although this cannot readily be distinguished because all state variables of one sample are not regarded totally independent. However, higher values in figure 4.7(c) seem to coincide especially to large differences in in the substrate concentrations shown in figure 4.7(b).

4.2.3. Results

As mentioned in paragraph 4.1, the designed experiments were simulated using the models with 10 different parameter sets which resulted from fitting the models to the batch data with different sets of noise. To each set of simulated data, 10 sets of noise were added, resulting in 100 sets of data. The models were then fitted to the 100 sets of data, each consisting of the preliminary batch data and one of the 100 data sets of the new experiment.

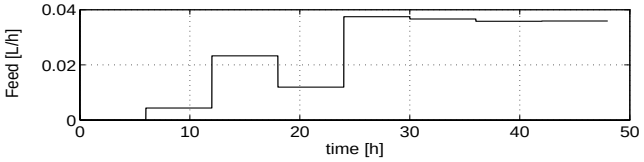

(a) Feedrate in L/h of a 3889 mM substrate solution.

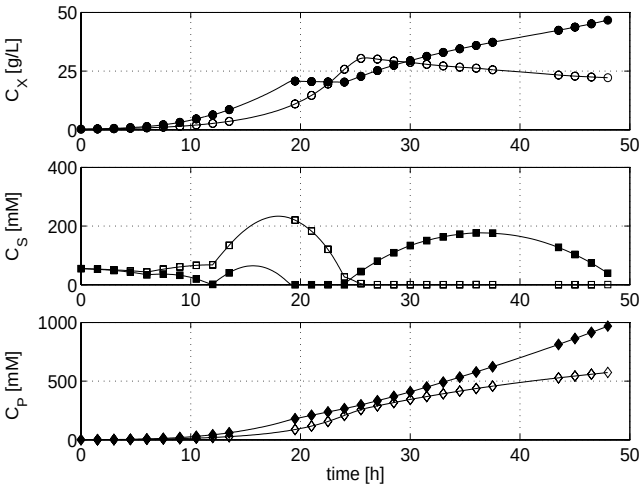

(b) Expected concentrations of biomass (C_X), substrate (C_S) and product (C_P) according to model Ferm1 with closed markers and according to Ferm2 with open markers.

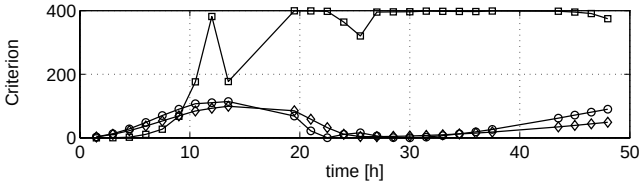

(c) Contribution to the HR criterion, of the suggested measurements of biomass as ∘, substrate as □ and product as ◊ Markers show the values, lines are a visual aid.

FIGURE 4.6.: Designed experiment according to the HR criterion. Initial substrate concentration: 55 mM.

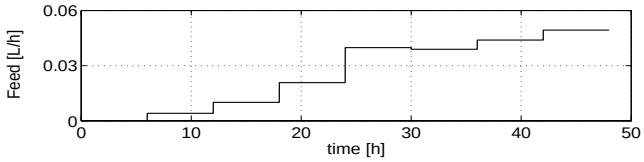

(a) Feedrate in L/h of a 3889 mM substrate solution.

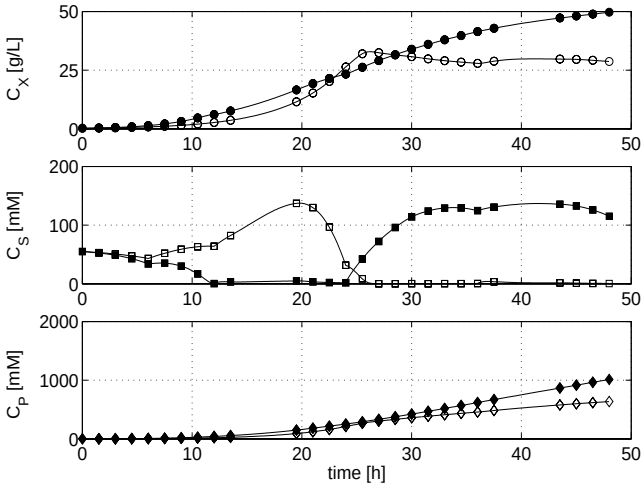

(b) Expected concentrations of biomass (C_X), substrate (C_S) and product (C_P) according to model Ferm1 with closed markers and according to Ferm2 with open markers.

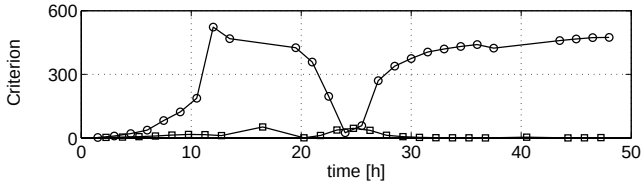

(c) Contribution of the suggested measurements to the ND criterion. Contribution of the difference in measured values as ∘ and a part directed by the shape of the responses as □. Markers show the values, lines are a visual aid.

FIGURE 4.7.: Designed experiment according to the ND criterion. Initial substrate concentration: 55 mM.

The reduced chi-squared values of the two competing models were calculated for each of the 100 fits. In each case, a proper low value was found for the 'true' model structure, as should be expected. Even values below 1 were reached, indicating that the fitted model were closer to the measured values than expected, based on the measurement variance. The ratio between the χ^2 values for the 'false' models and the 'true' models are shown in box-plots in figure 4.8. Higher values indicate better performance of the discriminating design criterion.

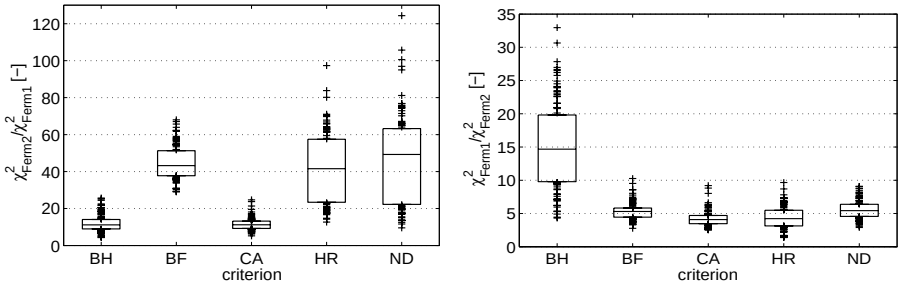

(a) Ratio between the reduced χ^2 of Ferm2 and Ferm1, fitted to data generated with Ferm1.

(b) Ratio between the reduced χ^2 of Ferm1 and Ferm2, fitted to data generated with Ferm2.

FIGURE 4.8.: Ratios between reduced χ^2 value of the 'false' and the 'true' models. The boxes have horizontal lines at the lower quartile, median and upper quartile. Points outside the quartiles are shown as +.

Except for the BH criterion, the discriminating power of each of the criteria was better when Ferm1 was the 'true' model.

As could be expected from the concentrations in figure 4.5(b), the CA criterion did not perform very well in the current example. As mentioned before, the reached value of this criterion was too low according to the original paper. It was suggested, to perform an experiment to improve the parameter estimation in such a case instead. It was surprising that the CA- and the BF criterion supposed such strongly different experiments, although the differences between the two criteria seem small. The difference mainly consists of the way to deal with dependent- or independent measurements and a slightly smaller influence of the measurement variance in weighting the criterion.

The partly large variances in the resulting $\tilde{\chi}^2$ values, as indicated by large boxes in figure 4.8, are mainly caused by the variance introduced by the different parameter values, which were used to generate data and not so much by the added noise. In the BF and CA criteria, large effects of the parameter inaccuracies result in reduced values of the design criterion through the weighting by the model variance, which might therefore explain smaller variances in the results using these criteria.

Although statistically, there is not yet a hard proof, it seems like the adjustments for use with dynamic experiments in the ND criterion gave a slight improvement compared to the HR criterion.

Unfortunately, the results of this simulative case study do not yield one clear preferred criterion. The highest discriminating power was achieved using the ND criterion when Ferm1 was the 'true' model and also the best average was achieved using this criterion. The smaller variation is on the other hand a positive characteristic of the BF criterion. The highest minimal discriminating power was achieved by the BH criterion.

4.3. Second Case: Catalytic Conversion

The second case is a catalytic conversion. This case deals with a common and important question, whether a decrease in reaction rate over time could be caused by product inhibition or rather by deactivation of the catalyst.

Again, only one substrate is converted to one product. The concentrations of substrate and product are the only measured state variables.

4.3.1. Prior Situation

The initial situation consists of two subsequent batch experiments with different initial concentrations of substrate and catalyst.

Three Michaelis-Menten type models were fitted to these data. The kinetic equations of these models are as follows:

Model Cat1:

$$r_C = 0 \tag{4.5}$$

$$-r_S = r_P = \frac{v_{max} \cdot C_C \cdot C_S}{K_m \cdot \left(1 + \frac{C_P}{Ki_P}\right) + C_S} \tag{4.6}$$

Again, the used symbols are as explained in appendix A on page 133. Subscript $_C$ is used to indicate the catalyst.

Model Cat2 is similar to Cat1, but with non-competitive instead of competitive product inhibition, so equation 4.6 is changed to:

$$-r_S = r_P = \frac{v_{max} \cdot C_C \cdot C_S}{K_m \cdot + C_{S1}} \frac{Ki_P}{C_P + Ki_P}, \tag{4.7}$$

but still, the amount of catalyst C does not change.

In model Cat3, instead of a product inhibition, a first order degradation of the catalyst

is included:

$$r_C = -k_d \cdot C_C \tag{4.8}$$

$$-r_S = r_P = \frac{v_{max} \cdot C_C \cdot C_S}{K_m + C_S} \tag{4.9}$$

The used data of the two batches without noise are shown in figure 4.9, together with the fitted curves of the three competing models.

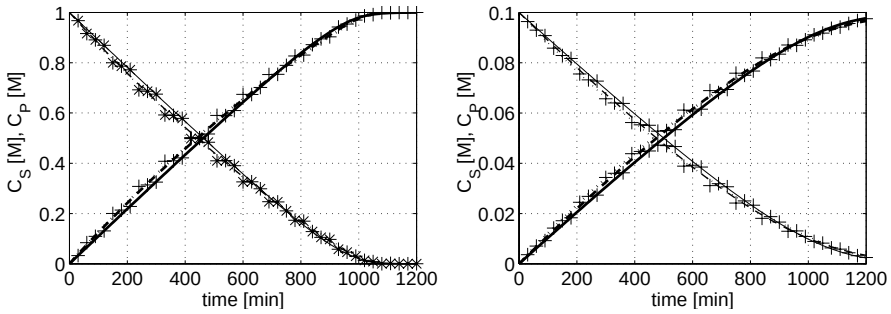

FIGURE 4.9.: Fit of the three competing models to the two batches. Markers show the 'measured' values whereas lines are the values of the fitted models. The fit of model Cat1 is shown in solid lines, Cat2 in dashed lines and Cat3 in dotted lines. Thin lines and $*$ show substrate concentrations; thick lines and $+$ are product concentrations. Initial concentrations of the experiment in the left plot were 0.1 mM catalyst, 1 M substrate and no product. For the right plot, they were 0.01 mM catalyst, 0.1 M substrate and no product.

The model parameters after fitting the model to the data of the batch experiments without noise are shown in table 4.2, together with estimated standard deviations using relative standard deviations of 5% and lower bounds on the measurement accuracies of 10 mM for both substrate (C_S) and product (C_P), for estimation of the standard deviation of the measured values according to equation 3.1 on page 47. In this case, the parameters are estimable more satisfactory, although partly high correlation coefficients exist between the parameters[2]. The mechanistic differences, however, cannot yet be determined by model fitting to the available data. All three models fit properly. The relative goodness of fit G, according to equation 2.35 on page 20 is also mentioned in the table. In the fermentation example shown above, these values did not have an influence on the resulting experiments, since only two models were used. In the current example, three different model pairs are available, so in the BH and ND criteria, the prior goodness

[2]Especially in model Cat2, with a correlation coefficient of -0.98 between v_{max} and Ki_P

of fit has an influence. However, at this point, the differences between the fits are rather small.

TABLE 4.2.: Model Parameters of the Competing Catalysis Models Before the Model Discriminating Experiment and the relative goodness at this point.

	Cat1		**Cat2**		**Cat3**		
Parameter	Value	σ	Value	σ	Value	σ	Unit
v_{max}	11.0	0.045	13.1	0.12	13.0	0.015	$mol.mol^{-1}.min^{-1}$
K_m	6.64	0.23	16.4	0.52	4.46	0.31	mM
Ki_P	193	8.9	1930	71			mM
k_d					0.0339	0.0132	h^{-1}
G	0.30		0.24		0.46		

The same standard deviations of the measured values were used to add normally distributed noise with mean 0 to the data and re-estimate the parameters as shown in the setup before.

4.3.2. Experimental Designs

A fed-batch experiment was designed with a fixed maximal duration of 2880 minutes (48 h). One feed is added containing 20 M substrate. This feed is described as periods of 240 minutes duration with constant feed rates and no feed in the first 240 minutes. The volume was restricted between 1.5 and 2.5 L, again in a similar matter as mentioned in paragraph 3.4.1, with samples of 10 mL, taken every 60 minutes. The initial volume was 1.7 L. There were no bounds used on the concentrations of substrate during the experiment.

The designed experiment consists of the parameters describing the feedrate over time and the initial concentrations of catalyst, substrate, and product. The initial concentrations of catalyst were bound between 0.001 and 0.2 mM, of substrate between 0.2 and 3 M and of product between 0 and 3 M. The feedrates were bound between 0 and 1 L/h.

The experiment was designed according to the 5 different design criteria and will be discussed in the following paragraphs.

Box and Hill (BH)

The designed experiment according to the criterion based on the criterion of Box and Hill is shown in figure 4.10, illustrated by the expected concentrations according to the competing models.

'Missing' measurements are caused by the lower limit on the volume.

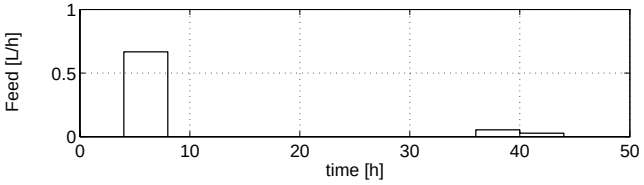

(a) Feedrate of a 20 M substrate solution.

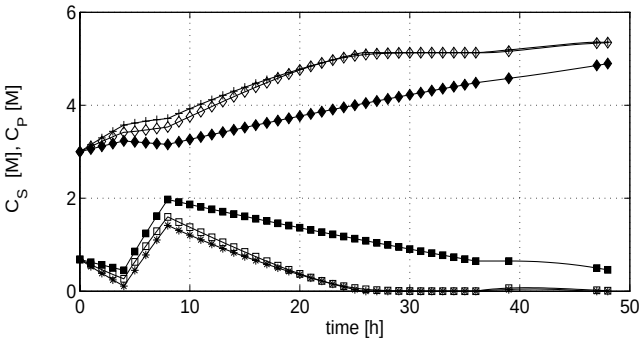

(b) Expected concentrations. According to model Cat1: □: substrate (C_S), ◊: product (C_P). Cat2: ■: C_S, ♦: C_P; Cat3: ∗: C_S, +: C_P.

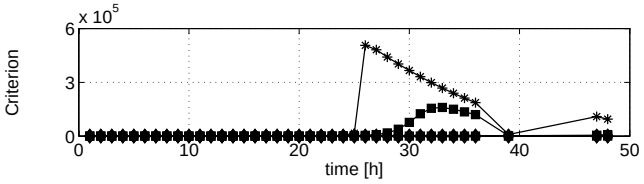

(c) Contribution of the suggested measurements to the BH criterion. Difference between model Cat1 and Cat2: ■: substrate (C_S), ♦: product (C_P); between Cat1 and Cat3: □: C_S, ◊: C_P; between Cat2 and Cat3: ∗: C_S, +: C_P. Lines are a visual aid.

FIGURE 4.10.: Designed experiment according to the BH criterion. Initial concentrations: 0.2 mM catalyst, 0.684 M substrate and 3 M product.

Similar to in the first case study, the difference between the expected model variances is determining the experiment to a much larger extend than the differences in the expected concentrations. The part of the criterion, driven by the model variances, accounts for 99.5% of the criterion.

The BH criterion is calculated as a summation over all measured values and all model pairs. The criterion for each state variable and each measured point is shown in figure 4.10(c) for each model pair.

As could be expected from figure 4.10, mainly the differences between model Cat2 and the other two models are of influence. Furthermore, it is mainly the measurement of substrate which contributes to the criterion. Especially the measurements in a range where one of the models from a model pair predicts very low substrate concentrations are of importance.

Buzzi-Ferraris and Forzatti (BF)

The designed experiment according to the BF criterion is shown in figure 4.11, illustrated by the expected concentrations according to the competing models. Again, skipped samples are caused by the lower bound on the volume.

In this experiment, the influence of the different model pairs is more evenly divided: model pairs Cat1-Cat2, Cat1-Cat3 and Cat2-Cat3 accounted for about 27%, 18% and 56% of the criterion.

The criterion was with $2 \cdot 10^4$ by far high enough to pass the minimal value according to the original BF criterion.

Chen and Asprey (CA)

The designed experiment according to the CA criterion is shown in figure 4.12, illustrated by the expected concentrations according to the competing models.

In this designed experiment, the model pairs Cat1-Cat2, Cat1-Cat3 and Cat2-Cat3 accounted for 28%, 24% and 48% of the criterion. In this case, the optimized criterion was with $5 \cdot 10^4$ high enough not to have problems regarding the minimal value suggested in the original criterion.

The criterion is shown over time for substrate and product in figure 4.12(c), showing that 98% of the criterion is accounted for by the substrate measurements, fairly evenly divided over time.

Hunter and Reiner (HR)

The designed experiment according to the HR criterion is shown in figure 4.13, illustrated by the expected concentrations according to the competing models. Obviously, the suggested experiment is very similar to the experiment according to the CA criterion shown in the prior paragraph.

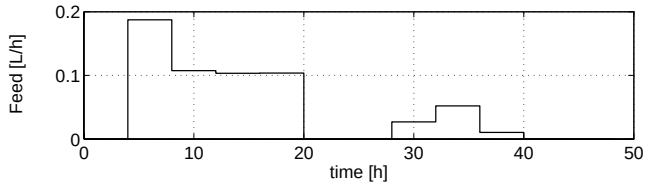

(a) Feedrate of a 20 M substrate solution.

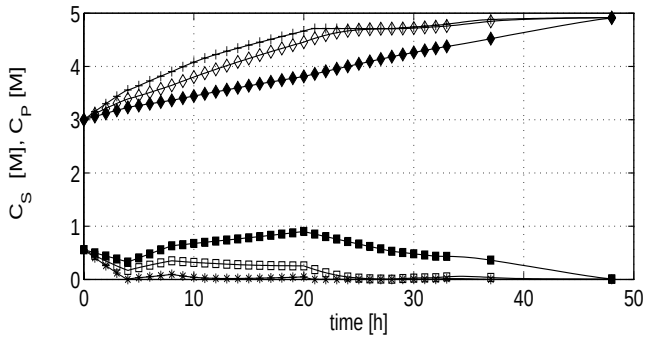

(b) Expected concentrations. According to model Cat1: □: substrate (C_S), ◊: product (C_P). Cat2: ■: C_S, ♦: C_P; Cat3: ∗: C_S, +: C_P.

FIGURE 4.11.: Designed experiment according to the BF criterion. Initial concentrations: 0.2 mM catalyst, 0.558 M substrate and 3 M product.

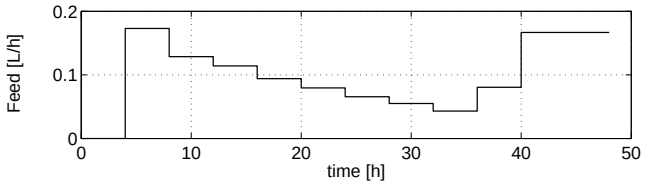

(a) Feedrate of a 20 M substrate solution.

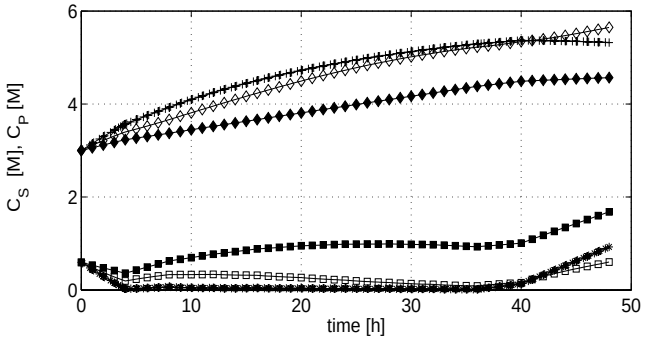

(b) Expected concentrations. According to model Cat1: □: substrate (C_S), ◊: product (C_P). Cat2: ■: C_S, ♦: C_P; Cat3: ∗: C_S, +: C_P.

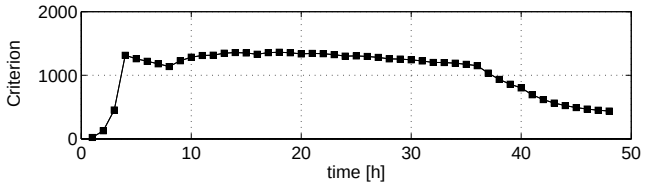

(c) Contribution of the suggested samples to the CA criterion.

FIGURE 4.12.: Designed experiment according to the CA criterion. Initial concentrations: 0.2 mM catalyst, 0.593 M substrate and 3 M product.

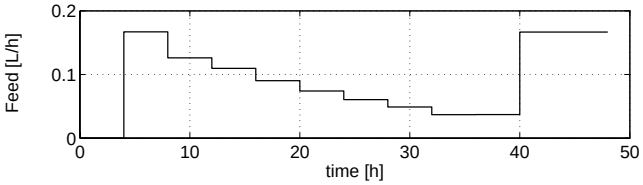

(a) Feedrate of a 20 M substrate solution.

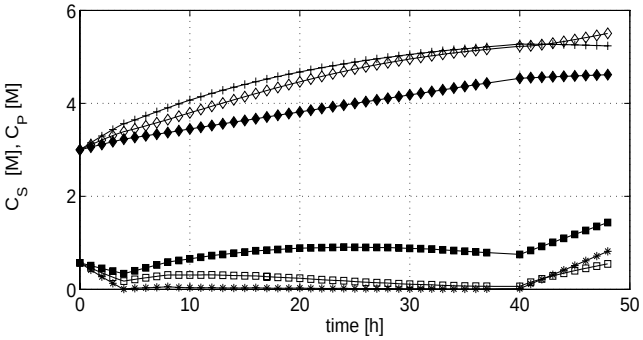

(b) Expected concentrations. According to model Cat1: □: substrate (C_S), ◊: product (C_P). Cat2: ■: C_S, ♦: C_P; Cat3: ∗: C_S, +: C_P.

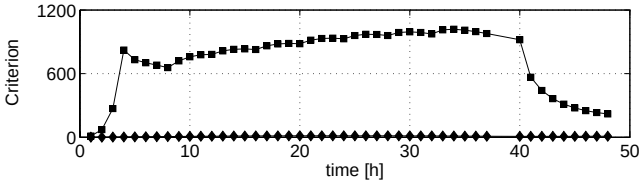

(c) Contribution of the suggested measurements to the HR criterion. ■: substrate, ♦: product. Lines are a visual aid.

FIGURE 4.13.: Designed experiment according to the HR criterion. Initial concentrations: 0.2 mM catalyst, 0.569 M substrate and 3 M product.

Skipped samples are again caused by problems regarding the lower bound on the volume.

In this designed experiment, the model pairs Cat1-Cat2, Cat1-Cat3 and Cat2-Cat3 accounted for 26%, 31% and 43% of the criterion.

The criterion is shown for each state variable and all time-points, as shown in figure 4.13(c). Again, the substrate measurements had more influence than the measurements of the product concentrations, accounting for almost 99% of the optimized criterion.

New Simple Criterion for Dynamic Experiments (ND)

In this case, the extensions to the HR criterion in the ND criterion did not lead to a different optimized experiment. Exactly the same experiment as suggested by the HR criterion shown in the former paragraph, was suggested using the ND criterion.

The pitfall of overrating very fast changing concentrations obviously did not occur in the suggested experiment using the HR criterion. Such a situation could not be produced within the experimental constraints. It also was apparently not possible to introduce more different shapes.

4.3.3. Results

Again, 100 data sets were generated with each model structure and each designed experiment. $\tilde{\chi}^2$ values were calculated for each model, fitted to the data of the two preliminary batch experiments and the newly simulated values with noise for all 100 data sets. The ratio between the $\tilde{\chi}^2$ values of the 'false' and the 'true' models are shown in the box-plots in figure 4.14. Higher values indicate better discrimination.

The first striking result is the large variance in the results using the BH criterion. This variance is mainly caused by the use of different sets of parameters for the generation of the data. The fact that the BH criterion especially aims at a large difference in the model variances of the competing models and therefore tends to suggest experiments where the influence of the insecurity in the parameters is very strong, explains this result. This also reflects in the fit of the 'true' model to the data, which is illustrated for instance in figure 4.15. The resulting $\tilde{\chi}^2$ values of the 'true' model after the designed experiment are higher than 1 because of the variance in the model parameters, which is not accounted for in the weighting of the residuals by the measurement standard deviation. This resulted in values around 1.5 after the designed experiments according to all criteria, except for the BH criterion which led to much higher values.

The BH criterion performed especially poor in discriminating between model Cat1 and Cat3. This was expected since the expected concentrations according to those two models are very similar, as discussed in paragraph 4.3.2 on page 76. Generally, the BH criterion performed worse than the other criteria in the current case.

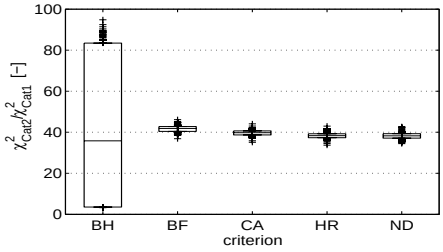

(a) Ratio between the reduced χ^2 of model Cat2 and Cat1, fitted to data generated with Cat1.

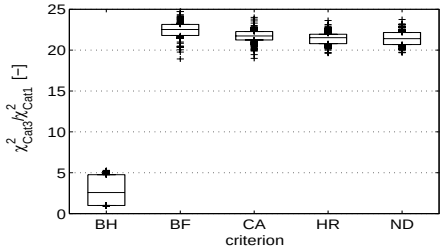

(b) Ratio between the reduced χ^2 of model Cat3 and Cat1, fitted to data generated with Cat1.

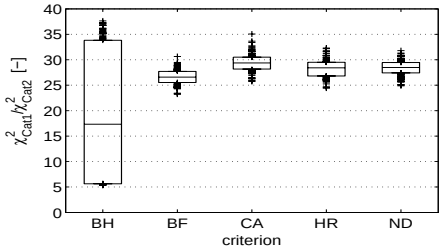

(c) Ratio between the reduced χ^2 of model Cat1 and Cat2, fitted to data generated with Cat2.

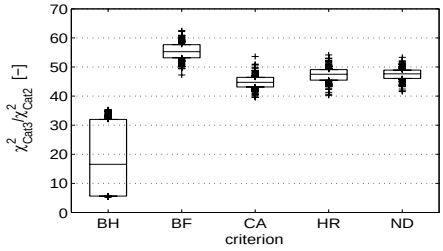

(d) Ratio between the reduced χ^2 of model Cat3 and Cat2, fitted to data generated with Cat2.

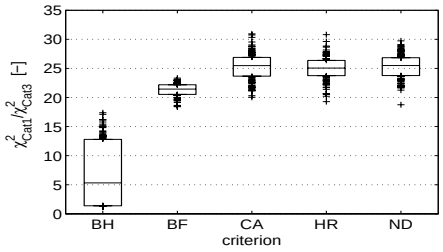

(e) Ratio between the reduced χ^2 of model Cat1 and Cat3, fitted to data generated with Cat3.

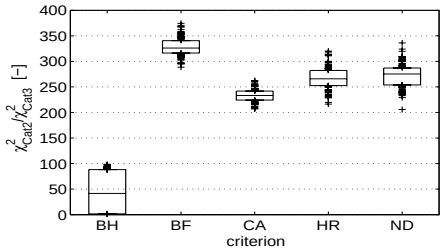

(f) Ratio between the reduced χ^2 of model Cat2 and Cat3, fitted to data generated with Cat3.

FIGURE 4.14.: Ratios between reduced χ^2 value of the 'false' and the 'true' models. The boxes have horizontal lines at the lower quartile, median and upper quartile. Points outside the quartiles are shown as +.

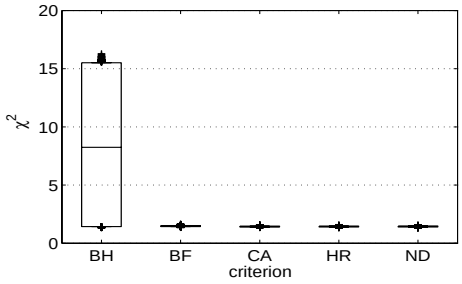

FIGURE 4.15.: Reduced χ^2 of Cat1, fitted to data generated with Cat1 itself as the 'true' model. Analogue to figure 4.14

The differences between the performances of the 4 other criteria are very small, as might also have been expected from the similar expected results. The discrimination between model Cat2 and Cat3 seems somewhat better using the BF criterion. On the other hand, this criterion performed slightly less good for discrimination between Cat1 and Cat3 when Cat3 was 'true'.

The differences between the results using the HR criterion and the ND criterion are only caused by the added random white noise, since exactly the same experiments were used.

4.4. Discussion and Conclusion

All model discriminating design criteria which are compared here are certainly useful and it is of course not the aim of this study to show useless criteria, but to compare their use in dynamic systems with potentially poor parameter estimates.

The use of the CA criterion was problematic in the fermentation experiment. As discussed in paragraph 4.2.2 on page 67, it was suggested in the original paper to perform an experiment for improvement of the parameter estimation in such a case. This might not be that simple, since still a series of competing models are available. One obvious option would be to design the parameter estimation experiment based on the model with the best fit so far. However, other discriminating design criteria did suggest proper discriminating experiments and this seems to be just a good example of the potential risks and problems in using the CA criterion. The potentially large and fast changes in model variances in dynamic systems with poor parameter estimates seem to be the major cause of these problems.

Note however, that the original CA criterion was especially developed for dynamic systems and it was shown to perform properly with a fermentation example with pa-

rameter estimates, which are comparable to the estimates in the catalytic conversion example in the current work. In the original paper, an example was given where the CA criterion was more efficient than the simple criterion of Hunter and Reiner without any weighting (so also not by the measurement variance as in the HR criterion used in the current work).

The BH criterion clearly produced different experimental designs than the other four criteria. In the used dynamic experiments, the criterion is driven by differences in the model variances, whereas the differences in the expected state variables have practically no direct influence. This might be different in steady state experiments such as in Takors et al. (1997), where the model variances do not reach such extreme and fluctuating values. In dynamic experiments, where the parameter sensitivities are integrated over time, extreme differences and changes in the model variance are very likely to be possible and such situations cause high values in the BH criterion. The BH criterion does also suggest useful experiments, but its results seem to be less certain. The intuitively strange use of the differences in the model variances is caused by the use of the maximal expected change in system entropy, as was also mentioned in paragraph 2.5.1 on page 28.

The differences between the CA and the BF criterion seem to be rather small on first thoughts, but these two criteria did turn out to result in different designs. The major difference lies in the fact that the model variance is calculated with all measured state variables and all samples being dependent for the BF criterion, whereas each sample time is regarded independent by the CA criterion. Intuitively, using all measurements dependent in calculating the model variance makes more sense because the parameters can only be adjusted once to fit to the new data. When a change in a parameter value would decrease the expected difference between two model predictions of one sample, but the same change would then increase the expected difference in another sample, this is an important characteristic which reduces the ability of the models to produce similar results and thus improves the expected model discrimination.

One possible disadvantage of the use of dependent samples as in the BF criterion, is that the calculations will include large matrices when many samples are used, which can cause relatively long calculation times, whereas with independent samples, the sparse matrices would reduce this problem. However, in our examples, this difference was not yet significant and more than 99% of the calculation time is used for the model simulations, so a real improvement of calculation times could only be reached by increasing the simulation speed and decreasing the amount of needed simulations.

Most studies on model discriminating experimental designs make use of the model variance. For instance the work by Chen and Asprey is just one of the examples where the use of model variances is shown to be beneficial in model discriminating experimental design. However, the potential pitfalls of the use of this characteristic value and the relatively high costs in terms of calculation times, which were also mentioned in paragraph 2.5.1 on page 32, are often not mentioned in those studies.

In the current examples, the criteria without the model variance (HR and ND) did suggest proper model discriminating experiments. It could be expected that these criteria would lead to more insecure results where re-estimation of the model parameters can undo the expected differences. The use of the model variance especially aims at diminishing this risk. The results of the fermentation example with Ferm1 as the true model do show a larger variance in the discriminating power of the experiments designed by HR and ND than by BF, but the discriminating power of all three experiments were very good. The average result of the ND criterion was even slightly better than the BF criterion. The other results do not show such a clear improvement in the reliability of the BF criterion as compared to the HR and ND criteria. In some cases, the HR and ND criteria even performed better, for instance in recognizing Cat1 as a false model when Cat3 would be correct. Generally, however, the differences between the performance of the BF criterion and the HR and ND criteria are rather small.

The differences between the performance of the HR and the ND criterion were generally even smaller. In the first case with the relatively poor parameter estimates, the ND performed slightly better than the HR criterion.

Based on the results of this study, it was decided to use the ND criterion for designing the second model discriminating experiment during development of the L-valine production process, as shown in paragraph. This choice was not only motivated by the proper performance in the current study, but certainly also by the decreased calculation times, compared to the BH, BF and CA criteria, as also mentioned in paragraph 2.5.1 on page 32. The difference in calculation time between the HR and ND criteria was negligible.

5. L-Valine Production Process Development

The practical application of the presented approach for model based process development is of special interest in the current work. The fermentative production of L-valine is the industrially relevant process, which is investigated here.

5.1. Material and Methods

5.1.1. Organism

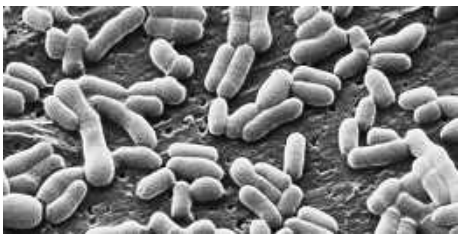

FIGURE 5.1.: Photo of *C. glutamicum* by electron microscopy.

The organism used in this study is the genetically modified strain *Corynebacterium glutamicum* ATCC 13032 Δ*ilvA*Δ*panBC*pJC1*ilvBNCD* as described by Radmacher et al. (2002). This strain was modified in order to improve the production of the amino acid L-valine by the group of Dr. L. Eggeling at the Institute of Biotechnology I of Research Centre Jülich. The modifications are shown in figure 5.2 on page 89.

An important special characteristic of the metabolic route towards L-valine is the fact that several enzymes of this route also catalyse similar reactions towards L-isoleucine synthesis (Eggeling et al., 1997). By deletion of the gene *ilvA*, which encodes threonine dehydratase, the synthesis of L-isoleucine via this route is blocked. This way, the total catalytic potential of these enzymes is available for L-valine synthesis. Due to this deletion, the strain is auxotrophic for L-isoleucine. This also offers the possibility of maintaining the L-isoleucine concentrations at a low level, which has been shown to increase

the expression of the genes *ilvBNC* by an attenuation control mechanism (Morbach et al., 2000). This is, however, probably of very limited importance in the used strain due to the overexpression of these genes on the plasmid, which led to an approximately 15 times increase in the enzyme activities (Cordes et al., 1992; Radmacher, 2001). Avoiding high concentrations of L-isoleucine is also expected to be beneficial, since high concentrations of the branched-chain amino acids have been shown to decrease the activity of the key enzyme of branched chain amino acid synthesis: acetohydroxyacid synthase (AHAS, see figure 5.2). This fact is, however, also expected to be of little importance in the final production experiments, since this enzyme is also inhibited by the other branched chain amino acids amongst which especially L-valine. This inhibition was shown to be maximal about 50% (Eggeling et al., 1987). Furthermore, a recent study with the used strain has indicated that the positive effect of L-isoleucine limitation on the biomass specific AHAS activity was stronger than the inhibiting effect of high L-valine concentrations (Lange et al., 2003).

The main aim of the deletion of the genes *panBC*, which are needed for the production of D-pantothenate from ketoisovalerate, was to increase the availability of pyruvate as the precursor of L-valine. Lack of D-pantothenate leads to a decrease in the production of coenzyme A and a corresponding decrease in the pyruvate dehydrogenase activity. The increased availability of pyruvate upon decreased pantothenic acid concentrations was also shown in a L-lysine overproducing strain, where the reduced concentrations however led to a decrease in L-valine and L-isoleucine and an increase in L-lysine production (An et al., 1999). A second beneficial effect of the deletion of *panBC* is the increased availability of ketoisovalerate for synthesis of L-valine when less is used for production of pantothenate. Due to this deletion the strain is auxotrophic for D-pantothenic acid.

The overexpression of the genes *ilvBNCD* on a plasmid increases the flux from pyruvate to ketoisovalerate and L-valine.

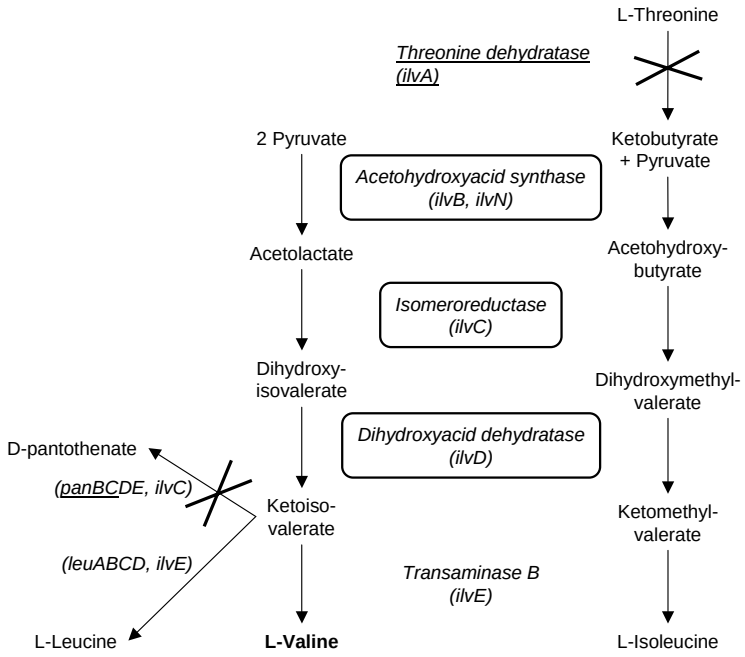

FIGURE 5.2.: Metabolic route for synthesis of L-valine and other branched chain amino acids, together with the genetic modifications in strain *Corynebacterium glutamicum* ATCC 13032 Δ*ilvA*Δ*panBC*pJC1*ilvBNCD*. The enzymes which catalyse the reactions are written in italic next to the reactions with the encoding genes between brackets. The deleted genes are underlined and the corresponding reactions are crossed out. The genes which are over-expressed on the plasmid are in rounded boxes. Note that several enzymes catalyse reactions for both L-valine and L-isoleucine biosynthesis.

5.1.2. Media

For all media, the used water was demineralized by reverse osmosis. The components were dissolved in demineralized water and sterilized by by filtration or by autoclavation for 20 minutes at 121°C. A syringe with a sterile filter (acrodisc® 0.2 μm, Pall Corporation, Ann Arbor, USA) was used for filtration of small volumes for use in shake flasks. The filter sterilized solutions for use in the stirred bioreactor were pumped through a filter which was autoclaved together with the bioreactor (0.2μm Sartobran®-300, Sartorius AG, Göttingen, Germany).

Complex Medium

Complex medium CGIII (Keilhauer et al., 1993) was used for the first preculture, which was inoculated directly with frozen working seed lots. The composition of this medium is mentioned in table 5.1. This medium was also used for the production of the seed lots.

TABLE 5.1.: Composition of the Complex Medium for the first preculture.

Substance	**Concentration**	
$glucose.H_2O$	22	$g.L^{-1}$
$NaCl$	5	$g.L^{-1}$
peptone	10	$g.L^{-1}$
yeast extract	10	$g.L^{-1}$
kanamycin stock solution	1	$mL.L^{-1}$

The glucose was dissolved and autoclaved separately. The kanamycin stock was sterilized by filtration. All other components were autoclaved together.

Defined Medium

The composition of the used defined culture medium was adapted from the minimal medium CGXII (Keilhauer et al., 1993; Morbach et al., 1996), which was also used during strain development at the IBT1 of the research centre. In some points, this medium was not ideal for our purposes or for an industrial production process, so some changes were made.

The trace element composition was taken from the composition which was optimized for another strain of *C. glutamicum* (WeusterBotz et al., 1997).

The composition of the medium is shown in table 5.2 on page 92.

In the precultures, also 5 g/L urea was added in order to keep the pH from decreasing too fast too soon. This amount of urea was also used during development of the strain but removed from the final medium composition because it caused the pH to rise rather fast in the first phase of the experiments (data not shown). This increase in pH depends

on the aeration and stirring rate and it is thought to be caused by a very strong urease activity of the used strain. This however remains to be tested. The wild-type of the used strain is reported to posses an energy-dependent urea uptake system which is synthesized under nitrogen limiting conditions (Siewe et al., 1998). In shake flask experiments with pH control, no beneficial effect of the urea was found.

In the experiments with the Ramos technology (see appendix C), also 42 g/L MOPS buffer was used as was also done during strain development at the IBT1, since in these experiments no pH control was available.

In the original medium, K_2HPO_4 was used instead of Na_2HPO_4. This way, only very little Na is available in the medium. However, the procedure used during strain development included the centrifugation of the preculture followed by resuspension of the cells in saline. This suspension was then used for inoculation of the production cultures, therewith introducing more Na in the medium. This is, of course, not very practicable and in fed-batch cultures, the concentration of Na would decrease over time. In pH-controlled shake flask experiments, different ratios between Na and K were compared (data not shown). Media with very low Na or K concentrations were shown to result in decreased growth. Media with both elements in appreciable concentrations were found to perform equally well. Based on these results, it was decided to replace K_2HPO_4 by Na_2HPO_4.

The 40 g/L glucose which is mentioned in table 5.2 was the standard concentration which was used in most shake flask experiments and in the first batch experiment in the stirred bioreactor. The initial glucose concentrations in planned fed-batch experiments was part of the experimental designs. For some experiments, the same holds for concentrations of L-isoleucine and pantothenic acid.

TABLE 5.2.: Medium composition of defined medium.

Substance	**Concentration**	
glucose [a]	40	$g.L^{-1}$
$(NH_4)_2SO_4$	20	$g.L^{-1}$
Urea [b]	5	$g.L^{-1}$
KH_2PO_4	1	$g.L^{-1}$
$Na_2HPO_4.2H_2O$	1	$g.L^{-1}$
$MgSO_4.7H_2O$	0.25	$g.L^{-1}$
L-isoleucine[a]	0.14	$g.L^{-1}$
$CaCl_2$ *stock solution*	1	$mL.L^{-1}$
protocatechuic acid stock solution	2	$mL.L^{-1}$
trace element solution I	1	$mL.L^{-1}$
trace element solution II	1	$mL.L^{-1}$
D-pantothenate stocksolution[a]	1	$mL.L^{-1}$
biotin stock solution	1	$mL.L^{-1}$
kanamycin stock solution	1	$mL.L^{-1}$

[a] concentration might differ in experiments where this compound is part of the experimental design
[b] only in (pre)cultures without pH regulation

Glucose was autoclaved separately for shake flask experiments and precultures and added filter sterilized in stirred bioreactors. The $CaCl_2$ *stock solution* is autoclaved along with the basic salt solution and all other stock solutions are added filter sterilized. Care was taken to avoid precipitations on the filter. The potent chelating compound protocatechuic acid (Liebl et al., 1989) forms a precipitate with the *trace element solution I* and at a low pH. The two solutions of trace elements produce a yellow precipitation together. Therefore, immediately after addition of the *protocatechuic acid stock solution* and after *trace element solution I*, the filter was first flushed with some water or glucose solution before addition of the following compound. Also after addition of all compounds which were added filter sterilized, the filter was flushed with some water to assure that no large amounts of the compounds stay on the filter.

Stock Solutions

Stock solutions were stored frozen at -20°C in aliquots of 2 or 15 mL. The composition of the stock solutions is shown in table 5.3 to 5.9

Table 5.3.: Calciumchloride Stock Solution

Substance	**Concentration**	
$CaCl_2.2H_2O$	10	$g.L^{-1}$

Table 5.4.: Protocatechuic Acid Stock Solution

Substance	**Concentration**	
protocatechuic acid	15	$g.L^{-1}$
$5M\ NaOH$ *solution*	20	$mL.L^{-1}$

Table 5.5.: Trace Elements Solution I

Substance	**Concentration**	
$FeSO_4.7H_2O$	28.5	$g.L^{-1}$
$MnSO_4.H_2O$	16.5	$g.L^{-1}$
$CuSO_4.5H_2O$	0.7625	$g.L^{-1}$
$ZnSO_4.7H_2O$	6.3	$g.L^{-1}$
$CoCl_2.6H_2O$	0.13	$g.L^{-1}$
$NiCl_2.6H_2O$	0.0425	$g.L^{-1}$
$Na_2MoO_4.2H_2O$	0.065	$g.L^{-1}$
$KAl(SO_4)_2.12H_2O$	0.028	$g.L^{-1}$
$Na_2SeO_3.5H_2O$	0.0193	$g.L^{-1}$
$H_2SO_4(95-97\%)$	2	$mL.L^{-1}$

Table 5.6.: Trace Elements Solution II

Substance	**Concentration**	
H_3BO_3	0.05	$g.L^{-1}$
$SrCl_2.7H_2O$	0.05	$g.L^{-1}$
$Ba_2Cl.2H_2O$	0.05	$g.L^{-1}$

Table 5.7.: D-Pantotheate

Substance	Concentration	
Ca-D(+)-pantothenate	0.238	$g.L^{-1}$

Table 5.8.: Biotin Stock Solution

Substance	Concentration	
biotin	0.85	$g.L^{-1}$

Table 5.9.: Kanamycin Stock Solution

Substance	Concentration	
kanamycin sulphate	25	$g.L^{-1}$

5.1.3. Fermentation

As far as not stated differently, experiments were performed at a pH of 7.6 and at $30°C$, shaken at 150 rpm with 25 mm amplitude in 500 mL shake flasks with 50 mL medium and 4 baffles or with a controlled dissolved oxygen tension (DO) kept at 30% of saturation with air in stirred bioreactors.

Seed Cultures

For production of seed lots, 50 mL complex medium (see table 5.1 on page 90) was inoculated with a frozen seed lot and cultivated under standard conditions (at $30°C$, shaken at 150 rpm with an amplitude of 25 mm in 500 mL Erlenmeyer flasks with 4 baffles). As soon as an OD_{600} of 5-10 was reached, the entire culture was added to 25 mL of an autoclaved 70% glycerol solution and mixed. This mixture was divided in aliquots of 1.5 mL and placed at $-80°C$. The resulted seed lots performed very well, regarding the short or absent lag times.

From the original culture provided by Dr. Eggeling, one set of master seed lots was produced this way. From this set, a series of working seed lots was produced which were used for the final experiments.

Precultures

At the start of an experiment, an entire 1.5 mL working seed lot is used to inoculate a 500 mL shake flask containing 50 mL complex medium (see table 5.1 on page 90). This culture was allowed to grow under standard conditions for about eight hours, after which it usually reached an OD_{600} of 10-15.

This culture is used to inoculate a second preculture, containing defined medium with urea (see table 5.2 on page 92) with 1-3% v/v. This culture was allowed to grow for about 14 hours (usually overnight) after which it was measured and used for inoculation of the production culture with 1-5% v/v, leading to an initial OD_{600} of less than 1 in the production culture. The second preculture was introduced in order to get rid of the influence of the complex components in the medium.

Stirred Bioreactor

All experiments which were planned by the experimental design techniques for model development as well as several other experiments have been performed in a stirred glass bioreactor. A schematic view of the reactor system is shown in figure 5.3.

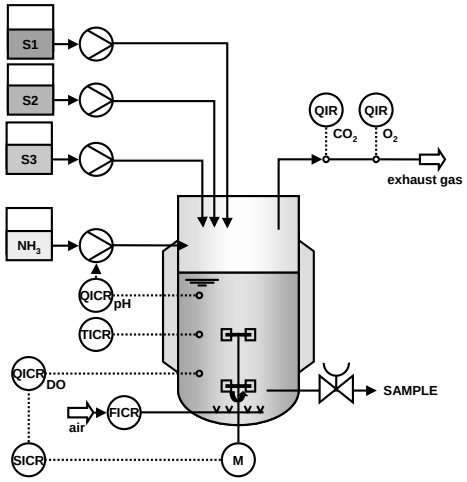

FIGURE 5.3.: Simplified schematic diagram of the stirred bioreactor system. Three feeds with substrates S1, S2 and S3 are added. The pH is measured and controlled by addition of ammonia. The temperature is controlled and the dissolved oxygen tension is controlled over the stirrer rate.

The 3-liter reactor (with about 2 L working volume) was equipped with electrodes for online measurement of the pH, temperature and DO (see also 5.1.4 on page 97) and a double 6 blade turbine impeller. The control of stirring rate, the pH at 7.6, the DO at 30% and the temperature at $30°C$ was done by the internal controllers of the Labfors system (Infors AG, Bottmingen, Switzerland). The pH was controlled by addition of a solution of about 25% m/v NH_3. The DO was controlled by adjustment of the stirring

rate between 100 and 700 rpm. At the start of the experiments, the aeration rate was 1 L/min. When the DO dropped below 30% during stirring at 700 rpm, the aeration was increased to 1.5 or 2 L/min. In the production experiment, higher aeration rates (up to 7 L/min, which however has little effect) and higher stirring rates (up to 1000 rpm) were used.

When foam developed, antifoam was added manually with a sterile syringe through a septum. In the first experiments, only antifoam 204 from Sigma (Sigma-Aldrich Chemie GmbH, Steinheim, Germany) was used. The first droplets of this antifoam always performed very well at first, but in some occasions in a later stage of the experiments, the effect of this antifoam was not satisfactory. Both silicon based antifoam M-30 from Serva (Serva, Heidelberg, Germany) and 7745 from Merck (Darmstadt, Germany) were shown to perform much better in this situation so in later experiments, either of these silicon based antifoams was used. In some experiments, both the antifoam from Sigma in an early stage and the silicon antifoam from Merck in a later stage were used, which seemed to be the most successful combination for our system. The antifoams were sterilized by autoclavation before use.

Feeds of glucose or other solutions were added into the reactor by Dosimat 665 systems (Metrohm AG, Herisau, Switzerland) with the feed rates adjusted manually. As a check on the proper addition by the Dosimats, the remaining volume after the experiment was measured and the weight of the Dosimats and the feed solutions together was measured and logged during the experiment. No problems were detected with the Dosimat systems.

Online data were logged using the software Medusa which has been developed in our institute.

Before taking a sample, about 10 mL of suspension was taken from the bioreactor and discarded to flush the sampling port. Directly after this, about 15 mL of suspension was taken from the bioreactor. The exact total volume taken from the reactor during sampling was estimated using a 10 mL graduated cylinder in order to estimate the remaining volume in the reactor as accurately as possible. Two 1.5 mL Eppendorf reaction vessels with the sample suspension were centrifuged (10 minutes, 13000 rpm, Biofuge pico, Hereaeus, Hanau, Germany) and the supernatant stored frozen at $-20°C$ for future measurement of amino acids, organic acids and glucose. These measurements were usually performed within 1 or 2 weeks after the fermentation to avoid problems with decomposition of the compounds which is known to occur even at $-20°C$ (Cooper et al., 1983). The OD_{600} and pH and in some samples also the glucose concentration of the suspension taken from the bioreactor, were measured immediately after taking the sample. In samples from several experiments, also 2 to 10 mL of the suspension (depending on the OD_{600}) was used for measurement of the biomass dry weight.

5.1.4. Analytics

pH

The pH value in the bioreactor was measured online using gel filled pH-electrodes (Mettler Toledo, Gießen, Germany). The electrodes were calibrated before autoclavation using buffers with a pH of 4 and 7 at room temperature. During fermentation, the pH of the samples, taken from the reactor was measured offline in a similar way. These offline values were used to adjust the calibration of the electrodes in the fermentation equipment.

DO

The dissolved oxygen tension (DO) was measured in the stirred bioreactor by a polarometric electrode (Ingold, Gießen, Germany). The electrode was calibrated, after autoclavation together with the bioreactor, by saturation of the medium at $30°C$ with nitrogen gas for the 0 and with air for 100%.

Temperature

The temperature was measured using a pT100 temperature probe. In the stirred bioreactor, the electrode was placed in the suspension and the temperature was controlled by adjusting the temperature of the water flowing through the double wall of the bioreactor. The temperature of the shake flasks was controlled by measuring and controlling the temperature in the room or cabinet in which the flasks were shaken.

CO_2 and O_2 in Exhaust Gas

From the outgoing gas stream, a constant flow of about 0.8 L/min was pumped through devices for measurement of CO_2 and O_2. The constant flow was achieved by a membrane pump and a manual flow meter (Kobold, Hofheim/Taunus, Germany) behind the two measurement devices which were placed in series. The CO_2 was measured by near infrared spectroscopy in a Binos 4b2 device (Leybold, Hanau, Germany). For measurement of the O_2 an Oxynos 100 (Rosemount, Hanau, Germany) was used, which uses a paramagnetic measurement method. The exhaust gas was first water-cooled using a condenser installed directly above the reactor, recycling the condensate. After this, the exhaust gas stream towards the gas analysers was cooled and dried again by an electric gas cooler (ECP1000, M&C Products Analysentechnik GmbH, Ratingen, Germany).

The analysers were calibrated before each experiment using the same flow rate. N_2 was used for setting the zero of both the CO_2 and O_2 measurements. A gas mixture containing 5% CO_2 was used for calibration of the CO_2 measurement and air was used for calibration of the O_2 measurement at 20.9%. The calibration was repeated at the

end of the experiment and the drift of the calibration was used to adjust the logged values, assuming the drift took place linearly over time.

OD_{600}

The main measure of the biomass concentration which was used, was the optical density at 600 nm (OD_{600}). The OD_{600} was measured using a spectrophotometer (UV-160, Shimadzu, Duisburg, Germany) with plastic cuvettes with a width of 1 cm. The samples were diluted in a 0.9% m/v NaCl solution (physiological saline) before measurement, to ensure an OD_{600} between 0.1 and 0.4.

The OD_{600} was used because it is much easier and faster to measure than the biomass dry weight, especially at low concentrations where very large samples are necessary for measurement of the dry weight as mentioned in the next paragraph.

Biomass Dry Weight

While using the OD_{600} as a measure of the concentration of biomass, it is assumed that the amount of active cell mass per volume of suspension is directly proportional to the OD_{600}. However, changes in the physiology of the cells under different conditions may very well influence the ratio between the OD_{600} and the amount of biomass. The cell volume is, for instance, known to be dependent on the osmolarity (Rönsch et al., 2003) and the size of the cells influences the optical density.

The biomass dry weight was measured as well as the OD_{600} during some experiments in the stirred bioreactor, in order to determine the ratio between the two measures and as a check on the assumption that this ratio is constant. For measuring the biomass dry weight in a sample, small 0.2μm filters (FP30/0,2 CA, Schleicher & Schuell, Dassel, Germany) were dried at 70°C, left to cool in an excicator and weighed. A sample with a known volume of 2-10 mL of suspension was filtered through the filter and the pellet was washed with an equal volume of physiological saline. The filter was then dried again at 70°C for about 24 hours and left to cool to room temperature in an excicator. The dried filters were weighed again and the biomass concentration was calculated by dividing the difference between the weight of the filter after and before use, by the sample volume.

Some results are shown in appendix B on page 139, showing a fairly constant ratio between the OD_{600} and biomass dry weight of 0.25 $g.L^{-1}.OD^{-1}$.

Glucose

Two methods of measurement of the glucose concentration in the fermentation suspension were used.

First, the glucose concentration in some samples was measured fast, directly after taking the samples, using the Accu-Chek® Sensor Comfort teststrips (Roche Diagnostics, Mannheim, Germany). Samples were diluted in physiological saline to assure that the

concentration was in the proper range of 0.1 to 6 g/L. In the used test strips, the glucose is converted to gluconolacton by glucoseoxidase. During this reaction, a small current is produced which is measured.

After a finished experiment, the glucose concentrations in the samples of supernatant were measured by an enzymatic assay in 96 well microtiter plates using hexokinase and glucose-6-phoshatedehydrogenase, similar to the Boehringer enzymatic analysis kit. The samples were diluted in water to about 0.3 g/L glucose. Standard solutions of 0.05-0.5 g/L glucose were measured at least in duplo on each plate. All samples were measured in duplo or triplo. In the assay, the glucose is converted to glucose-6-phosphate by hexokinase using ATP. This glucose-6-phosphate is then converted together with NAD to 6-phosphogluconate and NADH by glucose-6-phoshatedehydrogenase. The NADH was measured spectrophotometrically at 340 nm in a Thermo$_{max}$ microtiterplate-reader (Molecular Devices, Sunnyvale Ca., USA).

The enzymatic method in microtiter plates is more accurate and less expensive than the measurement in the teststrips mentioned above, but it takes much more time.

Amino Acids

The concentrations of several amino acids were determined in the stored samples of the supernatant by reversed phase high-performance liquid chromatography (HPLC, Sykam, Gilching, Germany) after derivatisation with ortho-phthaldialdehyde (OPA) (Lindroth and Mopper, 1979). The amino acids of interest were L-alanine, L-glycine, L-valine, L-isoleucine and L-leucine. Samples were first diluted with water in order to contain 10-200 μM of the relevant amino acids. The used standards contained 50 μM of the amino acids and 500 μM ammonium. A typical chromatogram of standard solutions is shown in figure 5.4.

The amino acids were derivatised with OPA and mercaptoethanol (OPA reagent, Pierce Europe BV, Oud-Beijerland, the Netherlands) for 1.5 minutes before they were separated on a reversed-phase column (Lichrospher 100 RP 18-5, 125 mm long, 4 mm diameter and 100 Å pore size, Merck, Darmstadt, Germany). During this pre-column derivatisation, the primary amines react with OPA and mercaptoethanol to the corresponding fluorescent isoindols. The elution from the column is done isocratically with a filtered solution containing 50% v/v of a 10 mM phosphate puffer of pH 7.2, 35% v/v methanol and 15% v/v acetonitril. Behind the column, the isoindols are detected fluorimetrically (Shimadzu RF-535 detector, excitation wavelength 330 nm, emission wavelength 450 nm, Shimadzu, Duisburg, Germany)

The isocratic elution with the used elution buffer at 0.9 mL/min, was found to be suitable for the fast separation of the relevant amino acids. Especially the separation of ammonium and L-valine was found to be rather difficult with the used system, which was originally used with a gradient with an increasing methanol concentration. This separation is very important for our purpose, because high concentrations of ammo-

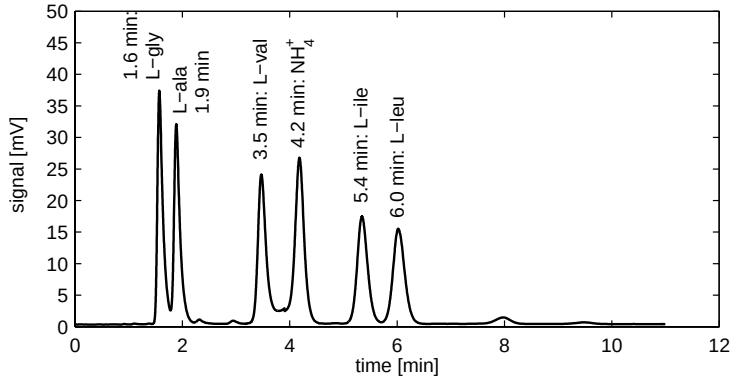

FIGURE 5.4.: Chromatogram of amino acid standards. The signals are labeled, including the retention time. All detected amino acids were added in concentrations of 50 μM whereas 0.5 mM ammonium was present.

nium and L-valine occur in the experiments and L-valine is, of course, a very important variable to be measured. In the initial phase of the experiments, there is only little L-valine available, but rather high concentrations of ammonium, which made the quantitative measurement of L-valine even more difficult at this stage. Either a relatively slow procedure with a long period with a low methanol concentration, or the fast isocratic elution with more methanol were found to be the best with respect to the separation of ammonium and L-valine in the used HPLC system (personal communication of Heidi Haase-Reiff, data not shown) and the isocratic procedure was preferred for its speed and simplicity.

Samples were diluted with water before measurement, in an attempt to have about the same concentration in the sample as in the standard solutions (50 μM). However, samples were diluted at least 50 times, because the measurement of more concentrated samples was problematic, probably due to limitation by OPA rather then the amino acids, as is addressed in more detail in appendix D on page 151.

Organic Acids

The concentrations of some organic acids in the supernatant were measured using a HPLC (Sykam, Gilching, Germany) with ion exchange chromatography (100 μL sample on a column: Aminex-HPX-87H, 300 $\times$ 7.8 mm, Biorad, München, Germany), with isocratic elution with 0.2 N H_2SO_4, 0.5 mL/min, 40°C. The separated acids were detected by UV detection at 215 nm (S3300, Sykam, Gilching, Germany). The organic

acids which were measured by this technique, were citrate, α-ketoglutarate, pyruvate, succinate, lactate, ketoisovalerate, acetate and fumarate. Samples were diluted in water before measurement if necessary, in order to get samples in the range of 0.2-5 times the standard concentrations of each acid, which are mentioned at figure 5.5, which shows a typical chromatogram of the standards.

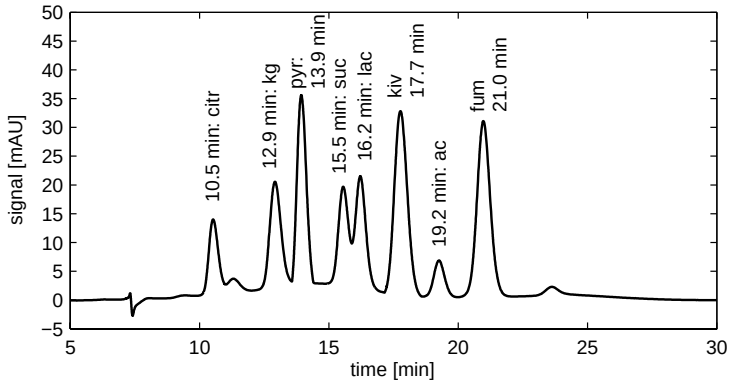

FIGURE 5.5.: Chromatogram of organic acid standards. The signals are labeled including the retention time. The used abbreviations and the corresponding concentrations are: citr: 0.2 mM citrate, kg: 0.2 mM α-ketoglutarate, pyr: 0.5 mM pyruvate, suc: 0.01 mM succinate, lac: 1 mM lactate, kiv: 0.5 mM keto-isovalerate, ac: 1 mM acetate and fum: 0.01 mM fumarate.

5.2. Modeling Based Process Development

5.2.1. Preliminary Experiments

The model based approach which is presented here, requires that all relevant characteristics of the process are either included in the models or kept within a range in which the influence does not change significantly. For instance certain media components such as trace elements, can be supplied in such a concentration from the start of the experiments, that they will not become limiting or inhibiting during the fermentations. Other factors such as the pH and the dissolved oxygen tension (DO), can be measured and controlled relatively well on-line with standard fermentation equipment. On the other hand, the factors which have an important influence on the course of the process and which we want to use in the development of the process, need to be included in the model. Therefore, before starting the model based procedure, it has to be decided which

factors are to be included in the models and for other factors appropriate initial concentrations or controlled set-points need to be determined. Some of these decisions can be made, based on theoretical knowledge on the biological and technical systems, but for some choices, experimental work might be required. Some examples of such experiments are the experiments which led to the adaptation of the CGXII medium as mentioned in paragraph 5.1.2 on page 90. Also the Ramos-experiments shown in appendix C on page 141 are examples of such preliminary experiments.

5.2.2. Initialization: Batch Data

The initialization of the model based approach was done using data from a simple batch experiment with initial concentrations of 222 mM glucose, 1.1 mM L-isoleucine and 1 μM pantothenic acid.

From these data, it is not yet possible to discriminate between effects caused by L-isoleucine and by pantothenic acid. These two compounds have therefore been regarded as 1 'complex' compound at this stage. A similar approach might be used when real complex media are used, although there are some obvious risks of regarding combinations of substances as one substance. In our case, assuming that it is always the same of the two compounds which gets limiting or inhibiting first when being used always in the same ratio, this simplification might be acceptable in this first example of the use of the model discriminating experimental design approach.

The measured and some derived results of the batch experiment are shown in figure 5.6. The yields, specific rates and reaction rates are used to set limits on the model parameter values (see also chapter 3) and to determine likely model structures as will also be discussed in the following paragraph.

Data Analysis and Modeling

First note that the results in figure 5.6 are rather inaccurate in the initial phase of the experiment, since the concentrations of biomass and product are very low and also the changes in measured concentrations are still very small.

The results show a relatively short period with a high specific growth rate, after which the growth still goes on for an appreciable period at a lower rate. The inhibition by product or limitation by depletion of L-isoleucine and pantothenic acid (being one variable together) were implemented in the Monod-type models in an attempt to describe this phenomenon. Furthermore, also since these approaches did not seem to be really successful, the option of ongoing growth after depletion of the substrates was introduced. Possible mechanistic explanations for such behaviour could be the decrease of the amount of these compounds per cell after depletion of the extracellular pools (which, of course, would be possible only in a very limited range) or the hypothesis that one of the introduced auxotrophies would not be complete, due to (possibly slow or 'ex-

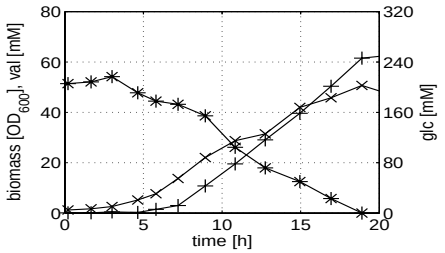

(a) Concentrations. Biomass as $\times$ in OD_{600}, glucose as $*$ in mM and L-valine as $+$ in mM

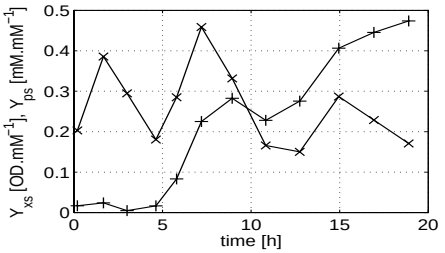

(b) Yields. Y_{xs} as $\times$ in $OD_{600}.mM^{-1}$, Y_{ps} as $+$ in $mmol_{val}.mmol_{glc}^{-1}$

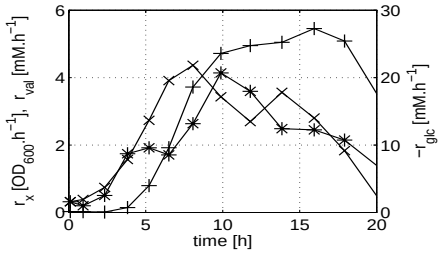

(c) Rates. r_X as $\times$ in $OD_{600}.h^{-1}$, r_{glc} as $*$ in $mM.h^{-1}$ and r_{val} as $+$ in $mM.h^{-1}$

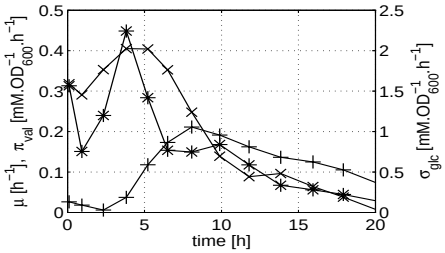

(d) Specific Rates. μ as $\times$ in h^{-1}, σ_{glc} as $*$ in $mM.OD_{600}^{-1}.h^{-1}$ and π_{val} as $+$ in $mM.OD_{600}^{-1}.h^{-1}$

FIGURE 5.6.: Results of the preliminary batch experiment. Lines are only a visual aid.

pensive') alternative metabolic pathways or alternative (possibly less effective) enzymes. The ongoing growth was implemented either as a minimal specific growth rate without the compounds, or as a minimum on the growth rate without these compounds. At the same time, depletion of glucose could still limit the rates further.

Two ways of dealing with multiple substrates were used: either the multiplication of Monod-terms, or the non-interactive way using the smallest of the rates according to the different substrates (see paragraph 2.3.2 on page 14). The additive way has not been used, since neither L-isoleucine nor pantothenic acid is regarded as sole essential substrate. Glucose is always needed as carbon and energy source for the organism and situations of glucose depletion were not allowed in the designed experiments.

The results show that a higher specific production rate is found in the period with a lower specific growth rate than during maximal growth. In some models, the organism was therefore assumed to be able to use more glucose for production of L-valine in the same time, when it cannot be used for growth due to growth limitation by other substrates. That way, when the growth rate would be limited by a limited availability of L-isoleucine or pantothenic acid, the corresponding decrease in the need for glucose for biomass production would not lead to a proportional decrease in glucose uptake, but (partly also) to a higher flux into the L-valine production.

This way, around 30 models were formulated. After estimation of the parameter values of these models, the chi-squared values were calculated for all model fits and the best eight models were selected for use in the following model discriminating design. The fit of the best and the worst of these eight models to the data are shown in figure 5.7 to illustrate the maximum range of differing model predictions. All eight models visually fit satisfactory with only small differences between the goodness of the fits as is also indicated by the relative 'prior' accuracies mentioned in figure 5.10.

All eight selected models have in common that some growth was possible after depletion of L-isoleucine or pantothenic acid.

The fitted values of the model parameters of the eight selected models and the estimated standard deviations of these parameters are shown in appendix E on page 153. Obviously, several parameters are poorly estimable from the batch data.

5.2.3. Model Discriminating Experiment I

An experiment was planned to discriminate between these eight models, using the adjusted design criterion of Box and Hill (BH criterion). The designed experiment is shown in figure 5.8, illustrated by the expected measured values of the two best fitting models. Here, L-isoleucine and pantothenic acid are still used in the same fixed ratio of 1.1 mM to 1 μM and regarded as one substrate.

Some clear differences between the competing models are expected, for instance in the final product concentrations of the two shown model predictions. It is, however, hard to judge the design, when many models are involved. Furthermore, in the criterion of

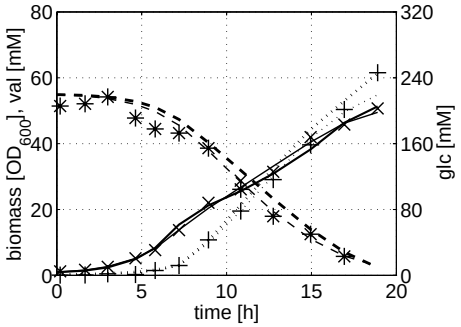

FIGURE 5.7.: Fit of the best (with thick lines) and worst (thin lines) of the 8 selected models to the first batch experiment. Markers show the measured values whereas lines are the simulated values of the fitted models. Biomass is shown in solid lines and $\times$ as OD_{600}. Dashed lines and $*$ indicate glucose concentrations in mM and L-valine concentrations are shown as dotted lines and $+$ in mM.

Box and Hill, it is often rather the differences in model variances than the differences in the expected concentrations, which determine the design. This holds especially when large variances of the model parameters occur, as is the case here. These differences in model variances and also relative differences in predicted concentrations, are likely to be high when limiting compounds change fast and reach very low values according to one of the models. This might explain why conditions of very low glucose concentrations were created twice, after 30 and 40 hours of fermentation. The expected concentrations according to all models stayed just above the allowed limit, which was very low in this experiment (10^{-6} mM).

This experiment has been performed and the resulting data are shown in figure 5.9, together with the specific rates derived from these results.

Data Analysis and Modeling

The results are not exactly as one of the models predicted. Although not all data are shown, this is also illustrated by the fact that model parameters of all models changed drastically upon re-estimation after the new experiment. The glucose uptake rate was lower than expected in the first 30 hours, but somewhat higher at the end of the experiment. Furthermore, the biomass concentration stayed below the expected values, but the growth rate did go on faster than expected after 30 hours. The relative goodness of fit of the eight models before and after the model discriminating experiment, calculated from the chi-squared values as mentioned in paragraph 2.4.3 on page 19, are shown in figure 5.10(a). Clearly, the differences between some fits have increased, indicating that

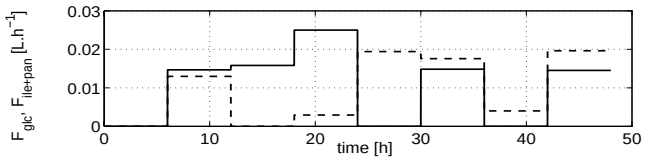

(a) Feedrates in L/h. Feed of a 500 g/L glucose solution as a solid line and of a solution containing 22 mM L-isoleucine and 20 μM pantothenic acid as a dashed line.

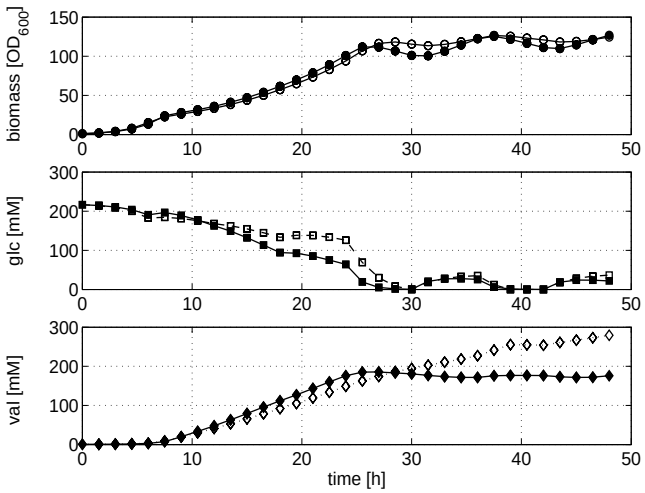

(b) Expected concentrations of the best model with closed markers and the second best fitting model with open markers. Biomass in OD_{600}, glucose in mM and L-valine in mM. Markers are placed at all measurement times.

FIGURE 5.8.: Planned model discriminating experiment I. The initial concentrations of biomass was an OD_{600} of 1. Initial concentrations of 217 mM glucose, 1.1 mM L-isoleucine, 1 μM pantothenic acid and 0.6 mM L-valine were used.

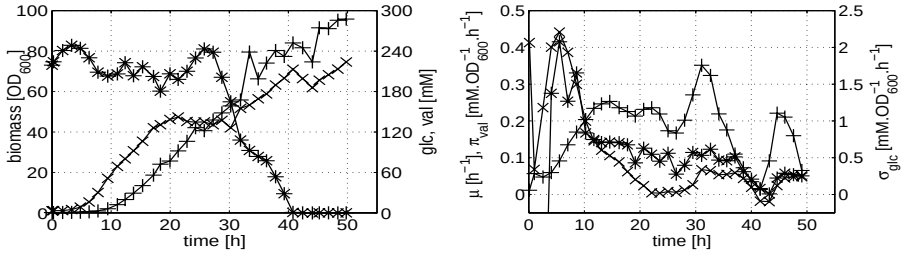

(a) Concentrations. Biomass as $\times$ in OD_{600}, glucose as $*$ in mM and L-valine as $+$ in mM

(b) Specific Rates. μ as $\times$ in h^{-1}, σ_{glc} as $*$ in $mM.OD^{-1}.h^{-1}$ and π_{val} as $+$ in $mM.OD^{-1}.h^{-1}$

FIGURE 5.9.: Results of model discriminating experiment I. Lines are only a visual aid.

the discrimination between these models improved. However, many of the models have reached a visually comparable fit, due to the partly strongly changed parameter sets. This is a general problem of the suggested procedure, which is likely to occur in the initial phase of the process development. When the inaccuracy of the model parameters are accounted for in the design criterion, as is the case here, it is only a slight adjustment of the parameter values which is regarded, but not the possibility of using a very distinct parameter set, possibly describing another local optimum in the parameter estimation problem. When a few of such distinct sets are known, which provide acceptable fits to the prior data, they could, however, be used as separate models in the model discriminating design criterion.

The amount of models taken into account for the model discriminating design should be limited, in order to keep calculation times at an acceptable level and to avoid the designed experiment to be more designed to keep the predictions of all models within the allowed bounds, than to find differences between the models. This, together with the fact that partly large changes in the parameter values occur upon re-estimation after a new experiment, makes it necessary to also reconsider 'rejected' models, as was also suggested by several others (Buzzi-Ferraris et al., 1990; Chen and Asprey, 2003).

The fit of the best model at this stage might be regarded satisfactory based on the direct visual image in figure 5.10, although it clearly fails to describe some effects properly. Purely based on the $\tilde{\chi}^2$ values, this may not always be very clear. The current situation provides a representative example: since we know that the rate of addition of L-isoleucine and pantothenic acid was increased after 26 hours[1], the clear increase in the growth rate after this point is qualified as important. The best fit, however, does not show this effect properly, but with a more or less constant growth rate, the simulated

[1]This corresponds more or less to 24 hours in the planned experiment, considering a delayed fermentation due to a reduced inoculum concentration and a lag-time.

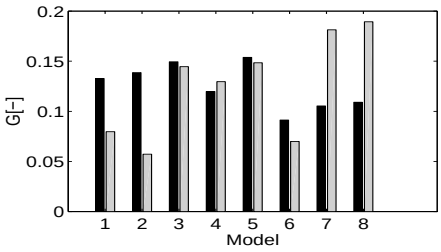

(a) Relative goodness of fit of eight of the competing models before the model discriminating experiment as solid black bars and after the experiment as grey bars. The models were given arbitrary numbers.

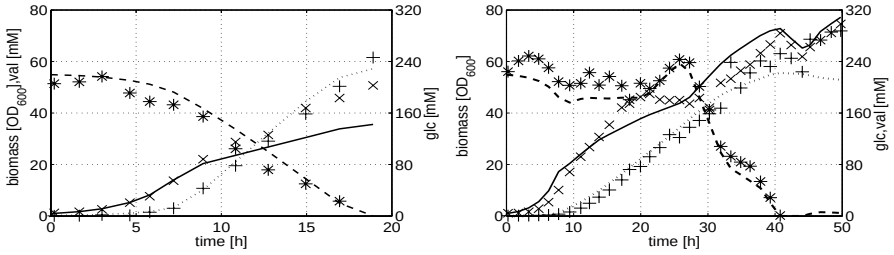

(b) Fit of the best model after model discriminating experiment I. The left plot shows the fit to the data of the first batch experiment and the right plot to the model discriminating experiment. Markers indicate measured values and lines simulated values. Biomass is shown as solid lines and $\times$ as OD_{600}, glucose in mM as dashed lines and $*$ and L-valine in mM as dotted lines and $+$.

FIGURE 5.10.: Results of fitted models after model discriminating experiment I.

concentrations stay relatively close to the measured ones. In such a situation, a clear trend in the residual plot occurs as can be seen in figure 5.11.

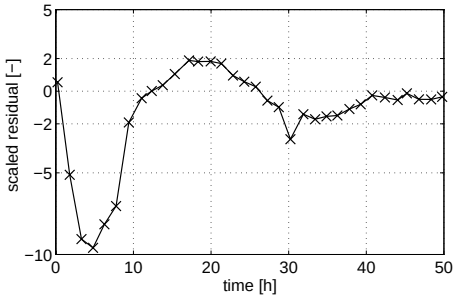

FIGURE 5.11.: Residuals between the measured biomass concentrations of model discriminating experiment I and the corresponding model predictions of the best fitting model after model discriminating experiment I. The residuals are scaled by the estimated standard deviations of the measured values.

The scaled residuals should form a horizontal line with only noise added to it, without clear trends. The simulated biomass concentrations are constantly higher than the measured ones during a long period before the mentioned change in the growth rate at 26 hours, resulting in positive residuals in this period. This is the other way around after this point, with negative residuals. Although the scaled residuals of the biomass measurements stay within the bounds of -2 to 2 in this period[2], a clear trend can be identified, which indicates that not all important features of the process are modeled properly.

The models which suggest the growth rate to be limited by glucose and inhibited by L-valine after 30 hours of fermentation, do not show the reaction upon the increased availability of L-isoleucine and pantothenic acid, whereas the models which presume these latter substrates to be limiting, react too strong. Therefore, inhibition of L-isoleucine and pantothenic acid uptake by L-valine was introduced in several models. This was also suggested by the finding that *C. glutamicum* contains an import system which imports different branched chain amino acids, so that the uptake of L-isoleucine through this system is inhibited competitively by L-valine (Boles et al., 1993; Ebbighausen et al., 1989).

Due to the fact that the glucose consumption rate was slightly higher than expected, and with the very low allowed expected glucose concentrations, some starvation effects

[2]This, of course, depends strongly on the used standard deviations, which were around 10%, 5% and 5% for biomass, glucose and L-valine respectively, with an increasing relative inaccuracy at low values. See also equation 3.1 on page 47 and the used values mentioned in appendix E on page 153.

seem to have occurred after about 41 hours. In this period, also the pH increased up to 7.8. Therefore, it was decided to discard the measurements from this point onwards. Noteworthy, the discriminating power of the experiment of course decreases very much upon discarding these points.

Such differences between the planned experiments and the achieved results are a general problem of performing off-line determined feed trajectories without feedback control on the resulting concentrations and is even more so a problem when the trajectories are based on poor models. One option to partly avoid this problem would be to use on-line measurement of the substrate concentration and feedback control of the trajectories. In that case, instead of feed trajectories, concentration profiles are planned. The output variables which show the differences between the models, are then the trajectories of the feeds needed to control the concentrations at their desired levels. One obvious drawback of such a system is the fact that an accurate online measurement system is needed.

5.2.4. Intuitiv Discrimination between L-Isoleucine and Pantothenic Acid

The results of an experiment in RAMOS shake flasks (see appendix C) have shown that both L-isoleucine and pantothenic acid can become limiting together at the same time and that both components clearly have different effects. This, together with the fact that the models after the first two experiments did not describe all important characteristics of the process satisfactory, were reasons to discriminate between the two compounds in the models. However, at this point, the available data did not support the fitting of models with both substances properly, since they have been used in identical ways and their concentrations could not be measured. Therefore, it was not possible to plan the next experiment on a model based way, but first, an intuitively planned experiment was needed.

The idea behind this experiment was a sequential limitation strategy: the experiment was started with a decreased pantothenic acid concentration. The cells were expected to run into a phase with pantothenic acid limitation. A pulse of L-isoleucine was added during this phase, in order to verify the fact that L-isoleucine was not the limiting factor. Then, pantothenic acid would be added, relieving the limitation until possibly L-isoleucine would get limiting. Glucose would be fed so that about 25 mM glucose would be present during the entire fermentation, which was expected to be neither limiting nor inhibiting.

The performed experiment and the resulting concentrations are shown in figure 5.12, together with the (specific) rates and yields which were derived from these data.

Data Analysis and Modeling

The specific L-valine production rates of the current experiment was lower than during model discriminating experiment I shown in figure 5.9 on page 107. It seems like the

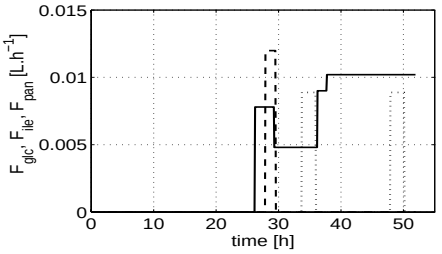

(a) Feedrates in L/h. Feed of a 500 g/L glucose solution as a solid line, of a 132 mM L-isoleucine solution as a dashed line and a 40 μM pantothenic mM acid solution as a dotted line.

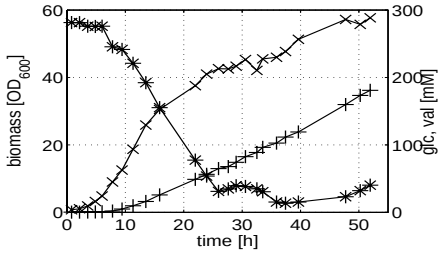

(b) Measured concentrations. Biomass as $\times$ in OD_{600}, glucose as $*$ in mM and L-valine as $+$ in mM

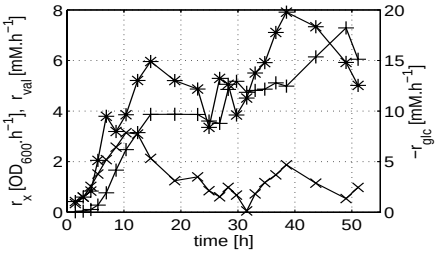

(c) Rates. r_X as $\times$ in $OD_{600}.h^{-1}$, r_{glc} as $*$ in $mM.h^{-1}$ and r_{val} as $+$ in $mM.h^{-1}$

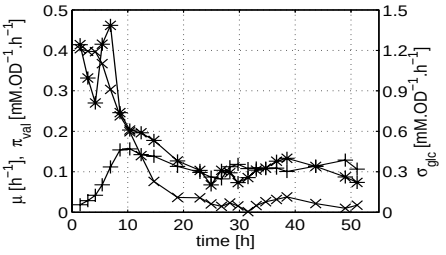

(d) Specific Rates. μ as $\times$ in h^{-1}, σ_{glc} as $*$ in $mM.OD^{-1}.h^{-1}$ and π_{val} as $+$ in $mM.OD^{-1}.h^{-1}$

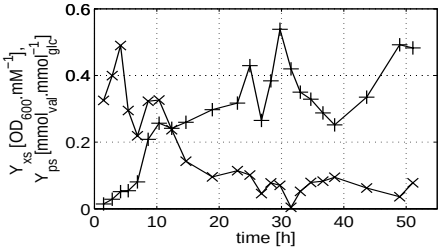

(e) Yields. Y_{xs} as $\times$ in $OD_{600}.mM^{-1}$, Y_{ps} as $+$ in $mmol_{val}.mmol_{glc}^{-1}$

FIGURE 5.12.: Results of the intuitively planned experiment for discrimination between L-isoleucine and pantothenic acid. Initial concentrations of L-isoleucine and pantothenic acid were 1.07 mM and 0.486 μM respectively.

limited availability of pantothenic acid in the current experiment limits not only the growth, but also the production rate. This is an effect which was not accounted for in the models so far. Since coenzyme A, which is formed from pantothenic acid, is used in many processes in the cell, there are several scenarios imaginable to describe this, but it was not a known characteristic before. This limitation of the production rate has been implemented in several models in slightly different ways, for instance by multiplied Monod terms, limited by glucose and by pantothenic acid, in the kinetics of L-valine production, or by a similar approach as the non-interactive approach used for multiple growth substrates.

A large set of more complex models was created this way and fitted to all data of the prior three experiments. Five models were selected which fit satisfactory, the best and the worst of which, based on their $\tilde{\chi}^2$, are shown in figure 5.13, indicating the maximal range of differing model predictions. The five models fit very satisfactory and only very

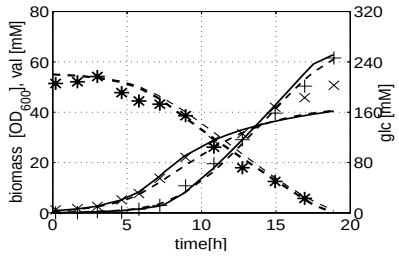

(a) Fit to the first batch experiment.

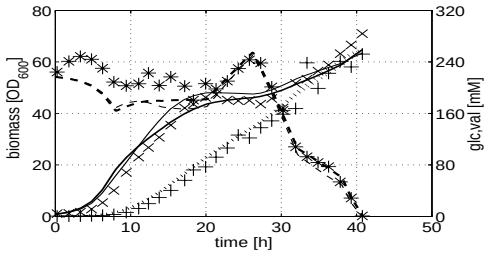

(b) Fit to model experiment I.

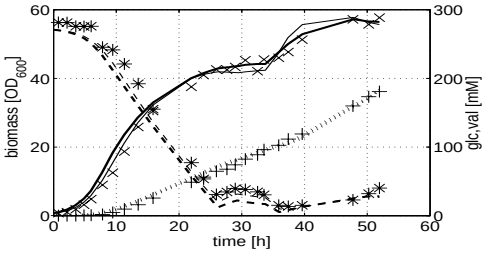

(c) Fit to the intuitively planned third experiment.

FIGURE 5.13.: Fit of the best as thick lines and worst as thin lines of the five selected models after the intuitively planned experiment. Markers indicate the measured values. Biomass is shown by solid lines and $\times$ in OD_{600}, glucose in mM by dashed lines and $*$ and L-valine in mM by dotted lines and $+$.

small differences are found between the five fits at this point. The model equations and

the estimated parameter values are shown in appendix F on page 162. Many model parameters are still poorly estimable from the available data.

5.2.5. Model Discriminating Experiment II

An experiment was planned to discriminate between the five selected models, using the ND criterion mentioned in paragraph 2.5.1 on page 32. The designed experiment is shown in figure 5.14, illustrated by the expected responses of the two best fitting models.

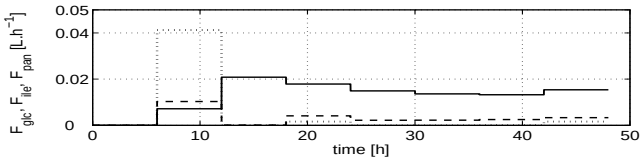

(a) Feeds in L/h. Flow of 500 g/L glucose feed as a solid line, of 55 mM L-isoleucine as a dashed line and of 50 μM pantothenic acid as a dotted line.

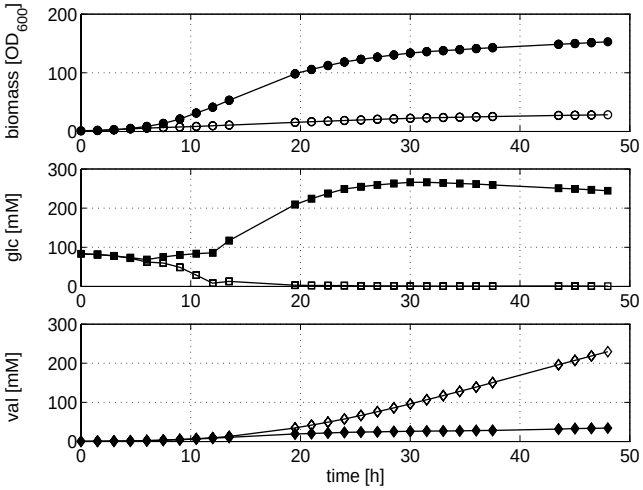

(b) Expected concentrations of the best model with solid markers and the second best fitting model with open markers. Biomass concentrations as OD_{600}, glucose in mM and L-valine in mM. Markers are placed at all measurement times.

FIGURE 5.14.: Designed model discriminating experiment II. Initial concentrations of L-isoleucine and pantothenic acid were 0.881 mM and 5.00 μM respectively.

The expected responses show large differences, for instance a very low glucose concentration during the largest part of the fermentation according to the best fitting model and rather high concentrations according to the second best model. This clearly indicates that a proper model discriminating experiment is expected, based on the current models.

The results of the performed experiment are shown in figure 5.15.

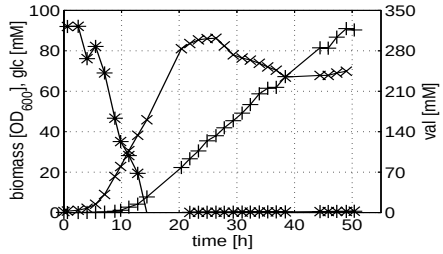

(a) Concentrations. Biomass as $\times$ in OD_{600}, glucose as $*$ in mM and L-valine as $+$ in mM

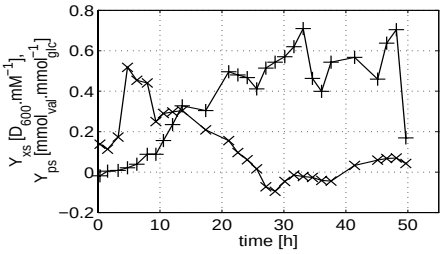

(b) Yields. Y_{xs} as $\times$ in $OD_{600}.mM^{-1}$, Y_{ps} as $+$ in $mmol_{val}.mmol_{glc}^{-1}$

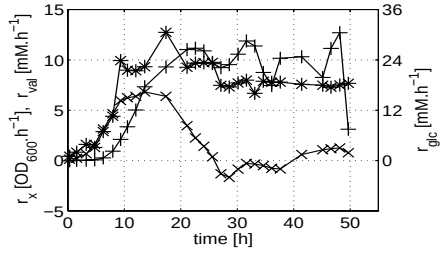

(c) Rates. r_X as $\times$ in $OD_{600}.h^{-1}$, r_{glc} as $*$ in $mM.h^{-1}$ and r_{val} as $+$ in $mM.h^{-1}$

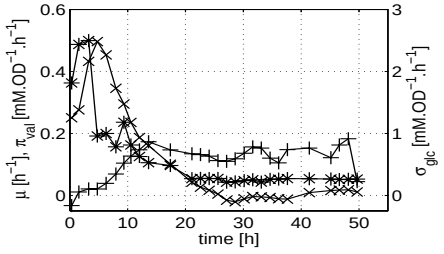

(d) Specific Rates. μ as $\times$ in h^{-1}, σ_{glc} as $*$ in $mM.OD^{-1}.h^{-1}$ and π_{val} as $+$ in $mM.OD^{-1}.h^{-1}$

FIGURE 5.15.: Results of model discriminating experiment II. Lines are only a visual aid.

Data Analysis and Modeling

After re-estimation of the model parameters, the relative goodness of the fits of the models was calculated. The parameters before and after re-estimation are shown in appendix F on page 162. The relative goodness of the fits of the competing models before and after the model discriminating experiment are shown in figure 5.16(a). The models were coded 2.1 to 2.5 to emphasize the fact that the models are different from the models mentioned before.

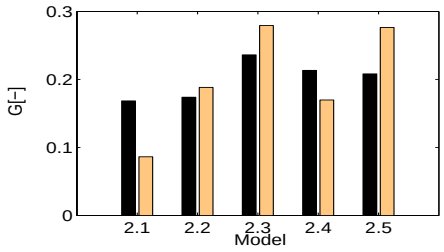

(a) Relative goodness of fit of the five used competing models before model discriminating experiment II as solid black bars and after the experiment as grey bars. The models were given arbitrary numbers.

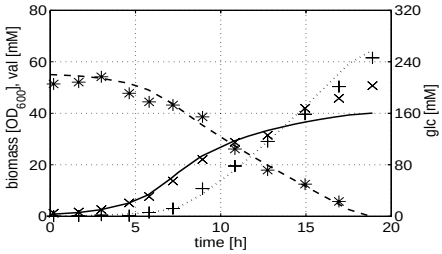

(b) Fit of the best fitting model after model experiment II to the first batch experiment.

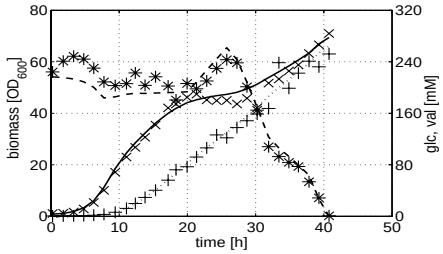

(c) Fit of the best fitting model after model experiment II to model discriminating experiment I.

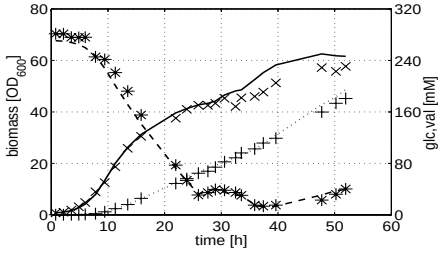

(d) Fit of the best fitting model after model experiment II to the intuitively planned third experiment.

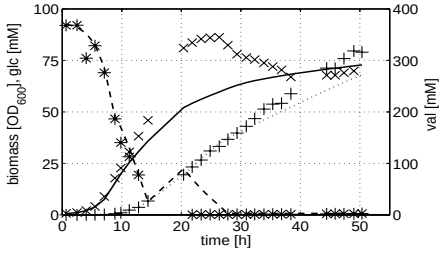

(e) Fit of the best fitting model after model experiment II to model discriminating experiment II.

FIGURE 5.16.: Results of fitted models after model discriminating experiment II. Markers indicate measured values and lines simulated values. Biomass is shown as solid lines and $\times$ as OD_{600}, glucose in mM as dashed lines and $*$ and L-valine in mM as dotted lines and $+$.

Due to the results of model discriminating experiment II, the discrimination between the five competing models has improved and model 2.3 and 2.5 are now being favored. These two models are very similar. They differ only in the way the decrease of the intracellular amount of L-isoleucine can depend on the L-valine production rate or on the amount of pantothenic acid which has been taken up so far as can be seen in appendix F. It might very well be that both model structures can not be distinguished properly within the region of interest, but this remains to be tested.

The new experiment cannot be described completely satisfactory by the used models. The problem lies in the fact that the only possibility for decrease of the biomass concentration which was included in the models was dilution. From the negative rates and specific rates in figure 5.15(c) and 5.15(d), it can be seen that the decrease around 30 hours is too large to be caused by dilution only. Such starvation effects were not goal of the modeling.

5.2.6. Optimized Process

The final goal of the 'modeling based process development' approach is the design of the optimized production process, possibly also with (model based) process control. Furthermore, performing an optimized production process can be very useful during process development to make sure that the developed model describes the process properly under the conditions of interest. In the current paragraph, an example is given of such an optimized production process.

The model

In the modeling and experimental design procedure presented so far, little attention has been paid to simplification of the models. Many introduced extensions to the models were expected to yield only small improvements of the fits. The positive effect of low amounts of parameters through the weighting of the reduced chi-squared values is rather weak. Furthermore, it was hypothesized that the design of experiments to discriminate between the extended models would not be less effective than designing to discriminate between simplified versions.

However, for use in process optimization and especially for process control, it is important to use models which are as simple as possible.

Certain parts of the resulting models have very little influence on the model predictions within the range of interest. This can be indicated by very large standard deviations of the parameter, and by very high or very low parameter values. Such indications have been used to simplify the best model 2.3 somewhat. The reduced model is shown in appendix F on page 162.

Off-line Optimized Process

This simplified model was used to calculate optimized feed trajectories and initial conditions. The criterion which was chosen to be optimized was the total volumetric productivity (see paragraph 3.4.3 on page 59). This criterion was calculated for each of the fixed measurement time-points in 1.5 h intervals. Of course, it can be expected that the highest value of the criterion is found at an earlier time than the maximal allowed duration of 48 h. At this point, the designed production experiment is then stopped.

The same limits and constraints which were used for the model discriminating experiments were used. However, the resulting optimized process, shown in appendix G on page 173, suggested a fast growth up to an OD_{600} of about 150. Such high concentrations of actively growing biomass have such a high oxygen uptake rate, that the DO could not be kept at the desired setpoint of 30% of saturation with air in the used equipment. Therefore, an extra constraint of a maximal expected biomass concentration of an OD_{600} of 70 was introduced.

The designed optimized experiment is shown in figure 5.17.

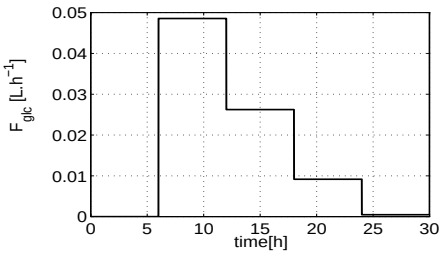

(a) Feed of 500 g/L glucose in L/h.

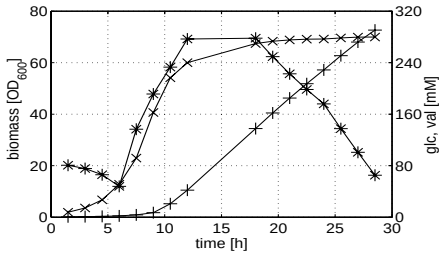

(b) Expected concentrations of the production experiment. $\times$ indicate biomass as OD_{600}, $*$ indicate glucose in mM and L-valine in mM is indicated by $+$. Markers are placed at all measurement times. Lines are only a visual aid.

FIGURE 5.17.: Designed production experiment. The designed initial concentrations were 91.7 mM glucose, 3.27 mM L-isoleucine and 10 μM pantothenic acid.

The feeds of L-isoleucine and of pantothenic acid are omitted from figure 5.17, because the feeds were clear below the minimal feeding rate during the entire experiment. Obviously, no important beneficial effect of extra feeding of these compounds was expected, enough could be supplied in the initial medium and the dilution effect by the feeds by itself is of course negative for the obtained total volumetric productivity.

The designed experiment has been performed and the results of this experiment are shown in figure 5.18.

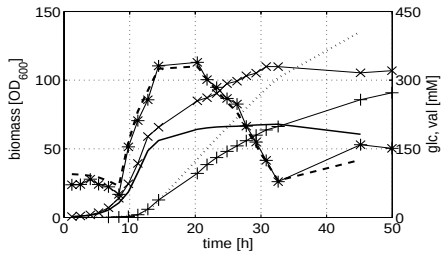

(a) Concentrations. Connected markers are measured values and lines without markers show the simulated values. Biomass as $\times$ and a solid line in OD_{600}, glucose as $*$ and a dashed line in mM and L-valine as $+$ and a dotted line in mM

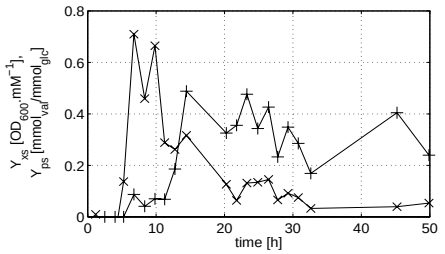

(b) Yields. Y_{xs} as $\times$ in $OD_{600}.mM^{-1}$, Y_{ps} as $+$ in $mmol_{val}/mmol_{glc}$

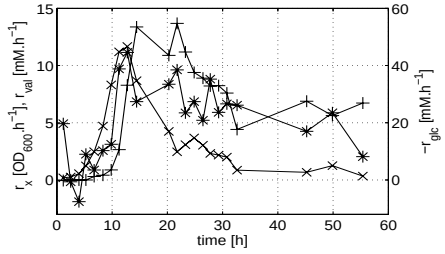

(c) Rates. r_X as $\times$ in $OD_{600}.h^{-1}$, r_{glc} as $*$ in $mM.h^{-1}$ and r_{val} as $+$ in mM, h^{-1}

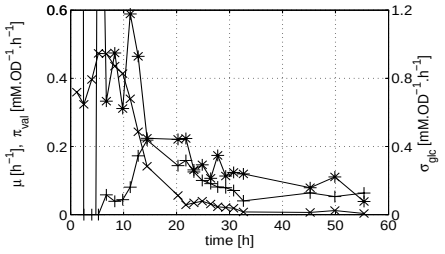

(d) Specific Rates. μ as $\times$ in h^{-1}, σ_{glc} as $*$ in $mM.OD^{-1}.h^{-1}$ and π_{val} as $+$ in $mM.OD^{-1}.h^{-1}$

FIGURE 5.18.: Results of the production experiment.

Model Validation

The optimized process was not only performed to demonstrate the use of the developed type of models for process optimization, but it also acts as a validation experiment for the model. A model should not only be judged by the way it describes prior data, but it should also be tested with data which were not used during model development.

In this respect, note that the model predictions shown by the thick lines in figure 5.18(a) are calculated with the model parameters as estimated before the production experiment, so the parameters have not been re-estimated after the optimized production experiment.

The first obvious discrepancy between the expected- and obtained results, is the fact that the biomass concentration gets higher than expected and the concentration of L-valine stays a lot lower than expected. The ongoing growth at a relatively low (specific) rate was already noted during the model discriminating experiments and implemented in the models in different ways, for instance by allowing growth without L-isoleucine or pantothenic acid. Furthermore, also higher specific production rates at lower specific growth rates were found and implemented in the models (see also paragraph 5.2.2 on page 102). The developed model did however still not predict these characteristics of the process properly in the production experiment.

Such differences are rather likely to occur when a strong extrapolation of the model predictions is performed outside the conditions which were used during model development, which was clearly the case here. This limited possible extrapolation is a well-known problem of the use of models. The limitations or inhibitions which occurred in the production experiment are likely to be of another nature than the limitations and inhibitions which were important in the prior experiments. This will also be discussed in paragraph 5.3 on page 121. This problem with strong extrapolation is an important reason why an 'optimized production experiment' such as performed here, is also a very useful experiment during model development and should not necessarily be performed only after the model has been determined very accurately.

The simulated glucose concentrations fit very satisfactory to the achieved measured concentration. The differences between the measured values and the expected values based on the designed experiment (i.e between the glucose concentrations in figure 5.17(b) and 5.18(a)), were largely caused by differences between the planned- and the actual performed experiment. This is also a well-known problem which could be circumvented by using some sort of feedback control based on online measured values, as discussed before.

Of course it should be mentioned that the used model was still partly relatively poorly estimable from the available data, as indicated by the partly high standard deviations of the model parameters as shown in appendix F on page 162. This is another reason why some discrepancy between the model predictions and the real experimentally obtained results is to be expected. Furthermore, when a model is not able to describe the prior

data perfectly, it is also likely to show some errors in its predictions.

Process Improvement

In figure 5.19, the volumetric productivities of all experiments are compared.

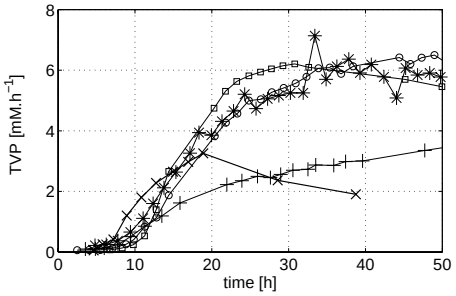

FIGURE 5.19.: Total volumetric productivities (TVP) of all experiments in $mM.h^{-1}$. $\times$: preliminary batch, $*$: model discrimination I, $+$: intuitive discrimination between L-isoleucine and pantothenic acid, $\circ$: model discrimination II, $\square$: production experiment.

The production experiment has been continued longer than planned and the results, shown in figure 5.19, show that the timing of the end of the process at about 30.5[3] hours was pretty good.

Clearly, the optimized experiment shows the highest volumetric productivity of all experiments in the period from 20 to 30 hours, reaching 6.2 $mM.h^{-1}$, which is more than 11% improvement compared to the next-best experiment at about 30 hours. In the model discriminating experiments, however, comparable total volumetric productivities were achieved at later time-points and higher product concentrations. By this time, the *expected* total volumetric productivity of the optimized experiment was actually a lot higher, but the very high production rate from 12 to 20 hours could not be maintained. Obviously, unexpected limitations or inhibitions occurred, as also mentioned in the preceding paragraph.

Noteworthy, the two experiments which were designed to discriminate between competing models, had a much better total volumetric productivity than the preliminary batch or the intuitively planned experiment. This can easily be explained when we realize that the difference between some models would only become apparent at higher product concentrations. Since no product was added to the cultures at the start of the experiments, the model discriminating experiments are likely to be designed to produce

[3]The designed experiment suggested to stop 28.5 hours after reaching an OD_{600} of 1, which corresponded to approximately 30.5 hours in the real experiment.

much product in a short time, e.g. have a high total volumetric productivity. This should also be taken into account when appreciating the 11% achieved improvement[4].

5.3. Biological Information from Modeling Based Process Development

Although the models are primarily aiming at describing the overall process and improving the process conditions, the results can also provide important information for a better understanding of the underlying biological processes and potentially also for further strain improvements.

5.3.1. Modeling

Models which allow for further growth after depletion of L-isoleucine or pantothenic acid seem to describe the process better, as was already mentioned in paragraph 5.2.2 on page 102. This is an important result and it would be interesting to investigate this aspect further. It is interesting to know whether this phenomenon is caused by alternative metabolic routes for production of these compounds or the production of biomass with a lower content of these compounds. The measurement of the total amount of L-isoleucine, free and bound in cell proteins, after long periods of L-isoleucine limitation, could for instance show whether alternative routes of L-isoleucine production are present in the cells and indicate the real minimal amount of L-isoleucine needed per amount of biomass. Recent results suggested that an alternative metabolic route for L-isoleucine may be present in the cells, but further research is still necessary (data not shown).

The decrease in the specific production rate upon strong limitation by pantothenic acid, which was found in the experiment in paragraph 5.2.4, is also very interesting. The possible effects of limited availability of coenzyme A, which is derived from pantothenic acid, are diverse and it seems likely that the available data are still too few to properly determine optimal profiles of pantothenic acid supply. With the used data, no important positive effect of reduced pantothenic acid concentrations was found within the used range. The theoretical idea behind limiting the pantothenic acid concentration and therewith the coenzyme A concentration, was to increase the availability of pyruvate for L-valine production. The fact that some pyruvate was even found extracellularly in the intuitively designed experiment with little pantothenic acid, as shown in figure 5.20(b) on page 123, is a good indication that this effect can be achieved. However,

[4] Allowing the addition of L-valine in the designed model discriminating experiments for model discrimination would probably have been very beneficial for model discrimination, although it might also make the modeling more difficult when differences between addition of L-valine and production of L-valine turn out to be important

the corresponding positive effect on the flux towards L-valine is not apparent. The fact that some extracellular pyruvate was also found at the end of the prolonged production experiment, as also shown in figure 5.22(b) on page 124, indicates that at this stage, it is not the availability of pyruvate which limits the production of L-valine. Large intracellular concentrations of pyruvate can also explain the production of L-alanine, which is also a member of the pyruvate family of amino acids, as will be discussed in the next paragraph.

Another interesting aspect is the fact that very high concentrations of glucose were used in the optimized production experiment. This positive effect of high glucose concentrations is reflected in the very high Kp value, the binding constant for production of L-valine from glucose. This value is with 56 mM much higher than can be expected for a real enzymatic binding constant. Compare for instance the Km value which was estimated for the PTS system for glucose uptake to be less than 0.6 mM and even for alternative systems with low affinity, values below 10 mM were reported (Gourdon et al., 2003). It is however not unusual that unphysiologically high concentrations lead to extra production or production of other products through overflow mechanisms. The underlying mechanisms of such processes are not yet all well understood.

5.3.2. By-products

The modeling based process development approach needs only measurement of the state variables which are used in the models. However, also other (by-)products can present important indications for the modeling and for understanding of the underlying biological processes, as is already apparent from the discussion on the measurement of extracellular amounts of pyruvate above. In figure 5.20 to 5.22, the extracellular concentrations of some amino acids and other organic acids of the last three experiments are shown.

The most striking result of the measured by-products of the intuitively planned experiment for discrimination between L-isoleucine and pantothenic acid, is the extremely high extracellular concentration of keto-iso-valerate. The net rate of the transamination from keto-iso-valerate to L-valine is very low in this experiment. This transamination is catalysed by two transaminases in *C. glutamicum* (McHardy et al., 2003). Radmacher, however, has shown that transaminase B, encoded by the gene *ilvA*, is the only transaminase which produces the branched-chain amino acids at a significant rate in the used strain (Radmacher et al., 2002). The available transaminase C activity, which is also able to produce L-valine with L-alanine as amino donor, is not likely to contribute significantly (Leyval et al., 2003). The amino donors of transaminase B are aliphatic amino acids, normally mainly glutamate. The resulting α-ketoglutarate can then be converted back to glutamate with ammonium by the enzyme glutamate dehydrogenase.

Interestingly, the production of L-leucine stays relatively low in the intuitive experiment. The production of L-leucine as a by-product can be expected, since it is also produced from keto-iso-valeric acid and its production was not hampered by genetic

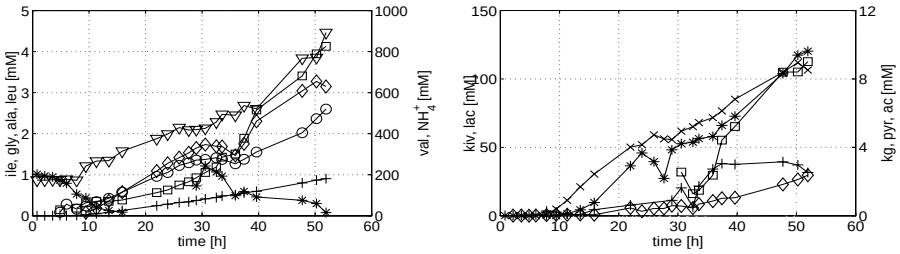

(a) Amino acids and ammonium, in mM. L-valine (val) is shown as $+$, L-isoleucine (ile) as $*$, L-glycine (gly) as $\circ$, L-alanine (ala) as $\square$, L-leucine (leu) as $\Diamond$ and ammonium as $\triangledown$.

(b) Organic acids, in mM. Keto-isovalerate (kiv) is shown as $\times$, α-ketoglutarate (kg) as $*$, pyruvate (pyr) as $+$, lactate (lac) as $\Diamond$ and acetate (ac) as $\square$.

FIGURE 5.20.: Concentrations of amino acids and organic acids in the intuitively planned experiment for discrimination between L-isoleucine and pantothenic acid.

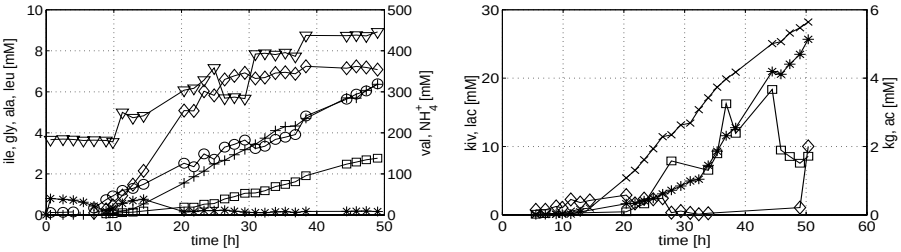

(a) Amino acids and ammonium, in mM. L-valine (val) is shown as $+$, L-isoleucine (ile) as $*$, L-glycine (gly) as $\circ$, L-alanine (ala) as $\square$, L-leucine (leu) as $\Diamond$ and ammonium as $\triangledown$.

(b) Organic acids, in mM. Keto-isovalerate (kiv) is shown as $\times$, α-ketoglutarate (kg) as $*$, lactate (lac) as $\Diamond$ and acetate (ac) as $\square$.

FIGURE 5.21.: Concentrations of amino acids and organic acids in model discriminating exsperiment II.

modifications. Although the concentration of its precursor keto-iso-valeric acid is very high in the intuitive experiment, the production of L-leucine is about 2 times lower than in the other two shown experiments. This corresponds to the lower production of L-valine. Noteworthy, the same transaminase is responsible for leucine- and valine production.

It remains a very interesting question, what causes the apparently very low (net) transamination rate towards L-valine (and L-leucine) in the intuitively planned experiment. The fact that a much higher specific L-valine production rate is found in, for instance, model discriminating experiment II, with a lower (but still appreciable) concentration of keto-iso-valerate, is an important indication that higher specific transamination activities can be achieved in the used strain. One obvious difference between the two experiments is of course the limited availability of pantothenic acid in the intuitively planned experiment. How the reduced pantothenic acid or reduced CoA concentrations may influence the transaminase activity is therefore an important question for further research.

In model discriminating experiment II, contrary to the intuitiv experiment mentioned above, no pyruvate was detected extracellularly. The traces of extracellular pyruvate in the intuitive experiment make it unlikely that the availability of pyruvate would be limiting the production of L-valine in that experiment.

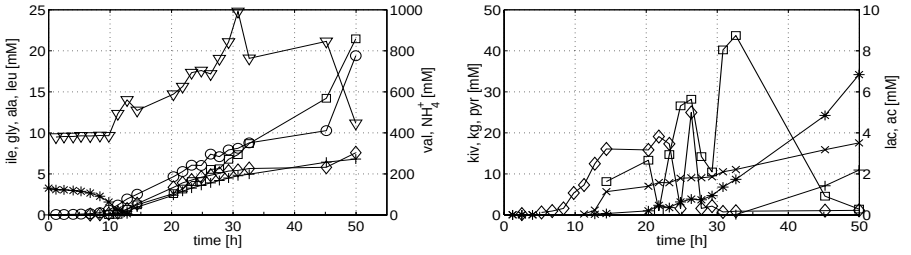

(a) Amino acids, in mM. L-valine (val) is shown as +, L-isoleucine (ile) as ∗, L-glycine (gly) as ○, L-alanine (ala) as □, L-leucine (leu) as ◊ and ammonium as ▽.

(b) Organic acids, in mM. Keto-iso-valerate (kiv) is shown as ×, α-keto-glutarate (kg) as ∗, pyruvate (pyr) as +, lactate (lac) as ◊ and acetate (ac) as □.

FIGURE 5.22.: Concentrations of amino acids and organic acids in the production experiment.

In the production experiment, relatively high concentrations of α-ketoglutarate, L-alanine and L-glycine were produced.

L-alanine is a common by-product for L-valine production, which can be expected to be produced when much pyruvate is available, since it is directly produced from pyruvate. A decreased availability of pantothenic acid was also shown to increase the production

of L-alanine in both an L-lysine producing strain (Tosaka et al., 1985) and an L-valine producing strain (Radmacher et al., 2002) of *C. glutamicum*, which was attributed to a decreased production of CoA and a corresponding decreased flow of pyruvate to acetyl-CoA. Radmacher (2001) has shown a positive influence of high oxygen supply on the production of L-valine related to L-alanine as is also discussed and confirmed in appendix C on page 141. Alanine was also a by-product of L-valine production in resting cells of *Brevibacterium* (Terasawa et al., 1990), with increasing amounts at lower ammonium concentrations. Although it is a known by-product, it remains an interesting question why the production of L-alanine was much faster in the production experiment, resulting in a much higher ratio between L-alanine and L-valine. The higher L-alanine production and its apparent increase upon reduced oxygen availability corresponds to the production of lactate and acetate.

Also L-glycine is a known by-product. It was also produced in appreciable amounts in a closely related strain which produces D-pantothenic acid (Chassagnole et al., 2003, 2002). Again, it remains an interesting question what causes the high production rate of this by-product in the production experiment in an absolute sense, but especially also relative to the L-valine production.

The high production rate of α-ketoglutarate in the production experiment was not expected. As stated before, this compound can be converted to L-glutamate by glutamate dehydrogenase using ammonium as amino-donor. The measurements of ammonium by HPLC after derivatisation with OPA (see also paragraph 5.1.4 on page 99), show high extracellular concentrations of ammonium[5], which is therefore not expected to limit this reaction at the used pH (Burkovski, 2003a,b). It would be interesting to investigate why this reaction is not fast enough to keep the concentration of α-ketoglutarate at a very low level. Notably, no extracellular glutamate is detected, but it would be interesting to measure the intracellular concentration of this compound, since it could be expected that large concentrations of glutamate may inhibit the net amination of ketoglutarate. However, when the glutamate pool in the cells would be so large, the question remains why this does not lead to a faster transamination with keto-iso-valerate, which is also found extracellularly after 15 hours of fermentation.

Another striking difference between the by-products of the production experiment and the other experiments, is the fast production of some lactate and acetate already in an early period, and the later decrease of these concentrations.

Lactate and acetate are by-products which are also produced by many organisms through overflow metabolism under limited oxygen supply or at very high substrate concentrations. Also the results of the Ramos experiments in appendix C on page 141 confirm the production of acetate and lactate in the used organism at limited oxygen availability. Very interestingly, the oxygen uptake rate was much higher in the produc-

[5]This measurement method is rather inaccurate for quantitative determination of ammonium concentrations, but this information is sufficient here.

tion experiment than in the prior experiments, as also indicated by the estimated oxygen transfer rates (OTR) shown in figure 5.23. The sudden peaks in the OTR in the pro-

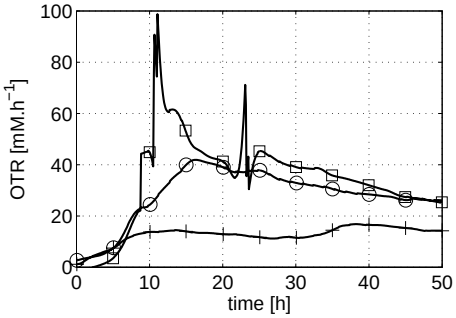

FIGURE 5.23.: Oxygen transfer rates in $mM.h^{-1}$. +: intuitive discrimination between L-isoleucine and pantothenic acid, ∘: model discrimination II, □: production experiment. Lines show the values derived from online measurements. Markers are only added to distinguish between the lines.

duction experiment are caused by changes in the aeration rate. The estimated oxygen transfer rates are rather inaccurate, since only small differences in the oxygen concentration in the gas phase are used to derive these values. The indicated differences between the oxygen transfer rates in the different experiments is however surely significant, as is also confirmed by the differences in the required stirrer speed (data not shown). The high OTR in the production experiment even provided difficulties to control the *DO* at the desired level of 30% of saturation with air , especially between 10-15 hours, where more than 1000 rpm stirrer speed was not even really sufficient, leading to a decrease in the *DO*, as shown in figure 5.24. It is not expected that the short decrease in the *DO* from 30 to 20% after about 13 hours had a large influence, but it cannot be excluded. Surely, the influence of the oxygen tension and the oxygen transfer is a very interesting field for further research, as also indicated in appendix C. The oxygen demand in the production experiment decreased again already after 15 hours, also indicated by a decrease in the required stirrer speed and the estimated OTR and it steadily decreased from this point onwards. It seems likely that the early production of lactate and acetate and the later uptake of these compounds was influenced by the high oxygen consumption rate in the first period and the decreased oxygen consumption in the later phase.

One other remarkable difference between the production experiment and all prior experiments is the long period of L-isoleucine depletion from about 15 hours onwards. Also in the intuitively planned experiment, a period of L-isoleucine depletion started at about the same time, but this was relieved by addition of L-isoleucine after about 28 hours,

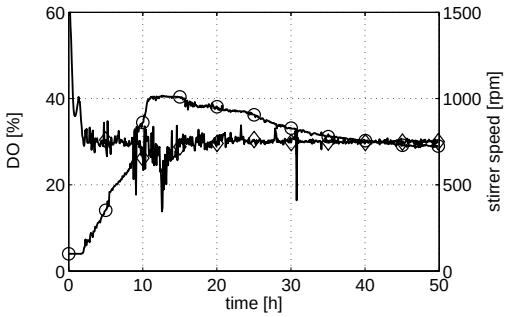

FIGURE 5.24.: Dissolved oxygen tension (DO, with ◊) and stirrer speed (in rpm with ○) in the production experiment. A DO of 100% corresponds to saturation with air. Markers are only added to distinguish between the lines of online measured values.

after which L-isoleucine was taken up again. To illustrate this aspect, the estimated total amount of isoleucine, taken up per gram biomass, is shown in figure 5.25. Note that

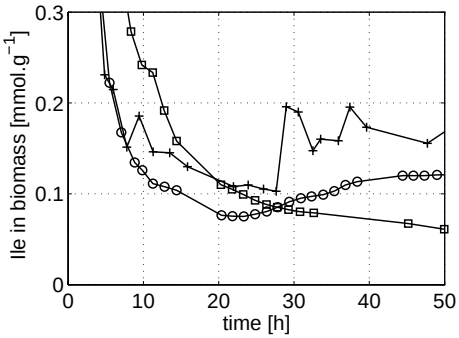

FIGURE 5.25.: Isoleucine used by the cells in $mmol$ per g biomass dry weight. +: intuitive discrimination between L-isoleucine and pantothenic acid, ○: model discrimination II, □: production experiment.

this amount is estimated from the amount which was supplied and it does not regard how much L-isoleucine degradation might have taken place in the cells. Furthermore, when alternative routes of L-isoleucine production would be present in the cells, this is also not regarded. Although such alternative metabolic routes towards ketobutyrate or L-isoleucine were not expected, it should not yet be excluded. The final amount of isoleucine which was taken up by the cells, is lower than the 142 $\mu mol.g^{-1}$ which was

reported for a very closely related pantothenate producing strain (Chassagnole et al., 2003), especially towards the end of the production experiment.

Many (by-)products increase to high concentrations in the late phases of the experiments. These high concentrations are likely to have an influence on the behaviour of the organism. Only the inhibiting effect of high concentrations of L-valine is used in the models to account for these effects. This is one of the obvious simplifications which might not allow proper description of the real effects, but within certain bounds, it may be sufficient for the use for optimization and control purposes. It could, for instance, very well be, that the osmolarity rather than the L-valine concentration is a major cause for decreased glucose uptake rates and decreased product yields (Gourdon et al., 2003), or possibly also an increased glucose uptake rate (Varela et al., 2003). The osmolarity could of course also be used as a state variable in the models, but this was not done in the used models up to now.

Carbon Balance

It could very well be, that not all important by-products are detected with the used analytics. This can be addressed using an elemental balance, such as a carbon balance. The way the carbon of the used substrates is divided among different products can also provide suggestions for possible improvements of the process or the strain. The C-balance of model discriminating experiment II and the production experiment are shown in figure 5.26.

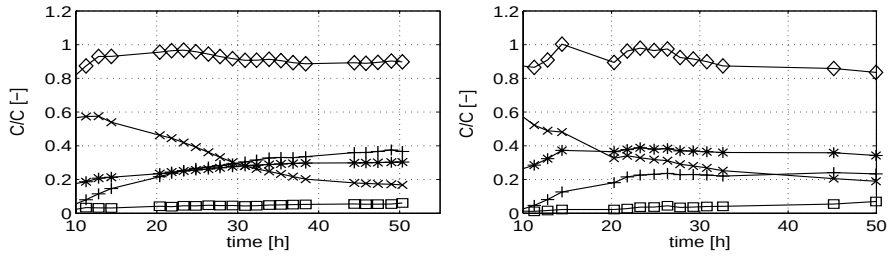

FIGURE 5.26.: Carbon balance. The left plot shows data from model discriminating experiment II and the right plot shows data from the production experiment. The total C-balance is shown as $\Diamond$, the fraction of the used C bound in L-valine is shown as $+$, in biomass as $\times$, in CO_2 as $*$ and the sum of all other measured amino-acids and organic acids as $\Box$.

In the production experiment, relatively much CO_2 and biomass are formed, compared to model discriminating experiment II. This could be expected, since only the total volumetric productivity was used as an optimization criterion. In an attempt to produce

L-valine as fast as possible, first, relatively much biomass should be produced as fast as possible, which is then used to produce the product. As mentioned before, even larger amounts of biomass were suggested by the optimization routine without the limit on the maximal biomass concentration. The large concentration of very active biomass is likely to produce much CO_2.

When the overall yield of product on glucose would be used as the design criterion, the opposite would happen: very little biomass is formed, which slowly produces L-valine (data not shown). This extreme situation does not seem very useful. In appendix G on page 173, the optimized expected process is shown where the yield is optimized with an additional constraint on the minimal final L-valine concentration, which was included by introducing a penalty function in the criterion when lower concentrations are reached. The process reaches exactly the minimal value in exactly the maximal allowed time.

The C-balances are not completely closed and the gap seems to be increasing over time. This is an indication that unknown by-products are produced in substantial amounts. In this respect, it must however be mentioned that especially the exact amounts of carbon in CO_2 and bound in biomass are rather inaccurate. The ratio between OD_{600} and dry biomass weight and the relative carbon content of the biomass are both not known exactly for the used organism and may also not be constant (see also appendix B). Nevertheless, it is likely that some unknown by-products are produced. It is, for instance, known that many of the relevant enzymes, also including the overexpressed ones, have a relatively broad substrate spectrum which could lead to the production of several keto-acid- or amino-acid analogues (Eggeling et al., 1997). This point is already illustrated by the fact that the same enzymes are responsible for the production of both L-valine and L-isoleucine. The partly very high concentrations of several intermediates is likely to lead also to the increase in other intracellular pools and therefore also possibly the excretion of intermediates which were not yet measured.

5.4. Conclusions

A model with 27 parameters was developed using the presented approach with four dynamic experiments. Two model discriminating design criteria were successfully used: the BH criterion and the ND criterion. Another experiment was planned using the same experimental design framework, maximizing the total volumetric productivity, reaching 6.2 $mM.h^{-1}$.

The developed model predicted especially the glucose consumption very satisfactory. However, also some discrepancy between the model predictions and the outcome of the experiments was identified, allowing for further model improvement.

This also provides a good example why it is important to try to use process relevant conditions, also during modeling and process development. Therefore, besides the model discriminating design criteria and the criteria for improvement of the parameter estima-

tion, also the use of criteria which aim at optimizing the production are useful during model development. Within the same framework, such criteria were easily implemented.

With the five dynamic experiments, also very much mechanistic information was obtained under process relevant conditions. Models which allow growth after depletion of L-isoleucine or pantothenic acid were for instance shown to describe the data better. This was the first indication that either the cells can grow on by diminishing the amounts of these compounds in the cell, or alternative metabolic routes towards these compounds were present. This is a clear example of how the fitting of mathematical models to the available data can help to elucidate underlying mechanisms.

Appendici

A. Nomenclature

TABLE A.1.: Symbols and Abbreviations.

Symbol	Description	Unit
ac	acetate	
ala	L-alanine	
C	concentration	
$\mathbf{c}$	vector for selection and weighting of a set of parameters for parameter estimating design	
$C - bal$	fraction of the carbon balance, accounted for by known and measured products	-
C_C	catalyst concentration	
C_E	concentration of enhancing (i.e. not essential) substrate E	
C_f	concentration in feed f	
C_I	concentration of inhibiting compound I	
C_P	product concentration, here L-valine	mM
C_S	substrate concentration	
C_{S1}	glucose concentration	mM
C_{S2}	L-isoleucine concentration	mM
C_{S2Int}	fictive concentration of isoleucine which has already been taken up by the biomass	mM
$C_{S2,intmin}$	minimal amount of isoleucine needed by the biomass.	$mM.OD_{600}{}^{-1}$
C_{S3}	pantothenic acid concentration	μM
$C_{S3,int}$	fictive concentration of pantothenic acid which has already been taken up by the biomass	μM
$C_{S3,intmin}$	minimal amount of pantothenic acid needed by the biomass.	$\mu M.OD_{600}{}^{-1}$
C_{ss}	steady state concentration	
$[CO_2]_{in}$	relative carbon dioxide tension in the gas flow into the reactor	-
$[CO_2]_{out}$	relative carbon dioxide tension in the gas flow out of the reactor	-
$\mathbf{Cor}_\theta$	correlation matrix of the parameter estimates	
$\mathbf{Cov}_\theta$	covariance matrix of the parameter estimates	

Table A.1.: Symbols and Abbreviations (continued)

Symbol	Description	Unit
$\mathbf{Cov_m}$	covariance matrix of the measurement	
CTR	carbon dioxide transfer rate	$M.h^{-1}$
C_X	biomass concentration	OD_{600}
d	degrees of freedom	
D_f	dilution of the suspension in the reactor by addition of feed f	h^{-1}
$D_i(t1:t2)$	integral dilution of the suspension in the reactor between timepoints t1 and t2	-
DO	dissolved oxygen tension	
F	flow/flux	$L.h^{-1}$
f	function	
F_f	flux of feed f	$L.h^{-1}$
$F_{g,in}$	gas flow into the reactor	$Ln.h^{-1}$
$F_{g,out}$	gas flow out of the reactor	$Ln.h^{-1}$
F_{S1}	feed rate of glucose feed	$L.h^{-1}$
F_{S2}	feed rate of isoleucine feed	$L.h^{-1}$
F_{S3}	feed rate of pantothenic acid feed	$L.h^{-1}$
G	measure of relative goodness of fit	-
g	function	
gly	L-glycine	
i	counter	
ile	L-isoleucine	
j	counter	
$\mathbf{j}$	vector of parameter sensitivities of suggested measurement	
$\mathbf{J}$	jacobian matrix (parameter sensitivities)	
$k_{S1extra}$	factor for extra use of glucose for productions when less is needed for growth	-
$k_{S3extra}$	factor for extra uptake of pantothenic acid which is not needed directly	-
k_d	degradation constant	h^{-1}
K_S	substrate binding constant analogue to Km	mM
kd_{S2}	constant for (diffusive) uptake of L-isoleucine which is not inhibited by L-valine	$mM.OD_{600}{}^{-1}.h^{-1}$
kiv	keto-isovalerate	
kg	α-ketoglutarate	
$Ki_{P,rp}$	inhibition constant for inhibition of L-valine production by L-valine	mM

Table A.1.: Symbols and Abbreviations (continued)

Symbol	Description	Unit
$Ki_{P,rs1}$	inhibition constant for inhibition of glucose uptake by L-valine	mM
$Ki_{P,rs2}$	inhibition constant for inhibition of L-isoleucine uptake by L-valine	mM
$Ki_{P,rxs2int}$	inhibition constant for inhibition of the growth rate limited by intracellular isoleucine, inhibited by high L-valine concentrations	mM
$Ki_{S2,rp}$	inhibition constant for inhibition of L-valine production by L-isoleucine	mM
Ki_P	inhibition constant for inhibition by product P	mM
Ki_S	inhibition constant for substrate inhibition	mM
Km	Michaelis-Menten binding constant	mM
Km_{S1}	Monod constant for growth on glucose	mM
Km_{S2}	Monod constant for growth on (extracellular) L-isoleucine	mM
Km_{S2Int}	Monod constant for growth on L-isoleucine which has already been taken up	mM
Km_{S3}	Monod constant for growth on (extracellular) pantothenic acid	μM
Km_{S3Int}	Monod constant for growth on pantothenic acid which has already been taken up	μM
Kp_{S1}	binding constant for L-valine production on glucose	mM
Kp_{S3}	binding constant for L-valine production, limited by pantothenic acid	μM
lac	lactate	
lb_θ	lower bound of the limited parameter space	
lb_y	lower bound on the measurement of y	
leu	L-leucine	
m	number of competing models	
$\mathbf{M}$	information matrix	g
M_r	mass of the suspension in the reactor	
m_s	maintenance constant	
m_{S1}	maintenance constant for glucose	$mM.{OD_{600}}^{-1}.h^{-1}$
m_{S2Int}	constant for degradation of intracellular L-isoleucine	$mM.{OD_{600}}^{-1}.h^{-1}$
m_{S3Int}	constant for degradation of intracellular pantothenic acid (or CoA)	$\mu M.{OD_{600}}^{-1}.h^{-1}$
N	number of measured values	
n_s	number of sampling times	

Table A.1.: Symbols and Abbreviations (continued)

Symbol	Description	Unit
$[O_2]_{in}$	relative oxygen tension in the gas flow into the reactor	-
$[O_2]_{out}$	relative oxygen tension in the gas flow out of the reactor	-
OTR	oxygen transfer rate	$M.h^{-1}$
p	number of model parameters / counter of the model parameters	
P_i	relative probability of model i	-
p_i	probability density function of the expected measurements according to model i	
r	rate	
R	expected change in system entropy	
r_p	product (here L-valine) formation rate	$mM.h^{-1}$
$r_{p,S1}$	L-valine production rate, limited by glucose	$mM.h^{-1}$
$r_{p,S3}$	L-valine production rate, limited by pantothenic acid which has already been taken up	$mM.h^{-1}$
r_s	substrate uptake rate	
r_{S1}	rate of glucose consumption (negative)	$mM.h^{-1}$
r_{S2}	rate of L-isoleucine consumption (negative)	$mM.h^{-1}$
r_{S3}	rate of pantothenic acid consumption (negative)	$\mu M.h^{-1}$
r_x	biomass production rate (growth rate)	h^{-1}
$r_{x,s1}$	growth rate when glucose would be limiting	h^{-1}
$r_{x,s2}$	growth rate when isoleucine would be limiting	h^{-1}
$r_{x,s2ext}$	growth rate limited by extracellular isoleucine	h^{-1}
$r_{x,s2int}$	growth rate limited by isoleucine which has already been taken up	h^{-1}
$r_{x,s3}$	pantothenic acid limited growth rate	h^{-1}
$r_{x,s3ext}$	growth rate limited by extracellular pantothenic acid	h^{-1}
$r_{x,s3int}$	growth rate limited by pantothenic acid which has already been taken up	h^{-1}
$\mathbf{S}$	weighting matrix containing the expected measurement (co)variances and model variances of two competing models (CA criterion)	
s_t	standard deviation of the timing of the measurement	h
t	time	h
t_{avg}	average timepoint between two offline measured points	h
t_{lag}	lagtime	h
TVP	total volumetric productivity	$mM.h^{-1}$

Table A.1.: Symbols and Abbreviations (continued)

Symbol	Description	Unit
$\mathbf{u}$	set of control variables	
ub_θ	upper bound of the limited parameter space	
V	volume of suspension in the bioreactor	L
$\mathbf{V}$	weighting matrix containing the expected measurement (co)variances and model variances of two competing models (BF criterion)	
v_{max}	maximal specific reaction rate	
val	L-valine	
$\mathbf{W_i}$	covariance matrix of the expectation of the measurements according to model i (model variances)	
x_i	state variable i	
y	(expected) measured value	
$\hat{y}_i$	model prediction of variable y_i	
Y_{PS}	yield of product on substrate	
Y_{PS1}	yield factor for production of L-valine from glucose	$mM.mM^{-1}$
Y_{PX}	ratio between production of L-valine and biomass	$mM.{OD_{600}}^{-1}$
Y_{XS}	yield of biomass on substrate	$OD_{600}.mM^{-1}$
Y_{XS}^{ov}	overall yield of biomass on substrate	$OD_{600}.mM^{-1}$
Y_{XS1}	yield factor for biomass growth on glucose	$OD_{600}.mM^{-1}$
Y_{XS2}	yield factor for biomass growth on isoleucine	$OD_{600}.mM^{-1}$
Y_{XS3}	yield factor for biomass growth on pantothenic acid	$OD_{600}.\mu M^{-1}$
$\tilde{\chi}^2$	reduced chi-squared measure of goodness of fit	-
δ_{Fglc}	density of the glucose feed	$g.L^{-1}$
δ_r	density of the suspension in the reactor	$g.L^{-1}$
μ	specific growth rate	h^{-1}
μ_{max}	maximal specific growth rate	h^{-1}
$\mu_{max,S1}$	maximal specific growth rate limited by glucose	h^{-1}
$\mu_{max,S2ext}$	maximal specific growth rate limited by extracellular isoleucine	h^{-1}
$\mu_{max,S2Int}$	maximal specific growth rate limited by isoleucine which has already been taken up by the cells	h^{-1}
$\mu_{max,S3ext}$	maximal specific growth rate limited by extracellular pantothenic acid	h^{-1}
$\mu_{max,S3Int}$	maximal specific growth rate limited by pantothenic acid which has already been taken up by the cells	h^{-1}
μ_S	specific growth rate, limited by substrate S	h^{-1}
π_{max}	maximal specific production rate	$mM.{OD_{600}}^{-1}.h^{-1}$

Table A.1.: Symbols and Abbreviations (continued)

Symbol	Description	Unit
$\pi_{max,S1}$	maximal specific L-valine production rate, limited by glucose	$mM.{OD_{600}}^{-1}.h^{-1}$
$\pi_{max,S3}$	maximal specific L-valine production rate, limited by pantothenic acid which has already been taken up	$mM.{OD_{600}}^{-1}.h^{-1}$
σ	standard deviation	
$\mathbf{\Sigma}$	matrix of measurement variances	
σ^2	measurement variance	
σ_i^{2*}	variance of the expectation of the values according to model i (i.e. 'model variance')	
σ_i^2	measurement variance of the expected values according to model i	
$\mathbf{\Sigma_{i,m}}$	matrix of measurement variances according to model i	
$\sigma_{i,t}$	standard deviation of the expected values according to model i due to variance in the timing of the measurement	
$\mathbf{\Sigma}_{i,t}$	matrix of (co)variances caused by variance in the timing of the measurement, according to model i	
$\mathbf{\Sigma}_{ij}$	weighting matrix containing the expected measurement (co)variance of the model predictions of model i and j	
$\sigma_{y,rel.min}$	minimal relative standard deviation of measurement y	
σ_{rel}	relative standard deviation	
σ_y	standard deviation measurement y	
$\boldsymbol{\theta}$	vector of model parameters	
$\hat{\boldsymbol{\theta}}$	vector of estimated model parameters	
θ_{lim}	parameter value in the limited parameter space	
θ_{unlim}	parameter value in the unlimited parameter space	
ξ	experiment (i.e. set of control variables describing the experiment)	
ξ^*	optimized experiment	

B. Ratio between OD_{600} and Dry Weight.

The optical densities at 600 nm and the biomass dry weight, measured as explained in paragraph 5.1.4 on page 97, of the batch experiment explained in paragraph 5.2.2 on page 102, are shown in figure B.1. A few measurements from the period after depletion of the glucose, which were not regarded in paragraph 5.2.2, are also shown here.

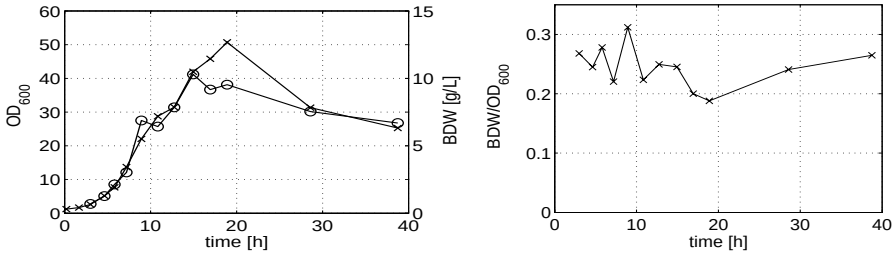

(a) OD_{600} as + and biomass dry weight as ∘ in g/L. (b) Ratio between OD_{600} and biomass dry weight.

FIGURE B.1.: OD_{600} and biomass dry weight of the preliminary batch experiment of paragraph 5.2.2 on page 102.

The ratio between the two characteristics seems fairly constant with a mean of 0.25 $g.L^{-1}.OD^{-1}$ and a standard deviation of 0.3. The two measurements at the highest concentrations have a bit a lower value.

C. The Influence of the Oxygen Supply.

The oxygen tension is expected to have a large influence on valine fermentations. For instance, Akashi et al. (1977) already mentioned a strong increase in the valine productivity by introduction of a strongly oxygen limited phase in the fermentation of a *Brevibacterium* strain.

To investigate this effect quickly, some experiments were performed in RAMOS equipment (Anderlei and Büchs, 2001; Anderlei et al., 2004). These are shake flasks with on-line measurement of the oxygen transfer rate (OTR) and the carbon dioxide transfer rate (CTR) between the gas phase and the liquid phase. The experiments were performed with the kind help of the company AC Biotec (www.ac-biotec.de).

Experiments were conducted with 250 mL shake flasks with different filling volumes of 10, 15, 20 and 30 mL. The experiments were performed in duplo in the RAMOS equipment and with a maximum of six similar flasks on another shaker for sampling during the experiment. The used shakers were run at 200 rpm with an amplitude of 50 mm and were placed together in a room at which the temperature was controlled at $30°C$.

Two experiments in the RAMOS equipment are mentioned here. In the first experiment, the standard initial concentrations of 1 mM L-ile and 1 μM pantothenic acid (pan) were used. Since these compounds turned out to be limiting the oxygen uptake rate even in the flasks with the largest filling volume, the second experiment was performed with increased concentrations of these two compounds: 3 mM L-ile and 3 μM pantothenic acid were used.

First RAMOS Experiment

As mentioned above, the first experiment resulted in the same substrate limitation in all flasks as can be seen from the OTR in figure C.1 graph in the first 21 hours.

Addition of only pantothenic acid did not seem to improve the OTR, but addition of isoleucine only did. However, the two compounds together allowed a much faster increase in the OTR. This was one important indication that the effects of both compounds should be regarded separately in the modeling.

Interestingly, although no differences were found in the OTR in the first 20 hours, the CTR does show a difference, with decreasing CTR at higher filling volumes as can be seen in figure C.2.

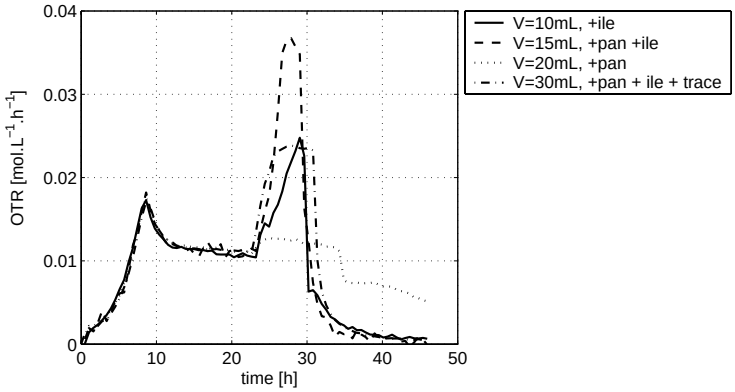

FIGURE C.1.: Oxygen transfer rates (OTR) in RAMOS flasks of the first experiment. The filling volumes are mentioned in the legend in the graph. After about 21 hours additions were made. The added substances are also mentioned in the graph, where ile indicates about 7 mM L-isoleucine in the flasks with 10 and 15 mL and about 3.5 mM in 30 mL. pan indicates the addition of 2 μM pantothenic acid in 15 and 20 mL and 1 μM in 30 mL. trace indicates the addition of 0.75 times the standard concentrations of trace solution I and biotin, shown in table 5.5 and 5.8 on page 94.

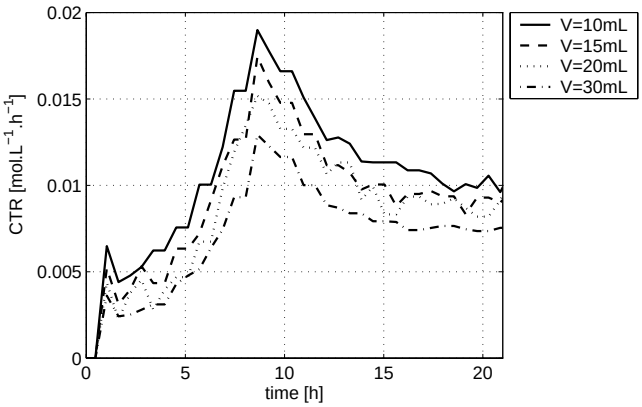

FIGURE C.2.: Carbon dioxide transfer rates (CTR) in RAMOS flasks of the first experiment. The filling volumes are mentioned in the legend in the graph.

The measurements of amino acids and other organic acids in the extra shake flasks, as well as pH and OD_{600} did not show any clear differences, except for the indication that more alanin and less ketoisovaleric acid are formed at smaller filling volumes. These data, being only two measurements for each filling volume, are shown in figure C.3.

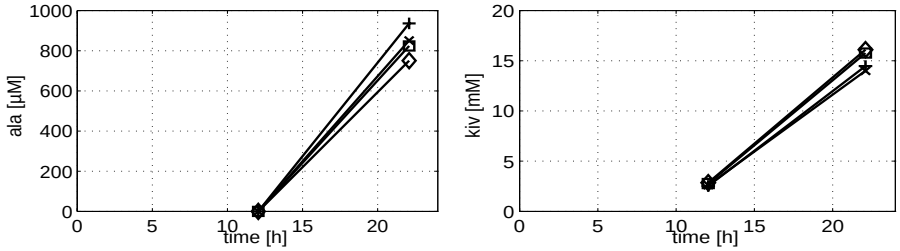

(a) L-Alanine, in μM.

(b) Keto-isovalerate (kiv) in mM.

FIGURE C.3.: Concentrations of amino acids and organic acids in the first RAMOS experiment. Concentrations in flasks with 10 mL volume as $+$, in 15 mL as $\times$, in 20 mL as $\square$ and in 30 mL as $\Diamond$. Lines are a visual aid.

Second RAMOS Experiment

In the second experiment, the expected differences in OTR values were found, where the OTR reaches a constant maximal value, limited by mass transfer between gas and liquid and therefore depending on the filling volume as shown in figure C.4.

It should be mentioned here that, unfortunately, the flasks which are used for taking samples during the experiment (not in the RAMOS device) were not shaken from 11.4 until 14.5 hours after the start of the experiment. This causes some discrepancies between the results from the RAMOS flasks and from the other flasks.

It seems like the reduced oxygen transfer at larger volumes decreases the growth somewhat, although only a relatively small influence was found as shown in figure C.5(a). Interestingly, the reduced oxygen uptake is not reflected in a change in the glucose uptake, which is shown in figure C.5(b) to be practically unaffected. A relatively small effect could, however, be masked by the problem regarding the shaking of the flasks and small effects might not be visible with the relatively low amount of samples.

However, the reduced oxygen availability does seem to lead to a stronger production of the typical overflow products acetate and lactate as shown in figure C.6 and a corresponding stronger decrease of the pH in figure C.7, which increases again after depletion of the glucose while the acids are metabolized further. Again, due to the limited amount of samples which could be taken, it cannot be completely excluded that these effects

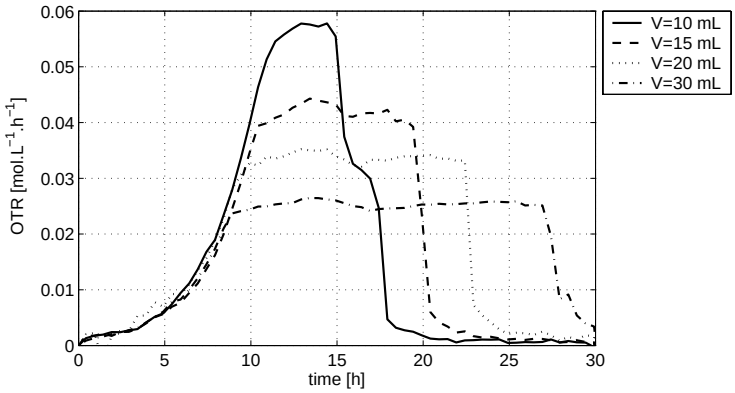

FIGURE C.4.: Oxygen transfer rates (OTR) in RAMOS flasks of the second experiment. The filling volumes are mentioned in the legend in the graph.

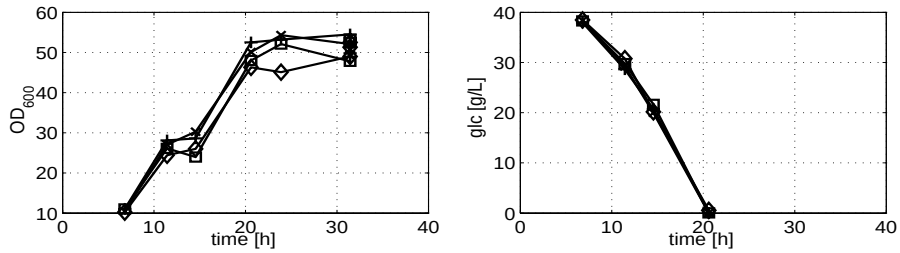

(a) OD_{600} in the second RAMOS experiment. The final value is connected to the measured densities in the RAMOS flasks, which were also stopped at that time.

(b) Glucose concentrations in the second RAMOS experiment.

FIGURE C.5.: OD_{600} and glucose concentrations. Concentrations in flasks with 10 mL volume as $+$, in 15 mL as $\times$, in 20 mL as $\square$ and in 30 mL as $\Diamond$. Lines are a visual aid.

are (partly) caused by an earlier depletion of glucose in the cultures with smaller filling volumes and a subsequent earlier start of further metabolizing the acids, reduction of the carbon dioxide concentrations and increase in the pH.

Upon depletion of the glucose, the CTR decreases steadily, whereas the physically limited OTR remains constant in the cultures with higher filling volumes, as can be seen in figure C.8. The decrease in OTR probably first appears when other products, which can be metabolized further (lactate, acetate) are also depleted. In the flasks with only

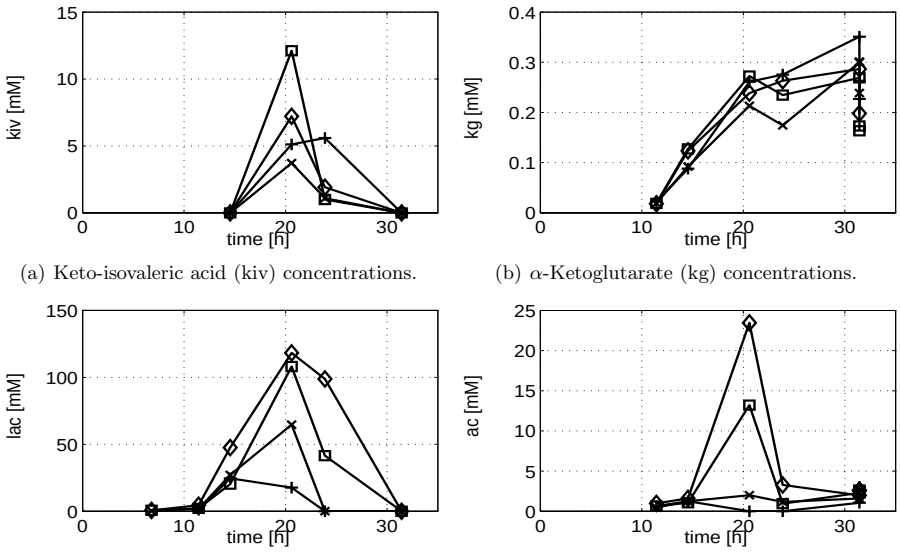

(a) Keto-isovaleric acid (kiv) concentrations.

(b) α-Ketoglutarate (kg) concentrations.

(c) Lactate (lac) concentrations.

(d) Acetate (ac) concentrations.

FIGURE C.6.: Concentrations of several organic acids in the second RAMOS experiment. Concentrations in flasks with 10 mL volume as $+$, in 15 mL as $\times$, in 20 mL as $\square$ and in 30 mL as $\Diamond$. Lines are a visual aid. The final concentrations are connected to markers indicating the final concentrations in the flasks in the RAMOS device.

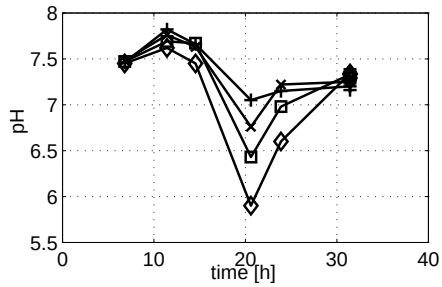

FIGURE C.7.: pH in RAMOS flasks of the second experiment. Values from flasks with 10 mL volume as +, 15 mL as ×, 20 mL as □ and 30 mL as ◊. Lines are a visual aid.

10 mL filling volume, the first decrease in the OTR might very well be caused by glucose depletion, with a subsequent period where the OTR is limited by the availability of other compounds which can be further metabolized, leading to a shoulder in the OTR profile.

Interestingly, the integral OTR and CTR values suggest that at larger filling volumes overall more oxygen was used, but less carbon dioxide was produced (data not shown).

The measured concentrations of several amino acids are shown in figure C.9.

The increased filling volumes only resulted in a decrease in L-valine production within the range used in this experiment. This suggests that for the used strain, it might not be beneficial to ferment at (very) low dissolved oxygen concentrations, as was suggested for instance by Akashi et al. (1977). However, it cannot yet be concluded whether moderate oxygen concentrations are better than high concentrations or not.

Interestingly, the alanine concentrations show the opposite from valine: at smaller volumes, less alanine is formed. Such an effect of more alanine formation with less valine formation and vice versa was also mentioned for instance by Radmacher (2001). Whether this is caused by a faster further metabolization of alanine, or a slower production of alanine can not yet be concluded. The same effect of increased alanine production and decreased valine production under anaerobic conditions was also published for an L-valine producing *Aerobacter aerogenes* (Hongo and Ueyeda, 1972).

Notable, the opposite trend in the alanine concentrations in the first RAMOS experiment (and the not clear trend in the valine concentrations in that experiment) might indicate a (small) positive effect of moderate oxygen tensions. Further investigation is therefore surely of interest. Fermentations at different moderate DO values could give more insight. Besides the very useful RAMOS technology used here, also other useful small scale techniques are nowadays available, for instance for measurement of the DO (Wittmann et al., 2003, 2001). For the proper control of this characteristic however, somewhat more elaborate techniques are needed, such as the stirred tank reactor used in the current work. Even in such systems it may prove difficult to control the

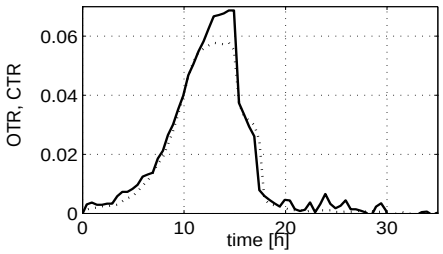

(a) OTR and CTR in the second RAMOS experiment in flasks with filling volume of 10 mL.

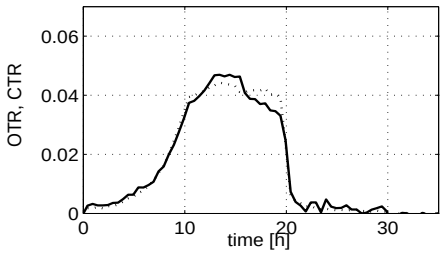

(b) OTR and CTR in the second RAMOS experiment in flasks with filling volume of 15 mL.

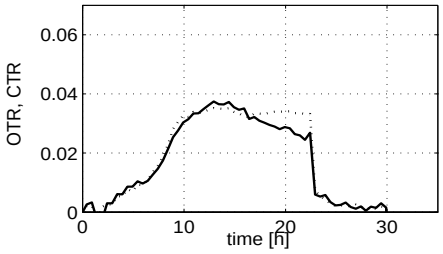

(c) OTR and CTR in the second RAMOS experiment in flasks with filling volume of 20 mL.

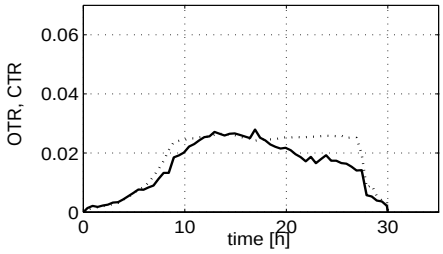

(d) OTR and CTR in the second RAMOS experiment in flasks with filling volume of 30 mL.

FIGURE C.8.: OTR as dotted lines in $mol.L^{-1}.h^{-1}$ and CTR as solid lines in $mol.L^{-1}.h^{-1}$ in the second RAMOS experiment.

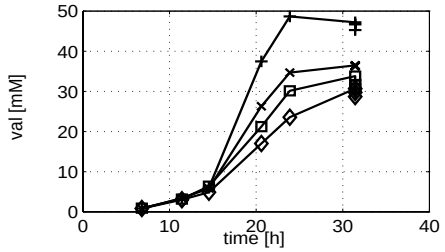

(a) L-Valine (val)concentrations in the second RAMOS experiment.

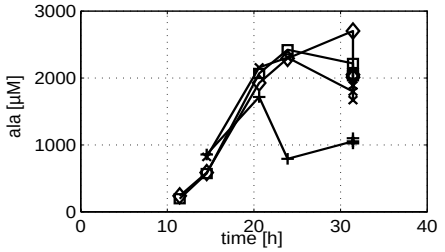

(b) L-Alanine (ala) concentrations in the second RAMOS experiment.

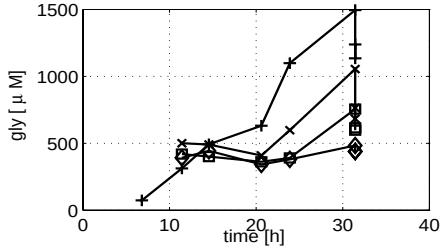

(c) L-Glycine (gly) concentrations in the second RAMOS experiment.

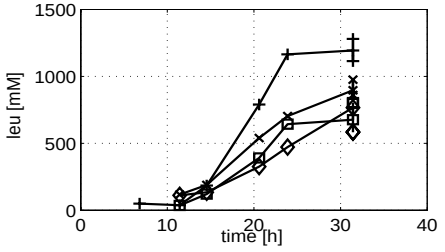

(d) L-Leucine (leu) concentrations in the second RAMOS experiment.

FIGURE C.9.: Concentrations of several amino acids in the second RAMOS experiment. Concentrations in flasks with 10 mL volume as $+$, in 15 mL as $\times$, in 20 mL as $\square$ and in 30 mL as $\lozenge$. Lines are a visual aid. The final concentrations are connected to markers indicating the final concentrations in the flasks in the RAMOS device.

DO properly at a low value in dynamic situations. If the oxygen tension does prove to have an important influence and relatively low values are beneficial for production but not so much for growth, controlling the *DO* at different levels in different stages of the fermentation could be considered. However, since no clear indications were found for beneficial effects of moderate oxygen tensions in the RAMOS experiments and since strong negative effects were found at very low oxygen availability, it was decided not to complicate the system any further by introducing the oxygen tension as a variable, as was for instance suggested by Ensari et al. (2003); Ensari and Lim (2003) for an L-lysine fermentation.

D. Dilution for Measurement of Amino Acids by HPLC.

It was noted that the amino acid concentration in one and the same sample, measured by the HPLC method explained in paragraph 5.1.4 on page 99, with different dilution factors led to strongly different values.

As an example, the measured concentrations of L-isoleucine and L-valine in a sample from a batch culture in a pH-controlled shake flask after 11 hours of fermentation, at an OD_{600} of about 8, using different dilution factors are shown in figure D.1.

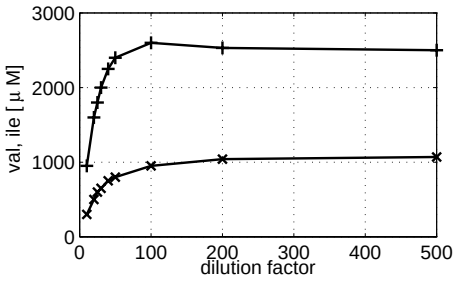

FIGURE D.1.: Effect of different dilution factors on the measured amino acid concentrations of L-isoleucine and L-valine. Measured concentrations in the fermentation broth (so accounted for the dilution) are shown in μM for L-valine as + and L-isoleucine as $\times$.

At small dilution factors, the measured concentrations are very low. This is probably caused by incomplete derivatisation with ortho-phtaldialdehyde (OPA), assuming that OPA (instead of the concentrations of amino acids) is limiting. This happens when other amino acids or ammonium are present in high concentrations.

Unfortunately, the used HPLC system uses a constant ratio between the amount of OPA solution and the amount of sample. Some quick attempts to increase the concentration of OPA in the OPA reactant did improve the measurement of low concentrations of amino acids at high concentrations of competing compounds. Unfortunately it also lead to black precipitates blocking the capillaries in the system.

Therefore, too small dilution factors had to be avoided. Of course, this depends on the

concentrations of amino acids and ammonium in the sample. In the example, a dilution of 100 times and more seems to be properly. However, it is of course also necessary to be in the linear concentration range and well above the lower accuracy bound of the measurement technique itself, best close to the used standards which were 50 μM for all amino acids.

Having already 20 g/L ammonium sulphate in the initial medium, pH control by addition of ammonium hydroxide and the production of large amounts of L-valine, make measurement of low concentrations of the other amino acids problematic throughout the fermentations.

E. Models used in the First Model Discriminating Experiment.

Model Equations

Model 1.1

$$r_x = \min(r_{x,S1}, r_{x,S2}) \tag{E.1}$$

$$r_{x,S1} = \frac{\mu_{max,S1} \cdot C_{S1} \cdot C_X}{Km_{S1} + c_{S1}} - m_{S1} \cdot C_X \tag{E.2}$$

$$r_{x,S2} = \frac{\mu_{max,S2} \cdot C_{S2} \cdot C_X}{C_{S2} + Km_{S2}} + \mu_{min,S2} \cdot C_X \tag{E.3}$$

$$r_{S2} = -\frac{r_x}{Y_{XS2}} \tag{E.4}$$

$$r_p = \frac{\pi_{max} \cdot C_{S1} \cdot C_X}{K_{p,S1} + C_{S1}} \cdot \frac{Ki_{rp,S2}}{Ki_{rp,S2} + C_{S2}} \tag{E.5}$$

$$r_{S1} = -\frac{\mu_{max,S1} \cdot C_{S1} \cdot C_X}{(Km_{S1} + C_{S1}) \cdot Y_{XS1}} - \frac{r_p}{Y_{PS1}} + \frac{r_{x,S1} - r_x}{Y_{XS1}} \tag{E.6}$$

Model 1.2

Model 1.2 is similar to model 1.1, with the following changes:
instead of equation E.5:

$$r_p = \frac{\pi_{max} \cdot C_{S1} \cdot C_X}{K_{p,S1} + C_{S1}} \cdot \frac{Ki_{rp,S2}}{Ki_{rp,S2} + C_{S2}} + (r_{x,S1} - r_x) \cdot Y_{PXS1xtra} \tag{E.7}$$

instead of equation E.6:

$$r_{S1} = -\frac{\mu_{max,S1} \cdot C_{S1} \cdot C_X}{(Km_{S1} + C_{S1}) \cdot Y_{XS1}} - \frac{\pi_{max} \cdot C_{S1} \cdot C_X}{(K_{p,S1} + C_{S1}) \cdot Y_{PS1}} \tag{E.8}$$

Model 1.3

Model 1.3 is similar to model 1.1, but with the following changes:

instead of equation E.2:

$$r_{x,S1} = \frac{\mu_{max,S1} \cdot C_{S1} \cdot C_X}{Km_{S1} + c_{S1}} \cdot \frac{Ki_{rx,P}}{Ki_{rx,P} + C_P} - m_{S1} \cdot C_X \tag{E.9}$$

instead of equation E.5:

$$r_p = \frac{\pi_{max} \cdot C_{S1} \cdot C_X}{K_{p,S1} + C_{S1}} \cdot \frac{Ki_{rp,P}}{Ki_{rp,P} + C_P} + (r_{x,S1} - r_x) \cdot Y_{PXS1xtra} \tag{E.10}$$

furthermore, instead of E.6:

$$r_{S1} = -\frac{\mu_{max,S1} \cdot C_{S1} \cdot C_X}{(Km_{S1} + C_{S1}) \cdot Y_{XS1}} \cdot \frac{Ki_{rx,P}}{Ki_{rx,P} + C_P} - \frac{\pi_{max} \cdot C_{S1} \cdot C_X}{(K_{p,S1} + C_{S1}) \cdot Y_{PS1}} \tag{E.11}$$

Model 1.4

Model 1.4 is similar to model 1.1, but with the following changes:
instead of equation E.2:

$$r_{x,S1} = \frac{\mu_{max,S1} \cdot C_{S1} \cdot C_X}{Km_{S1} + c_{S1}} \cdot \frac{Ki_{rx,P}}{Ki_{rx,P} + C_P} - m_{S1} \cdot C_X \tag{E.12}$$

instead of equation E.5:

$$r_p = \frac{\pi_{max} \cdot C_{S1} \cdot C_X}{K_{p,S1} + C_{S1}} \cdot \frac{Ki_{rp,P}}{Ki_{rp,P} + C_P} \cdot \frac{Ki_{rp,S2}}{Ki_{rp,S2} + C_{S2}} \tag{E.13}$$

furthermore, instead of E.6:

$$r_{S1} = -\frac{\mu_{max,S1} \cdot C_{S1} \cdot C_X}{(Km_{S1} + C_{S1}) \cdot Y_{XS1}} \cdot \frac{Ki_{rx,P}}{Ki_{rx,P} + C_P} - \frac{r_p}{Y_{PS1}} + \frac{r_{x,S1} - r_x}{Y_{XS1}} \tag{E.14}$$

Model 1.5

Model 1.5 is similar to model 1.4, with the following difference:
instead of equation E.13:

$$r_p = \frac{\pi_{max} \cdot C_{S1} \cdot C_X}{K_{p,S1} + C_{S1}} \cdot \frac{Ki_{rp,P}}{Ki_{rp,P} + C_P} \cdot \frac{Ki_{rp,S2}}{Ki_{rp,S2} + C_{S2}} + (r_{x,S1} - r_x) \cdot Y_{PXS1xtra} \tag{E.15}$$

instead of equation E.14:

$$r_{S1} = -\frac{\mu_{max,S1} \cdot C_{S1} \cdot C_X}{(Km_{S1} + C_{S1}) \cdot Y_{XS1}} \cdot \frac{Ki_{rx,P}}{Ki_{rx,P} + C_P} - \frac{r_p}{Y_{PS1}} \tag{E.16}$$

Model 1.6

Model 1.6 is similar to model 1.2, with the following change:
instead of equation E.3:

$$r_{x,S2} = \frac{\mu_{max,S2} \cdot C_{S2} \cdot C_X}{C_{S2} + Km_{S2}} + r_{xS2,min} \tag{E.17}$$

Model 1.7

Model 1.7 is similar to model 1.3, with the following change:
instead of equation E.3:

$$r_{x,S2} = \frac{\mu_{max,S2} \cdot C_{S2} \cdot C_X}{C_{S2} + Km_{S2}} + r_{xS2,min} \tag{E.18}$$

Model 1.8

Model 1.8 is similar to model 1.5, with the following change:
instead of equation E.3:

$$r_{x,S2} = \frac{\mu_{max,S2} \cdot C_{S2} \cdot C_X}{C_{S2} + Km_{S2}} + r_{xS2,min} \tag{E.19}$$

Parameter Estimates

The estimated model parameters are shown with the corresponding standard deviations, which were calculated from the model simulations and the accuracy of the measurements according to paragraph 2.4.2 on page 18. The standard deviation of the measured values is estimated using equation 3.1 on page 47, with a relative standard deviation of 10, 10 and 5% for the measurements of biomass, glucose and L-valine respectively. The used lower accuracy bounds on the measurements were an OD_{600} of 0.1, 0.3 mM glucose and 2.5 mM L-valine.

TABLE E.1.: Model Parameters of the Competing Fermentation Models Before Model Discriminating Experiment I.

Model	1.1		1.2		
Parameter	Value	σ	Value	σ	Unit
$\mu_{max,S1}$	0.887	0.0214	1.07	0.465	h^{-1}
Km_{S1}	211	114	278	424	mM
m_{S1}	$7.04{\cdot}10^{-5}$	0.0199	0.0308	0.0404	h^{-1}
Y_{XS1}	0.432	0.142	0.554	0.354	$OD.mM^{-1}$
$\mu_{max,S2}$	20	$9.7{\cdot}10^{7}$	13	$9.6{\cdot}10^{8}$	h^{-1}
Km_{S2}	0.074	$1.0{\cdot}10^{6}$	0.16	$2.2{\cdot}10^{7}$	mM
Y_{XS2}	20.4	7.1	19.6	10.6	$OD.mM^{-1}$
π_{max}	0.547	0.269	0.90	30.03	$mM.OD^{-1}.h^{-1}$
Kp_{S1}	179	140	395	3261	mM
Y_{PS1}	0.701	0.439	1.8	10.1	$mM.mM^{-1}$
$Ki_{S2,rp}$	0.288	0.116	0.100	0.0133	mM
$\mu_{min,S2}$	0.0914	0.0110	0.249	0.765	h^{-1}
$Y_{PX,S1extra}$			0.100	1.69	$mM.OD^{-1}$

Model	1.3		1.4		
Parameter	Value	σ	Value	σ	Unit
$\mu_{max,S1}$	1.08	0.035	0.846	0.780	h^{-1}
Km_{S1}	274	73	182	1370	mM
m_{S1}	0.0077	0.0118	0.0072	0.0130	h^{-1}
Y_{XS1}	0.463	0.083	0.342	0.093	$OD.mM^{-1}$
$\mu_{max,S2}$	12.2	3154	16.3	$1.8{\cdot}10^{7}$	h^{-1}
Km_{S2}	0.0105	0.0085	0.15	$4.0{\cdot}10^{5}$	mM
Y_{XS2}	18.0	5.4	18.8	7.72	$OD.mM^{-1}$
π_{max}	0.092	0.444	0.460	2.12	$mM.OD^{-1}.h^{-1}$
Kp_{S1}	$5.56{\cdot}10^{-4}$	0.356	130	1058	mM
Y_{PS1}	1.63	3.60	1.24	1.83	$mM.mM^{-1}$
$Ki_{S2,rp}$			0.325	0.078	mM
$\mu_{min,S2}$	0.100	0.012	0.0974	0.0117	h^{-1}
$Y_{PX,S1extra}$	0.692	0.254			$mM.OD^{-1}$
$Ki_{P,rp}$	2000	$1.37{\cdot}10^{4}$	1824	$1.78{\cdot}10^{5}$	mM
$Ki_{P,rx}$	168	304	100	891	mM

Table E.1: Model Parameters of the Competing Fermentation Models Before Model Discriminating Experiment I. (continued)

Model	1.5		1.6		
Parameter	Value	σ	Value	σ	Unit
$\mu_{max,S1}$	1.09	0.020	0.937	1.06	h^{-1}
Km_{S1}	274	88	278	1194	mM
m_{S1}	0.0109	0.00592	$1.44{\cdot}10^{-5}$	0.0638	h^{-1}
Y_{XS1}	0.464	0.060	0.437	0.297	$OD.mM^{-1}$
$\mu_{max,S2}$	6.44	$1.15{\cdot}10^{6}$	13.2	$6.56{\cdot}10^{6}$	h^{-1}
Km_{S2}	0.00249	1122	0.0676	$4.58{\cdot}10^{4}$	mM
Y_{XS2}	18.11	7.45	15.8	11.7	$OD.mM^{-1}$
π_{max}	0.0978	0.5918	0.321	27.6	$mM.OD^{-1}.h^{-1}$
Kp_{S1}	$5.56{\cdot}10^{-4}$	6.55	82.4	327	mM
Y_{PS1}	1.68	4.12	1.80	18.2	$mM.mM^{-1}$
$Ki_{S2,rp}$	6.36	27.5	0.319	0.991	mM
$\mu_{min,S2}$	0.100	0.0139			h^{-1}
$r_{x,min,S2}$			3.09	0.381	h^{-1}
$Y_{PX,S1extra}$	0.677	0.311	0.101	2.23	$mM.OD^{-1}$
$Ki_{P,rp}$	1529	$2.99{\cdot}10^{4}$			mM
$Ki_{P,rx}$	166	325			mM

Model	1.7		1.8		
Parameter	Value	σ	Value	σ	Unit
$\mu_{max,S1}$	0.976	1.20	0.946	2.77	h^{-1}
Km_{S1}	278	2735	278	3159	mM
m_{S1}	$1.07{\cdot}10^{-6}$	0.0156	$2.57{\cdot}10^{-8}$	0.0592	h^{-1}
Y_{XS1}	0.391	0.0875	0.369	0.170	$OD.mM^{-1}$
$\mu_{max,S2}$	8.13	$3.40{\cdot}10^{9}$	13.1	$9.13{\cdot}10^{6}$	h^{-1}
Km_{S2}	$6.06{\cdot}10^{-4}$	$2.09{\cdot}10^{4}$	0.142	$1.32{\cdot}10^{5}$	mM
Y_{XS2}	15.7	8521	14.2	10.7	$OD.mM^{-1}$
π_{max}	0.0812	1.20	0.337	37.2	$mM.OD^{-1}.h^{-1}$
Kp_{S1}	0.00403	10.6	80.8	379	mM
Y_{PS1}	1.65	6.33	1.75	18.4	$mM.mM^{-1}$
$Ki_{S2,rp}$			0.262	0.640	mM
$r_{x,min,S2}$	3.15	0.396	3.37	0.442	h^{-1}
$Y_{PX,S1extra}$	0.890	0.393	0.100	2.65	$mM.OD^{-1}$
$Ki_{P,rp}$	1261	$2.58{\cdot}10^{4}$	1639	$1.05{\cdot}10^{5}$	mM
$Ki_{P,rx}$	208	3078	100	1522	mM

TABLE E.2.: Model Parameters of the Competing Fermentation Models After Model Discriminating Experiment I.

Model	1.1		1.2		
Parameter	Value	σ	Value	σ	Unit
$\mu_{max,S1}$	0.600	0.147	0.496	0.0255	h^{-1}
Km_{S1}	105	78.8	34.8	12.2	mM
m_{S1}	0.0181	0.00854	0.0128	0.00255	h^{-1}
Y_{XS1}	0.271	0.0146	0.604	0.0334	$OD.mM^{-1}$
$\mu_{max,S2}$	4.39	239	16.6	0.133	h^{-1}
Km_{S2}	2.20	124	0.430	$8.83{\cdot}10^{-5}$	mM
Y_{XS2}	20.1	0.699	18.6	0.224	$OD.mM^{-1}$
π_{max}	0.266	0.0210	1.18	0.419	$mM.OD^{-1}.h^{-1}$
Kp_{S1}	20.8	8.52	105	66.5	mM
Y_{PS1}	1.02	0.165	0.360	0.00971	$mM.mM^{-1}$
$Ki_{S2,rp}$	0.467	0.0938	4.33	4.50	mM
$\mu_{min,S2}$	0.0292	0.00430	0.017	0.00699	h^{-1}
$Y_{PX,S1extra}$			0.766	0.0113	$mM.OD^{-1}$

Model	1.3		1.4		
Parameter	Value	σ	Value	σ	Unit
$\mu_{max,S1}$	0.436	0.00677	0.501	0.0125	h^{-1}
Km_{S1}	4.27	2.30	30.0	1.24	mM
m_{S1}	0.0456	0.00825	0.0235	0.0105	h^{-1}
Y_{XS1}	0.534	0.0758	0.276	0.0257	$OD.mM^{-1}$
$\mu_{max,S2}$	19.9	1.28	19.3	69677	h^{-1}
Km_{S2}	0.123	0.00771	0.384	1395	mM
Y_{XS2}	19.2	0.615	17.8	0.635	$OD.mM^{-1}$
π_{max}	0.150	0.0107	0.276	0.0240	$mM.OD^{-1}.h^{-1}$
Kp_{S1}	4.40	7.48	5.87	7.02	mM
Y_{PS1}	1.59	2.44	1.01	0.267	$mM.mM^{-1}$
$Ki_{S2,rp}$			0.329	0.0783	mM
$\mu_{min,S2}$	0.0308	0.00462	0.0436	0.00430	h^{-1}
$Y_{PX,S1extra}$	0.459	0.0778			$mM.OD^{-1}$
$Ki_{P,rp}$	1923	4538	481	185	mM
$Ki_{P,rx}$	143	64.8	613	3390	mM

Table E.2: Model Parameters of the Competing Fermentation Models After Model Discriminating Experiment I. (continued)

Model	1.5		1.6		
Parameter	Value	σ	Value	σ	Unit
$\mu_{max,S1}$	0.436	0.0101	0.487	0.0251	h^{-1}
Km_{S1}	0.0328	0.147	32.7	9.56	mM
m_{S1}	0.0220	0.0101	0.00979	0.0171	h^{-1}
Y_{XS1}	0.555	0.0293	0.630	0.117	$OD.mM^{-1}$
$\mu_{max,S2}$	15.8	819	17.0	$1.78{\cdot}10^5$	h^{-1}
Km_{S2}	3.38	175	0.0786	808	mM
Y_{XS2}	17.9	0.626	14.1	0.829	$OD.mM^{-1}$
π_{max}	0.455	0.207	0.145	0.418	$mM.OD^{-1}.h^{-1}$
Kp_{S1}	300	266	412	1815	mM
Y_{PS1}	1.76	0 571	1.80	7.79	$mM.mM^{-1}$
$Ki_{S2,rp}$	0.500	0.268	9.40	49.6	mM
$\mu_{min,S2}$	0.0358	0.00493			h^{-1}
$r_{x,min,S2}$			1.86	0.125	h^{-1}
$Y_{PX,S1extra}$	0.386	0.113	0.661	0.0222	$mM.OD^{-1}$
$Ki_{P,rp}$	1969	4978			mM
$Ki_{P,rx}$	179	18.6			mM

Model	1.7		1.8		
Parameter	Value	σ	Value	σ	Unit
$\mu_{max,S1}$	0.448	0.0178	0.426	0.00569	h^{-1}
Km_{S1}	4.29	1.94	2.38	2.04	mM
m_{S1}	0.0304	0.0148	0.0346	0.00607	h^{-1}
Y_{XS1}	0.568	0.0314	0.558	0.0438	$OD.mM^{-1}$
$\mu_{max,S2}$	19.0	23356	17.8	$1.55{\cdot}10^5$	h^{-1}
Km_{S2}	1.20	1475	0.331	2900	mM
Y_{XS2}	16.8	0.648	16.9	0.596	$OD.mM^{-1}$
π_{max}	0.313	0.566	0.446	0.370	$mM.OD^{-1}.h^{-1}$
Kp_{S1}	455	1208	317	606	mM
Y_{PS1}	1.68	1.13	1.80	0.909	$mM.mM^{-1}$
$Ki_{S2,rp}$			0.651	0.618	mM
$r_{x,min,S2}$	1.73	0.162	1.68	0.165	h^{-1}
$Y_{PX,S1extra}$	0.666	0.0475	0.427	0.268	$mM.OD^{-1}$
$Ki_{P,rp}$	1751	5685	2000	5933	mM
$Ki_{P,rx}$	220	39.5	196	30.1	mM

TABLE E.3.: Estimated Lag-Times of the First Batch Experiment, Before Model Discriminating Experiment I.

Model	$t_{lag,exp1}[h]$
1.1	1.09
1.2	0.969
1.3	1.35
1.4	1.13
1.5	1.33
1.6	0.633
1.7	0.800
1.8	0.648

TABLE E.4.: Estimated Lag-Times of the First Batch Experiment ($t_{lag,exp1}$) and After Model Discriminating Experiment I ($t_{lag,exp2}$), After Model Discriminating Experiment I.

Model	$t_{lag,exp1}[h]$	$t_{lag,exp2}[h]$
1.1	0.0037	1.92
1.2	0.401	2.33
1.3	0.381	2.00
1.4	0.508	2.48
1.5	0.537	2.44
1.6	0.0377	2.00
1.7	0.656	2.38
1.8	0.333	2.00

F. Models used in the Second Model Discriminating Experiment.

Model Equations

Model 2.1

$$r_x = \min(r_{x,S1}, r_{x,S2}, r_{x,S3}) \tag{F.1}$$

$$r_{x,S1} = \frac{\mu_{max,S1} \cdot C_{S1} \cdot C_X}{Km_{S1} + c_{S1}} \tag{F.2}$$

$$r_{x,S2} = r_{x,S2ext} + r_{x,S2int} \tag{F.3}$$

$$r_{x,S3} = r_{x,S3ext} + r_{x,S3int} \tag{F.4}$$

$$r_{x,S2ext} = \frac{\mu_{max,S2ext} \cdot C_{S2ext} \cdot C_X}{C_{S2ext} + Km_{S2ext}(1 + C_P/Ki_{P,rxs2})} + kd_{S2} \cdot C_X \cdot C_{S2} \tag{F.5}$$

$$r_{x,S2int} = \frac{\mu_{max,S2int} \cdot (C_{S2int}/C_X - S2intmin) \cdot C_X}{K_{m,S2int} + (C_{S2int}/C_X - S2intmin)} \tag{F.6}$$

$$r_{x,S3ext} = \frac{\mu_{max,S3ext} \cdot C_{S3ext} \cdot C_X}{S3_{ext} + K_{m,S3ext}} \tag{F.7}$$

$$r_{x,S3int} = \frac{\mu_{max,S3int} \cdot C_X(C_{S3int}/C_X - S3_{intmin})}{K_{m,S3int} + (C_{S3int}/C_X - S3_{intmin})} \tag{F.8}$$

$$r_{S2ext} = -\frac{r_{x,S2ext}}{Y_{xs2}} \tag{F.9}$$

$$r_{S2int} = -r_{x,S2ext} - m_{S2int} \cdot (C_{S2int}/C_X - S2intmin) \cdot C_{S3int} \tag{F.10}$$

$$r_{S3ext} = -\frac{r_{x,S3ext} + k_{S3extra} \cdot (r_{x,S3} - r_x)}{Y_{xs3}} \tag{F.11}$$

$$r_{S3int} = -r_{x,S3ext} - m_{S3int} \cdot (C_{S3int}/C_X - S3intmin) \cdot C_X \tag{F.12}$$

$$r_p = \min(r_{p,S1}, r_{p,S3}) \tag{F.13}$$

$$r_{p,S1} = \frac{\pi_{max,S1} \cdot C_{S1} \cdot C_X}{K_{p,S1}(1 + \frac{C_{S2int}/C_X - S2intmin_{rp}}{Ki_{rp,S2int}}) + C_{S1}} + \frac{k_{S1extra}(r_{x,S1} - r_x)}{Y_{ps1}} \tag{F.14}$$

$$r_{p,S3} = \frac{\pi_{max,S3} \cdot C_X(C_{S3int}/C_X - S3intmin)}{K_{p,S3} + (C_{S3int}/C_X - S3intmin)} \cdot \frac{C_P}{Ki_{P,rp} + C_P} \tag{F.15}$$

$$r_{S1} = -\frac{rx}{Y_X S1} - \frac{rp}{Y_P S1} - m_{S1} \cdot C_X \tag{F.16}$$

Model 2.2

Model 2.2 is similar to model 2.1, with the following changes:
instead of equation F.2:

$$r_{x,S1} = \frac{\mu_{max,S1} \cdot C_{S1} \cdot C_X}{K_{m,S1} + c_{S1}} \cdot \frac{Ki_{P,rxS1}}{Ki_{P,rxS1} + C_P} \tag{F.17}$$

instead of equation F.3:

$$r_{x,S2} = r_{x,S2ext} \tag{F.18}$$

so equation F.6 can be omitted.
instead of equation F.13 to F.15:

$$r_p = \frac{\pi_{max,S1} \cdot C_{S1} \cdot C_X}{K_{p,S1} + C_{S1}} \cdot \frac{Ki_{P,rp}}{Ki_{P,rp} + C_P} \cdot \frac{(C_{S3int}/C_X - S3_{intmin,rp})}{Kp_{S3int} + (C_{S3int}/C_X - S3_{intmin,rp})} + \frac{k_{S1extra}(r_{x,S1} - r_x)}{Y_{p,s1}} \tag{F.19}$$

Model 2.3

Model 2.3 is similar to model 2.1, but with the following changes:
instead of equation F.6:

$$r_{x,S2int} = \mu_{max,S2int} \cdot C_{S2int} \cdot \frac{Ki_{P,rxs2int}}{Ki_{P,rxs2int} + C_P} \tag{F.20}$$

instead of equation F.14:

$$r_{p,S1} = \frac{\pi_{max,S1} \cdot C_{S1} \cdot C_X}{C_{S1} + K_{p,S1}(1 + \frac{C_{S2int}/C_X}{Ki_{rp,S2int}})} + \frac{k_{S1extra}(r_{x,S1} - r_x)}{Y_{ps1}} \tag{F.21}$$

Model 2.4

Model 2.4 is similar to model 2.1, but with the following changes:
instead of equation F.5:

$$r_{x,S2ext} = \frac{\mu_{max,S2ext} \cdot C_{S2ext} \cdot C_X}{C_{S2ext} + K_{m,S2ext}(1 + C_P/Ki_{P,rxs2})} \tag{F.22}$$

instead of equation F.6:

$$r_{x,S2int} = \mu_{max,S2int} \cdot C_{S2int} \tag{F.23}$$

instead of equation F.14:

$$r_{p,S1} = \frac{\pi_{max,S1} \cdot C_{S1} \cdot C_X}{K_{p,S1}(1 + \frac{C_{S2int}/C_X}{Ki_{rp,S2int}}) + C_{S1}} + \frac{k_{S1extra}(r_{x,S1} - r_x)}{Y_{p,s1}} \tag{F.24}$$

instead of equation F.15:

$$r_{p,S3} = \frac{\pi_{max,S3} \cdot C_X(C_{S3int}/C_X)}{K_{p,S3} + (C_{S3int}/C_X)} \cdot \frac{C_P}{Ki_{P,rp} + C_P} \tag{F.25}$$

Model 2.5

Model 2.5 is similar to model 2.3, with the following difference:
instead of equation F.10:

$$r_{S2int} = -r_{x,S2ext} - m_{S2int} \cdot (C_{S2int}/C_X - S2intmin) \cdot r_p/Y_{ps1} \tag{F.26}$$

Reduced model for the production experiment

The reduced model is based on model 2.3, but with the following difference:
instead of equation F.12:

$$r_{S3int} = -r_{x,S3ext} \tag{F.27}$$

Parameter Estimates

The estimated model parameters are shown with the corresponding standard deviations, which were calculated in a similar way as the parameters shown in appendix E.

Table F.1.: Model Parameters of the Competing Fermentation Models Before Model Discriminating Experiment II.

Model	2.1		2.2		2.3		
Parameter	Value	σ	Value	σ	Value	σ	Unit
$\mu_{max,S1}$	0,438	0,0395	0,411	0,00614	0,437	0,0153	h^{-1}
Km_{S1}	14,1	20,6	0,00715	0,878	15,0	8,53	mM
m_{S1}	0,0688	0,0145	0,0495	0,0156	0,0720	0,0133	$mM.OD^{-1}.h^{-1}$
Y_{XS1}	0,428	0,0302	0,363	0,0207	0,434	0,0298	$OD^{-1}.mM$
$\mu_{max,S2}$	1,29	1,69	3,01	3,45	0,895	2,97	h^{-1}
Km_{S2}	1,09	2,36	3,37	4,93	3,14	8,79	mM
Y_{XS2}	66,3	50,1	133	58,4	11,9	4,86	$OD^{-1}.mM$
$\pi_{max,S1}$	0,644	5,71	0,211	0,306	0,0883	0,0679	$mM.OD^{-1}.h^{-1}$
Kp_{S1}	46,0	563	19,6	7,91	53,3	207	mM
Y_{PS1}	0,631	0,0411	0,650	0,0404	0,645	0,0364	$mM.mM^{-1}$
$\mu_{max,S3}$	5,12	13,9	41,2	165	6,30	11,7	h^{-1}
Km_{S3}	6,40	18,4	2,99	12,8	8,64	15,9	μM
Y_{XS3}	93,3	15,4	28,7	3,59	82,3	42,1	$OD.\mu M^{-1}$
$\mu_{max,S2Int}$	81,7	378			22,3	66,1	h^{-1}
Km_{S2Int}	10,4	55,1					$mM.OD^{-1}$
$C_{S2IntMin,rx}$	0,00771	0,00942					$mM.OD^{-1}$
m_{S2Int}	21,5	43,4			20,8	52,5	$OD.mM^{-1}.h^{-1}$
kd_{S2}	0,00153	0,00280			0,0229	0,00981	–
$Ki_{P,rs2}$	1,86	1,58	2,47	0,854	1,00	2,47	mM
$\mu_{max,S3Int}$	2,69	1765	10,4	92,6	13,9	552	h^{-1}
Km_{S3Int}	0,915	605	0,755	6,96	0,249	9,93	$\mu M.OD^{-1}$
m_{S3Int}	0,0850	0,0850	0,460	0,238	0,124	0,597	h^{-1}
$C_{S3IntMin,rx}$	0,00963	0,00344	0,00394	0,00152	0,0101	0,00206	$\mu M.OD^{-1}$
$k_{S3extra}$	0,139	0,605	0,0608	0,291	0,864	0,286	–
$Ki_{S2,rp}$	$2{,}02{\cdot}10^{-4}$	0,00300					mM^{-1}
Kp_{S3}	0,870	1,64	0,923	1,40	0,143	0,594	$\mu M.OD^{-1}$
$C_{S3IntMin,rp}$	0.431	0,00560	0,00592	0,00240	0,00910	0,00243	$\mu M.OD^{-1}$
$k_{S1extra}$	0,332 0	0,135	0,232	0,0279	0,506	0,0992	–
$Ki_{P,rp}$	487	309	184	61,1	483	296	mM
$\pi_{max,S3}$	10,1	19,1			14,7	65,8	$mM.OD^{-1}.h^{-1}$
$C_{S2IntMin,rp}$	0,00770	0,0110					$mM.OD^{-1}$
$Ki_{P,rs1}$			155	41,3			mM
$Ki_{P,rxs2int}$					12,7	15,6	$mM.h-1$

Table F.1: Model Parameters of the Competing Fermentation Models Before Model Discriminating Experiment II. (continued)

Model	2.4		2.5		
Parameter	Value	σ	Value	σ	Unit
$\mu_{max,S1}$	0.407	0.0217	0.432	0.122	h^{-1}
Km_{S1}	0.0713	10.1	10.6	62.4	mM
m_{S1}	0.0850	0.0140	0.0675	0.0133	$mM.OD^{-1}.h^{-1}$
Y_{XS1}	0.396	0.0257	0.435	0.0320	$OD^{-1}.mM$
$\mu_{max,S2}$	0.500	1.24	0.500	2.87	h^{-1}
Km_{S2}	5.00	16.9	3.00	22.2	mM
Y_{XS2}	10.6	5.03	10.4	7.15	$OD^{-1}.mM$
$\pi_{max,S1}$	0.344	0.150	0.0799	0.0788	$mM.OD^{-1}.h^{-1}$
Kp_{S1}	55.6	57.6	9.59	213	mM
Y_{PS1}	0.718	0.0458	0.626	0.0366	$mM.mM^{-1}$
$\mu_{max,S3}$	4.70	15.7	6.26	25.6	h^{-1}
Km_{S3}	10.0	35.2	8.71	36.1	μM
Y_{XS3}	16.9	11.1	76.9	65.8	$OD.\mu M^{-1}$
$\mu_{max,S2Int}$	71.6	40.0	37.6	55.0	h^{-1}
m_{S2Int}	4.21	2.74			$OD.mM^{-1}.h^{-1}$
m_{S2Int}			0.250	0.359	mM^{-1}
kd_{S2}	41.4	34.0	0.0174	0.0122	–
$Ki_{P,rs2}$			6.99	12.9	mM
$\mu_{max,S3Int}$	4.92	68.7	14.0	700	h^{-1}
Km_{S3Int}	0.433	6.21	0.353	17.8	$\mu M.OD^{-1}$
m_{S3Int}	$1.40{\cdot}10^{-5}$	0.0205	0.0505	0.336	h^{-1}
$C_{S3IntMin,rx}$	0.0107	0.00185	0.0105	0.00186	$\mu M.OD^{-1}$
$k_{S3extra}$	0.482	0.287	0.790	0.744	–
$Ki_{S2,rp}$	$9.54{\cdot}10^{-4}$	$8.27{\cdot}10^{-4}$			mM^{-1}
Kp_{S3}	0.228	0.680	0.277	1.96	$\mu M.OD^{-1}$
$C_{S3IntMin,rp}$			0.00848	0.00756	$\mu M.OD^{-1}$
$k_{S1extra}$	0.0669	0.0666	0.465	0.0921	–
$Ki_{P,rp}$			370	171	mM
$\pi_{max,S3}$	0.467	1.31	14.1	109	$mM.OD^{-1}.h^{-1}$
$Ki_{P,rxs2int}$			18.7	17.0	$mM.h-1$

TABLE F.2.: Estimated Lag-Times of the First Batch Experiment ($t_{lag,exp1}$), Model Discriminating Experiment I ($t_{lag,exp2}$), and the Subsequent Intuitively Planned Experiment ($t_{lag,exp3}$) After these Three Experiments.

Model	$t_{lag,exp1}[h]$	$t_{lag,exp2}[h]$	$t_{lag,exp3}[h]$
2.1	$6.56 \cdot 10^{-4}$	1.75	1.12
2.2	$2.76 \cdot 10^{-4}$	1.79	1.50
2.3	$2.82 \cdot 10^{-4}$	1.69	1.51
2.4	$4.08 \cdot 10^{-4}$	1.77	1.12
2.5	$1.09 \cdot 10^{-4}$	1.77	1.54

TABLE F.3.: Model Parameters of the Competing Fermentation Models After Model Discriminating Experiment II.

Model	2.1		2.2		
Parameter	Value	σ	Value	σ	Unit
$\mu_{max,S1}$	0.441	0.00591	0.420	0.00412	h^{-1}
Km_{S1}	14.63	0.951	0.00586	0.107	mM
m_{S1}	0.0814	0.00900	0.00135	0.0107	$mM.OD^{-1}.h^{-1}$
Y_{XS1}	0.426	0.0162	0.339	0.0106	$OD^{-1}.mM$
$\mu_{max,S2}$	1.30	0.409	4.32	2.45	h^{-1}
Km_{S2}	1.09	0.600	3.12	2.19	mM
Y_{XS2}	65.1	9.52	140	33.4	$OD^{-1}.mM$
$\pi_{max,S1}$	0.643	0.623	0.209	0.0252	$mM.OD^{-1}.h^{-1}$
Kp_{S1}	46.0	53.8	9.93	2.67	mM
Y_{PS1}	0.638	0.0275	0.577	0.0225	$mM.mM^{-1}$
$\mu_{max,S3}$	5.12	2.69	19.4	263	h^{-1}
Km_{S3}	6.39	3.56	1.573	0.714	μM
Y_{XS3}	91.7	4.21	16.1	6.84	$OD.\mu M^{-1}$
$\mu_{max,S2Int}$	81.1	1793			h^{-1}
Km_{S2Int}	10.6	234			$mM.OD^{-1}$
$C_{S2IntMin,rx}$	0.00753	0.00141			$mM.OD^{-1}$
m_{S2Int}	21.9	6.08			$OD.mM^{-1}.h^{-1}$
kd_{S2}	0.00151	0.00139			–
$Ki_{P,rs2}$	1.84	0.498	1.30	0.364	mM
$\mu_{max,S3Int}$	2.63	558	7.40	47.5	h^{-1}
Km_{S3Int}	0.924	197	0.949	6.34	$\mu M.OD^{-1}$
m_{S3Int}	0.0815	0.0242	$6.63{\cdot}10^{-4}$	0.206	h^{-1}
$C_{S3IntMin,rx}$	0.0114	0.00135	0.00669	0.00162	$\mu M.OD^{-1}$
$k_{S3extra}$	0.114	0.221	0.978	0.293	–
$Ki_{S2,rp}$	$2.33{\cdot}10^{-4}$	$3.28{\cdot}10^{-4}$			mM^{-1}
Kp_{S3}	0.862	5.01	0.939	0.179	$\mu M.OD^{-1}$
$C_{S3IntMin,rp}$	0.00197	0.00235	0.00790	0.00207	$\mu M.OD^{-1}$
$k_{S1extra}$	0.265	0.0363	0.135	0.0163	–
$Ki_{P,rp}$	491	200	680	610	mM
$\pi_{max,S3}$	10.2	57.1			$mM.OD^{-1}.h^{-1}$
$C_{S2IntMin,rp}$	0.00793	0.00144			$mM.OD^{-1}$
$Ki_{P,rs1}$			657	414	mM

Table F.3: Model Parameters of the Competing Fermentation Models After Model Discriminating Experiment II. (continued)

Model	2.3		2.4		
Parameter	Value	σ	Value	σ	Unit
$\mu_{max,S1}$	0.428	0.00329	0.40033	0.00397	h^{-1}
Km_{S1}	0.485	0.0403	0.401	0.0712	mM
m_{S1}	0.0384	0.00920	0.114	0.0131	$mM.OD^{-1}.h^{-1}$
Y_{XS1}	0.367	0.00119	0.367	0.00862	$OD^{-1}.mM$
$\mu_{max,S2}$	1.02	2.85	0.335	0.137	h^{-1}
Km_{S2}	2.01	4.95	1.63	1.11	mM
Y_{XS2}	14.9	1.42	12.0	1.52	$OD^{-1}.mM$
$\pi_{max,S1}$	0.0986	0.00590	0.606	0.427	$mM.OD^{-1}.h^{-1}$
Kp_{S1}	55.4	11.4	79.0	68.3	mM
Y_{PS1}	0.670	0.0274	0.932	0.0590	$mM.mM^{-1}$
$\mu_{max,S3}$	7.43	5.95	2.31	1.42	h^{-1}
Km_{S3}	9.30	7.63	7.85	5.22	μM
Y_{XS3}	95.0	18.0	8.49	3.92	$OD.\mu M^{-1}$
$\mu_{max,S2Int}$	31.5	27.0	87.6	43.6	h^{-1}
m_{S2Int}	16.6	12.3	5.43	2.71	$OD.mM^{-1}.h^{-1}$
kd_{S2}	0.0306	0.00349			$-$
$Ki_{P,rs2}$	0.467	0.684	25.1	7.37	mM
$\mu_{max,S3Int}$	12.9	133	7.06	34.4	h^{-1}
Km_{S3Int}	0.282	2.90	0.563	2.80	$\mu M.OD^{-1}$
m_{S3Int}	$1.06{\cdot}10^{-6}$	0.320	$1.95{\cdot}10^{-5}$	0.0293	h^{-1}
$C_{S3IntMin,rx}$	0.00942	0.00137	0.0118	0.00223	$\mu M.OD^{-1}$
$k_{S3extra}$	0.931	0.0425 0.785	0.0697		$-$
$Ki_{S2,rp}$			$4.89{\cdot}10^{-4}$	$2.10{\cdot}10^{-4}$	mM^{-1}
Kp_{S3}	0.112	0.414	0.0616	0.0272	$\mu M.OD^{-1}$
$C_{S3IntMin,rp}$	0.00876	0.00123			$\mu M.OD^{-1}$
$k_{S1extra}$	0.327	0.0212	0.193	0.0113	$-$
$Ki_{P,rp}$	591	122			mM
$\pi_{max,S3}$	15.2	55.0	0.127	0.0316	$mM.OD^{-1}.h^{-1}$
$Ki_{P,rxs2int}$	4.94	3.75			$mM.h-1$

Table F.3: Model Parameters of the Competing Fermentation Models After Model Discriminating Experiment II. (continued)

Model	2.5		2.3 reduced		
Parameter	Value	σ	Value	σ	Unit
$\mu_{max,S1}$	0.418	0.00371	0.417	0.00380	h^{-1}
Km_{S1}	0.570	0.0466	0.00716	$7.74{\cdot}10^{-4}$	mM
m_{S1}	0.0179	0.00832	0.0348	0.00212	$mM.OD^{-1}.h^{-1}$
Y_{XS1}	0.385	0.0148	0.344	0.0717	$OD^{-1}.mM$
$\mu_{max,S2}$	0.130	0.0300	1.19	13.7	h^{-1}
Km_{S2}	0.0322	0.208	1.92	31.5	mM
Y_{XS2}	18.6	3.87	13.3	2.03	$OD^{-1}.mM$
$\pi_{max,S1}$	0.0870	0.00717	0.105	0.00833	$mM.OD^{-1}.h^{-1}$
Kp_{S1}	55.6	17.2	55.6	3.42	mM
Y_{PS1}	0.595	0.0214	0.698	0.218	$mM.mM^{-1}$
$\mu_{max,S3}$	6.31	12.4	6.78	10.1	h^{-1}
Km_{S3}	9.06	14.2	9.03	13.8	μM
Y_{XS3}	84.1	101	95.0	9.26	$OD.\mu M^{-1}$
$\mu_{max,S2Int}$	52.4	34.6	33.9	56.4	h^{-1}
m_{S2Int}	0.0256	0.0318			mM^{-1}
m_{S2Int}			16.6	18.0	$OD.mM^{-1}.h^{-1}$
kd_{S2}	0.00965	0.00611	0.0351	0.00796	–
$Ki_{P,rs2}$	1.12	7.20	0.263	1.63	mM
$\mu_{max,S3Int}$	14.9	144	12.7	70.9	h^{-1}
Km_{S3Int}	0.220	2.19	0.330	1.85	$\mu M.OD^{-1}$
m_{S3Int}	$3.62{\cdot}10^{-5}$	0.262			h^{-1}
$C_{S3IntMin,rx}$	0.00914	0.00167	0.00918	2.68E-04	$\mu M.OD^{-1}$
$k_{S3extra}$	0.822	0.703	0.936	0.0456	–
Kp_{S3}	0.187	1.45	0.118	0.274	$\mu M.OD^{-1}$
$C_{S3IntMin,rp}$	0.00798	0.00392	0.00849	$5.04{\cdot}10^{-4}$	$\mu M.OD^{-1}$
$k_{S1extra}$	0.419	0.0237	0.345	0.0283	–
$Ki_{P,rp}$	620	142	398	88.9	mM
$\pi_{max,S3}$	14.5	122	15.2	38.0	$mM.OD^{-1}.h^{-1}$
$Ki_{P,rxs2int}$	0.849	0.737	5.03	6.23	$mM.h-1$

TABLE F.4.: Estimated Lag-Times of the First Batch Experiment ($t_{lag,exp1}$), Model Discriminating Experiment I ($t_{lag,exp2}$), the Subsequent Intuitively Planned Experiment ($t_{lag,exp3}$) and of Model Discriminating Experiment II ($t_{lag,exp4}$), After these Four Experiments.

Model	$t_{lag,exp1}[h]$	$t_{lag,exp2}[h]$	$t_{lag,exp3}[h]$	$t_{lag,exp4}[h]$
2.1	$6.71 \cdot 10^{-4}$	1.00	1.03	0.801
2.2	$2.76 \cdot 10^{-4}$	1.56	1.39	1.31
2.3	0.241	1.67	1.96	0.908
2.4	0.00358	1.51	1.42	0.247
2.5	$1.09 \cdot 10^{-4}$	1.50	1.72	1.65

G. Alternative Off-line Optimized Production Experiments

The experiment in paragraph 5.2.6 on page 116 was designed by optimizing the expected total volumetric productivity with an extra limitation with respect to the maximal biomass concentration: the OD_{600} should stay below 70. Without this extra limitation, much higher biomass concentration were expected, as shown in paragraph G.1.

Besides the total volumetric productivity, also other criteria could be of interest for process optimization. For instance a maximal final product concentration or the absence of problematic by-products are often of interest to facilitate the down-stream processing. The overall yield of product on substrate can be of interest when substrate costs form a significant part of the production costs. As another example, this overall yield is also optimized off-line just like the total volumetric productivity. The suggested experiment is mentioned in paragraph G.2.

G.1. Total Volumetric Productivity

The optimized process with respect to the total volumetric productivity, without the extra limitation on the maximal optical density, is shown in figure G.1, together with the expected results. This experiment could not be performed due to limitations with respect to the oxygen transfer between the gas phase and the liquid phase in the used fermentation equipment.

The expected maximal total volumetric productivity was with 14.0 $mM.h^{-1}$ higher than the expected value with the extra limitation on the biomass concentration, which was 10.2 $mM.h^{-1}$.

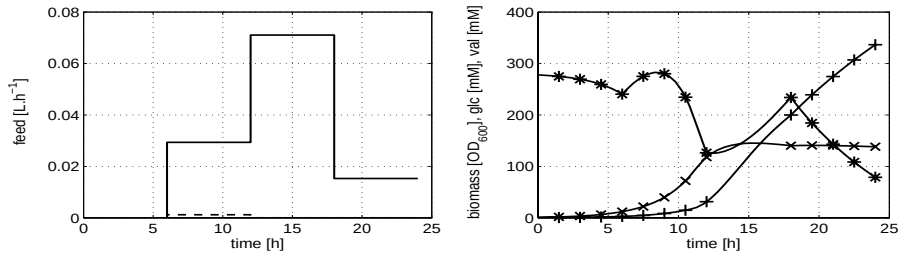

(a) Suggested experiment. Feed rates of a 500 g/L glucose solution as a solid line and of a 55 mM L-isoleucine solution as a dashed line. Initial concentrations were 50 g/L glucose, 10 mM L-isoleucine and 4.60 μM pantothenic acid. No further feed of pantothenic acid was needed.

(b) Expected results of the suggested experiment. Biomass in OD_{600} as $\times$, glucose in mM as $*$ and L-valine in mM as $+$.

FIGURE G.1.: Suggested experiment for a maximized TVP, without limitations with respect to the biomass concentration.

G.2. Overall Yield of Product on Substrate

Optimization of the yield of product on substrate suffers from the risk of suggesting very low final product concentrations because of the positive effect of using little substrate for biomass production. Since this can not be a realistic optimal process, a penalty function was introduced to prevent such very low final product concentrations. The used optimization criterion was

$$\xi^* = \arg\max_{\xi} \frac{P_{end}}{S_{used,int}} - \begin{cases} f_s \cdot (P_{min} - P_{end}) & : \quad P_{end} < P_{min} \\ 0 & : \quad P_{end} \geqq P_{min} \end{cases} \tag{G.1}$$

where ξ is again the description of the experiment, P_{end} is the final concentration of L-valine, $S_{used,int}$ is the integral concentration of substrate which was available, corrected for changes in volume and sampling. The scaling factor f_s is an arbitrarily chosen factor, with which the impact of the penalty function can be influenced. High values will make it more unlikely that the optimal value will be found at a lower concentration than the minimal desired concentration P_{min}.

A minimal concentration of 250 mM L-valine was used in the current example and the factor f_s was set to 0.06. Note that here, just like with the optimization with respect to the productivity, again the criterion was calculated for each suggested measurement timepoint and the best value was chosen, resulting in possibly shorter production experiments than the maximal allowed duration. All constraints, such as the maximal duration of 48 h, the way the feeds were described, etc. were the same as for the optimization of the total volumetric productivity.

The suggested experiment and the corresponding expected results are shown in figure G.2.

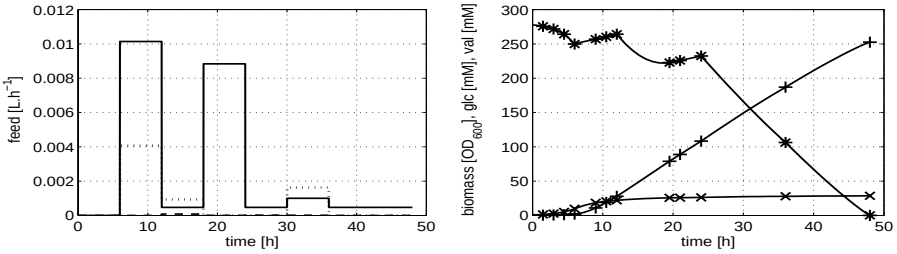

(a) Suggested experiment. Feed rates of a 500 g/L glucose solution as a solid line, of a 55 mM L-isoleucine solution as a dashed line and of a 50 μM pantothenic acid solution as a dotted line. Initial concentrations were 50 g/L glucose, 0.85 mM L-isoleucine and 7.67 μM pantothenic acid.

(b) Expected results of the suggested experiment. Biomass in OD_{600} as a line with $\times$, glucose in mM with $*$ and L-valine in mM with $+$. The markers indicate sampling times.

FIGURE G.2.: Suggested experiment for a maximized overall yield of L-valine on glucose.

The optimized experiment would use the maximal allowed duration of 48 hours. The expected final concentration is just above the limit of 250 mM and the glucose would be just depleted at this point. A maximal overall yield of 49% $\frac{mol}{mol}$ or 32% $\frac{g}{g}$.

This would be more than 10% increase, compared to the maximal yield of about 29% $\frac{g}{g}$, which was reached in model discriminating experiment II. This 29% was however already at least as high as the yield mentioned for the industrial production of L-valine by a *Brevibacterium* mentioned in Drauz et al. (2003) and it remains to be tested if the increased yield can be achieved. The maximal momentary yields which were achieved so far, were reached in model discriminating experiment II in a period without biomass growth and the data are shown in figure 5.15(b) on page 114. These results are of course rather inaccurate since they are only based on the differences between subsequent (splined) measured values of both L-valine and glucose. This also explains the partly strong fluctuations. The achieved momentary yields do however correspond well to the molecular yield of 67% which was reported for production of L-valine from glucose by non-growing cells of *Brevibacterium* by Terasawa et al. (1990). Also the suggested maximal overall yield of 49% $\frac{mol}{mol}$ seems to correspond reasonably to these results. This value is of course lower due to the fact that some glucose also has been used for biomass growth.

Summary

Fast development of production processes is crucial for successful industrial use of biotechnology in order to keep development costs low and time-to-market short. On the other hand, it can also be very important to optimize the process to keep production costs low. The use of mathematical models can be very helpful for faster process development and for optimization and control of the final process. Furthermore, especially when the models have a mechanistic meaning, they can provide useful information for further strain development. The development of the model itself is often difficult and time-consuming.

A framework for modeling and optimization was written in the MATLAB environment. The system allows the use and simulation of dynamic multivariable experiments. Models can be fitted to the experimental data and the accuracy of the parameter estimates can be regarded. Also the accuracy of the model fit can be addressed and the different models can be compared. Importantly, the programs also provide options for the design of informative experiments. These can be either experiments for discrimination among rival models, for improvement of the parameter estimation or for improvement of the production process with respect to, for example, the overall volumetric productivity. Constraints can be provided on the designed experiments. The constraints which were used in this work, included limits on the allowed feedrates and initial conditions as well as limits on the expected concentrations and suspension volume throughout the designed experiment.

A general sequential experimental design procedure was presented where first model discriminating experiments are suggested until one model structure would be chosen. If necessary, subsequent experiments can then be designed for improvement of the parameter estimation.

For the design of experiments for parameter estimation, a D-optimal design criterion was implemented.

Four different model discriminating design criteria were adapted from criteria found in literature, for the use with dynamic multivariable experiments. Three of them (BH, BF and CA) regarded the model variance and one (HR) not. A fifth criterion (ND) was developed, based on the criterion without variance. The five criteria were used and compared in a simulative study with two examples. The system entropy criterion (BH) lead to more insecure results. Problems were encountered in the use of the CA criterion for discrimination between partly poorly estimable fermentation models. The positive influence of the use of a model variance was not clear in the current examples, but the

model variance accounted for about 90% of the calculation time. With larger models and longer experiments, this is bound to get even more. The ND criterion performed slightly better than the HR criterion in one of the simple examples.

The system for modeling and experimental design was used for process development of L-valine production by a genetically modified *C. glutamicum*. With four experiments, a model was developed and selected. Both the BH and the ND criterion were used for the design of these experiments.

The selected model was used for calculation of optimal feed trajectories for optimization of the total volumetric productivity of the valine production process. This process was performed without further control strategies, leading to the production of 6.2 $mM.h^{-1}$ L-valine in a fermentation of 30 h, an 11% increase compared to the best prior experiments.

The model was shown to predict especially the glucose uptake rate very satisfactory in the optimized experiment, i.e. in the region of interest. Also some discrepancies between the model predictions and the actual experimental results were identified, providing indications for model improvement. These discrepancies are caused by the strong extrapolation of the model outside the conditions which were used before. Therefore, the use of optimized feed trajectories is also recommended during model development.

Furthermore, interesting information on the used biological system under process relevant conditions was gathered, providing important indications for further research and possibly also strain improvement.

Zusammenfassung

Es ist wichtig, die Entwicklungszeit von industriellen Bioprozessen zu verkrzen, um somit die Entwicklungskosten niedrig und 'time-to-market' kurz zu halten. Anderseits ist es auch sehr wichtig, die Prozesse zu optimieren, um die Produktionskosten niedrig zu halten. Mathematische Modellierung ist ein wichtiges Werkzeug für die schnelle Prozessentwicklung und für die Prozessoptimierung. Vor allem mechanistische Modelle können dabei auch noch viele wichtige Informationen für die weitere Stammentwicklung liefern. Die Entwicklung der Modelle kann aber schwierig und Zeitaufwändig sein.

Ein System für die Modellierung und Optimierung dynamischer Experimente mit mehreren Zustandsvariablen ist in der MATLAB Umgebung entwickelt worden. In diesem System können die Modelle an experimentelle Daten angepasst werden, und die Parametergenauigkeit kann betrachtet werden. Darüberhinaus kann auch die Genauigkeit der Modellanpassung geprüft werden und Modelle können miteinander verglichen werden. Wichtig ist auch die Möglichkeit der gezielten Planung von Versuchen. Diese können entweder zur Modelldiskriminierung, Parameterschätzung oder Prozessoptimierung benutzt werden. Zur Prozessoptimierung kann zum Beispiel die erwartete totale volumetrische Produktivität maximiert werden. Weiter können Randbedingungen angegeben werden, sowie maximale und minimale Anfangskonzentrationen und Zufütterraten. Neben diesen direkten Grenzen der erlaubten Optimierungsparameter sind auch Grenzen für die erwarteten Substratkonzentrationen und das Volumen während des ganzen Versuches implementiert worden.

Ein Verfahren zur sequentiellen Versuchsplanung ist vorgestellt worden. Hierbei werden zuerst modelldiskriminierende Experimente vorgeschlagen, bis eine Modellstruktur selektiert worden ist. Danach können, wenn nötig, weitere Versuche zur Verbesserung der Parametergenauigkeit geplant werden.

Das D-optimale Kriterium ist für die Versuchsplanung zur Parameterschätzung implementiert worden.

Vier Kriterien zur modelldiskriminierenden Versuchsplanung sind für dynamische multivariable Experimente angepasst und implementiert worden. Drei dieser Kriterien (BH, BF, CA) enthalten die Modellvarianz. Das HR Kriterium benutzt die Modellvarianz nicht. Basierend auf diesem HR Kriterium ist ein weiteres Kriterium (ND) ohne Modellvarianz entwickelt worden, was sich speziell für dynamische Experimente eignen soll. Die fünf Kriterien sind in einer simulativen Studie mit zwei Beispielen miteinander verglichen worden. Das BH Kriterium, das als einziges das Konzept der Systementropie benutzt, hat zu unsichereren Ergebnissen geführt. Das CA Kriterium hat in einem der Beispiele

nicht gut funktioniert. Die Modellvarianz hat nicht eindeutig zu besserer Versuchsplanung geführt. Außerdem brauchten die Kriterien mit der Modellvarianz zehnfach mehr Rechenzeit als die Kriterien ohne Modellvarianz und dieser Unterschied wird noch größer bei größeren Modellen und längeren Experimenten. In einem Beispiel hat das neue ND Kriterium zu etwas bessere Ergebnisse als das HR Kriterium geführt.

Das System zur Modellierung und Versuchsplanung ist für die Prozessentwicklung eines L-Valin-Produktionsprozesses mit einem genetisch modifizierten *C. glutamicum* eingesetzt worden. Nach vier Experimenten ist ein makrokinetisches Modell entwickelt und selektiert worden. Sowohl das BH Kriterium als auch das ND Kriterium sind hierbei verwendet worden.

Anhand dieses Modells ist ein fed-batch Experiment zur Maximierung der totalen volumetrischen Produktivität geplant worden. Die Durchführung dieses Prozesses ergab eine Produktion von 6.2 mMh^{-1} L-Valin in einer Fermentationdauer von 30 Stunden, was eine 11-prozentige Erhöhung im Vergleich zu vorherigen Experimenten darstellt.

Das Modell hat vor allem die Glukoseverbrauchsrate des optimierten Experimentes sehr gut vorhergesagt. Es sind aber auch Unterschiede zwischen den erwarteten und den experimentellen Ergebnissen identifiziert worden, die für eine Verbesserung des Modells benutzt werden können. Die Unterschiede werden durch eine starke Extrapolation außerhalb der bisher benutzten Verhältnisse verursacht. Es wird darum sehr empfohlen, auch während der Modellentwicklung schon Versuche zur Prozessoptimierung durchzuführen.

Weiterhin sind in den fünf Versuchen auch viele prozessrelevante Informationen gesammelt worden, die für ein besseres biologisches Verständnis und möglicherweise für weitere Stammentwicklung nützlich sind.

Acknowledgements

This thesis results from work I performed at the Institute of Biotechnology of Research Centre Jülich (IBT).

I have really enjoyed working in the very stimulating environment at the institute and I am grateful to *Prof. C. Wandrey*, for making this possible. I am impressed by the great variety of interesting projects, which are worked on at the institute. Furthermore, I would like to thank Prof. Wandrey for supporting me and putting trust in me. I think the nice German word for a supervisor of a PhD student covers it very well: it could be literally translated as 'PhD-father'.

In the first place, however, *Dr. Ralf Takors* has been my supervisor. I thank him very much for his confidence in me and the many fruitful, interesting and open discussions. I am grateful to Ralf for supervising the project and support and stimulation to present my work inside, but especially also outside the institute.

Although the work which is reported here has been performed at the Research Centre in Jülich, this thesis is submitted at the Rheinisch-Westfälischen Technischen Hochschule Aachen under supervision of *Prof. J. Büchs*. I thank Prof. Büchs for his supervision. Furthermore, I appreciate the fruitful and interesting discussions very much. I especially would like to mention the suggestion of the experiments with the Ramos equipment and the extensive discussion of the results thereof.

I feel I am very lucky with the students who came to work with me in Jülich. *Christian Bollmann, Barbara Kaiser, Diana Steinbuesch* and *Sandra Stollwerk* were all very motivated, motivating and a pleasure to work with. They helped me a lot with the work in the laboratory and made the work more fun. For this, I am very thankful to them.

Several biologists at the Institute of Biotechnology-I have helped me with discussions on the biological mechanisms behind the process and the used strain. I especially like to thank *Prof. Bott, Eva Radmacher, Christian Lange, Andreas Krug* and *Dr. L. Eggeling*.

I am obliged to AC Biotec: *Dr. Tibor Anderlei* and *Dr. Simon Curvers* for the opportunity to use the Ramos equipment and their help in performing the experiments and discussing the results.

I would like to thank *Heidi Haase-Reiff* here for her help with the HPLC measurements.

The members of the *Fermentation group* have helped me a lot inside and outside the work. They also contributed very much to the very pleasant working atmosphere and I have enjoyed the numerous discussions about many subjects, either related to the work or not. I thank all who made may time in Jülich such a pleasant one.

One of the reasons why the IBT provides such a stimulating and pleasant working environment is the great infrastructure including the library, electronic- and mechanic workplaces and computer network. In this respect I also would like to thank *Horst Kiehl* and *Andreas Franz* for keeping my computer running, which was clearly crucial for my work.

I am grateful to *Lasse Greiner* for the successful and most enjoyable cooperation, providing an appealing example of how modeling can be useful (Brik Ternbach and Greiner, 2004). I also appreciate his help with LaTeX very much.

Last but not least, I would like to use this opportunity to thank the '*home front*'. My friends and family always kept supporting me and there was always an open door. Special thanks also go to *Miranda Morin*, who could even forgive me when I went to spend some time at work when she was with me in Jülich.

Bibliography

K. Akashi, H. Shibai, and Y. Hirose. Effect of oxygen supply on L-valine fermentation. *Journal of Fermentation Technology*, 55(4):364–368, 1977.

G.H. An, K.B. Song, and A.J. Sinskey. Redirection of carbon flux to lysine in a recombinant of Corynebacterium lactofermentum ATCC 21799 by limited supply of pantothenate. *Journal of Bioscience and Bioengineering*, 88(2):168–172, 1999.

T. Anderlei and J. Büchs. Device for sterile online measurement of the oxygen transfer rate in shaking flasks. *Biochemical Engineering Journal*, 7(2):157–162, 2001.

T. Anderlei, W. Zang, M. Papaspyrou, and J. Büchs. Online respiration activity measurement (OTR, CTR, RQ) in shake flasks. *Biochemical Engineering Journal*, 17(3): 187–194, 2004.

J.F. Andrews. A mathematical model for the continuous culture of microorganisms utilizing inhibitory substrates. *Biotechnology and Bioengineering*, 10:707–723, 1968.

A.C. Atkinson. Developments in the design of experiments. *International Statistical Review*, 50:161–177, 1982.

A.C. Atkinson and V.V. Fedorov. Optimal design: experiments for discriminating between several models. *Biometrika*, 62(2):289–303, 1975.

R. Auer and F.C. Thyrion. Kinetics of the total oxidation of methane over a La0.9Ce0.1CoO3 perovskite catalyst. *Industrial and Engineering Chemistry Research*, 41(4):680–690, 2002.

R. Babuška, H.B. Verbruggen, and E.J.L. van Can. Fuzzy modeling of enzymatic penicillin-G conversion. *Engineering Applications of Artificial Intelligence*, 12:79–92, 1999.

J.E. Bailey. Towards a science of metabolic engineering. *Science*, 252:1668–1675, 1991.

J.E. Bailey. Mathematical modeling and analysis in biochemical engineering: Past accomplishments and future opportunities. *Biotechnology Progress*, 14:8–20, 1998.

R.K. Bajpai, M. Reuss, and W. Held. Regulation phenomena in methanol consuming yeasts - an experiment with model discrimination. *Biotechnology and Bioengineering*, 23(3):499–521, 1981.

R. Bajramovic and P.M. Reilly. Explanation for an apparent failure of Box-Hill procedure for model discrimination. *Canadian Journal of Chemical Engineering*, 55(1):82–86, 1977.

M. Baltes, R. Schneider, C. Sturm, and M. Reuss. Optimal experimental design for parameter estimation in unstructured growth models. *Biotechnology Progress*, 10: 480–488, 1994.

H. Bandemer and A. Bellmann. *Statistische Versuchsplanung*. Mathematik für Ingenieure und Naturwissenschaftler. B.G. Teubner Verlagsgesellschaft, Stuttgart Leipzig, 4 edition, 1994.

N. Bayan, C. Houssin, M. Chami, and G. Leblon. Mycomembrane and S-layer: two important structures of Corynebacterium glutamicum cell envelope with promising biotechnology applications. *Journal of Biotechnology*, 104(1-3):55–67, 2003.

T. Becker, T. Enders, and A. Delgado. Dynamic neural networks as a tool for the online optimization of industrial fermentation. *Bioprocess and Biosystems Engineering*, 24: 347–354, 2002.

R.J. Berger, E.H. Stitt, G.B. Marin, F. Kapteijn, and J.A. Moulijn. Eurokin - chemical reaction kinetics in practice. *Cattech*, 5(1):30–60, 2001.

F. Bergter and W.A. Knorre. Computer-simulation of growth and product formation by Saccharomyces cerevisiae. *Zeitschrift Fur Allgemeine Mikrobiologie*, 12(8):613–629, 1972.

R. Berkholz, D. Rohlig, and R. Guthke. Data and knowledge based experimental design for fermentation process optimization, 2000. (03) Berkholz R/BioControl Jena GmbH/D 07745 Jena/GERMANY (42) English Article (44) 383QE.

D. Birkes and Y. Dodge. *Alternative Methods of Regression*. John Wiley & Sons, New York, 1993.

G. Birol, B. Kirdar, and Z.I. Onsan. A simple structured model for biomass and extracellular enzyme production with recombinant saccharomyces cerevisiae ypb-g. *Journal of Industrial Microbiology & Biotechnology*, 29(3):111–116, 2002.

M.F. Biselli. *Enzymkatalysierte Racematspaltunüg von Aminosäuren mit integrierter Rückführung: dargestellt am Beispiel der Umsetzung von D,L-Alanin zu L-Alanin*. PhD thesis, Universität Bonn, 1992.

A. Bodalo-Santoyo, J.L. Gomez-Carrasco, E. Gomez-Gomez, J. Bastida-Rodriquez, M.F. Maximo-Martin, and A.M. Hidalgo-Montesinos. Production of optically pure L-valine in fluidized and packed bed reactors with immobilized L-aminoacylase. *Journal of Chemical Technology and Biotechnology*, 74(5):403–408, 1999.

E. Boles, H. Ebbighausen, B. Eikmanns, and R. Krämer. Unusual regulation of the uptake system for branched-chain amino-acids in Corynebacterium glutamicum. *Archives of Microbiology*, 159(2):147–152, 1993.

R. Bona and R. Moser. Modelling of growth of Corynebacterium glutamicum under biotin limitation. *Bioprocess Engineering*, 17(2):121–125, 1997.

D.-M. Borth. A total entropy criterion for the dual problem of model discrimination and parameter estimation. *Journal of the Royal Statistical Society Series B-Statistical Methodology*, 37:77–87, 1975.

A.N.R. Bos, L. Lefferts, G.B. Marin, and M.H.G.M. Steijns. Kinetic research on heterogeneously catalysed processes: A questionnaire on the state-of-the-art in industry. *Applied Catalysis A: General*, 160:185–190, 1997.

G.E.P. Box and W.J. Hill. Discrimination among mechanistic models. *Technometrics*, 9:57–71, 1967.

R.D. Boyd, K.J. Touchette, G.C. Castro, M.E. Johnston, K.U. Lee, and I.K. Han. Recent advances in amino acid and energy nutrition of prolific sows - review. *Asian-Australasian Journal of Animal Sciences*, 13(11):1638–1652, 2000.

M.A. Brik Ternbach and L. Greiner. Kinetic study of homogeneous alkene hydrogenation by model discrimination. *Advanced Synthesis & Catalysis*, 2004. accepted for publication.

A.L. Burke, T.A. Duever, and A. Penlidis. Discriminating between the terminal and penultimate models using designed experiments: An overview. *Industrial and Engineering Chemistry Research*, 36(4):1016–1035, 1997.

A. Burkovski. Ammonium assimilation and nitrogen control in Corynebacterium glutamicum and its relatives: an example for new regulatory mechanisms in actinomycetes. *Fems Microbiology Reviews*, 27(5):617–628, 2003a.

A. Burkovski. I do it my way: regulation of ammonium uptake and ammonium assimilation in Corynebacterium glutamicum. *Archives of Microbiology*, 179(2):83–88, 2003b.

G. Buzzi-Ferraris and P. Forzatti. A new sequential experimental design procedure for discriminating among rival models. *Chemical Engineering Science*, 38(2):225–232, 1983.

G. Buzzi-Ferraris, P. Forzatti, and Paolo Canu. An improved version of a sequential design criterion for discriminating among rival multiresponse models. *Chemical Engineering Science*, 45(2):477–481, 1990.

G. Buzzi-Ferraris, P. Forzatti, G. Emig, and H. Hofmann. Sequential experimental design for model discrimination in the case of multiple responses. *Chemical Engineering Science*, 39(1):81–85, 1984.

H.J.L. Can, v., H.A.B. Braake, C. Hellinga, K.C.A.M. Luyben, and J.J. Heijnen. An efficient model development strategy for bioprocesses based on neural networks in macroscopic balances. part I. *Biotechnology and Bioengineering*, 62:666–680, 1997.

C. Chassagnole, A. Diano, F. Letisse, and N.D. Lindley. Metabolic network analysis during fed-batch cultivation of Corynebacterium glutamicum for pantothenic acid production: first quantitative data and analysis of by-product formation. *Journal of Biotechnology*, 104(1-3):261–272, 2003.

C. Chassagnole, F. Letisse, A. Diano, and N.D. Lindley. Carbon flux analysis in a pantothenate overproducing Corynebacterium glutamicum strain. *Molecular Biology Reports*, 29(1-2):129–134, 2002.

M. Chatterjee and S.P. Chatterjee. Valine production from hydrocarbon by Micrococcus Varians. *Folia Microbiologica*, 27(4):228–236, 1982.

S.P. Chattopadhyay and A.K. Banerjee. Production of valine by a Bacillus Sp. *Zeitschrift Fur Allgemeine Mikrobiologie*, 18(4):243–254, 1978.

B.H. Chen and S.P. Asprey. On the design of optimally informative dynamic experiments for model discrimination in multiresponse nonlinear situations. *Industrial and Engineering Chemistry Research*, 42(7):1379–1390, 2003.

B. Cheng, R.L. Fournier, and P.A. Relue. The inhibition of Escherichia coli lac operon gene expression by antigene oligonucleotides - mathematical modeling. *Biotechnology and Bioengineering*, 70(4):467–472, 2000.

H. Christensen, N.J. Garton, R.W. Horobin, D.E. Minnikin, and M.R. Barer. Lipid domains of mycobacteria studied with fluorescent molecular probes. *Molecular Microbiology*, 31(5):1561–1572, 1999.

T.F. Coleman and Y.Y. Li. An interior trust region approach for nonlinear minimization subject to bounds. *Siam Journal on Optimization*, 6(2):418–445, 1996.

M.J. Cooney and K.A. McDonald. Optimal dynamic experiments for bioreactor model discrimination. *Applied Microbiology and Biotechnology*, 43(5):826–837, 1995.

A.J. Cooper, J.Z. Ginos, and A. Meister. Synthesis and properties of the alpha-keto acids. *Chemical Reviews*, 83(3):321–358, 1983.

C. Cordes, B. Mockel, L. Eggeling, and H. Sahm. Cloning, organization and functional-analysis of ilva, ilvb and ilvc genes from Corynebacterium glutamicum. *Gene*, 112(1): 113–116, 1992.

N. Costa-Riu, A. Burkovski, R. Kramer, and R. Benz. Por-A represents the major cell wall channel of the gram-positive bacterium Corynebacterium glutamicum. *Journal of Bacteriology*, 185(16):4779–4786, 2003a.

N. Costa-Riu, E. Maier, A. Burkovski, R. Kramer, F. Lottspeich, and R. Benz. Identification of an anion-specific channel in the cell wall of the gram-positive bacterium Corynebacterium glutamicum. *Molecular Microbiology*, 50(4):1295–1308, 2003b.

M.W. Covert and B.O. Palsson. Transcriptional regulation in constraints-based metabolic models of Escherichia coli. *Journal of Biological Chemistry*, 277(31):28058–28064, 2002.

J.N. Dabes, R.K. Finn, and C.R. Wilke. Equations of substrate-limited growth - case for Blackman kinetics. *Biotechnology and Bioengineering*, 15(6):1159–1177, 1973.

D. Degenring, C. Froemel, G. Dikta, and R. Takors. Sensitivity analysis for the reduction of complex metabolism models. *Journal of Process Control*, 14(7):729–745, 2004.

H. Dette and I. Roder. Optimal discrimination designs for multifactor experiments. *Annals of Statistics*, 25(3):1161–1175, 1997.

N.R. Draper and F. Pukelsheim. An overview of design of experiments. *Statistical Papers*, 37(1):1–32, 1996.

K. Drauz, Hoppe B., A. Kleemann, H.-P. Krimmer, W. Leuchtenberger, and C. Weckbecker. Amino acids. In *Ullmann's Encyclopedia of Industrial Chemistry*. John Wiley & Sons, Weinheim, 6 edition, 2003.

A. Drysch, M. El Massaoudi, C. Mack, R. Takors, A.A. de Graaf, and H. Sahm. Production process monitoring by serial mapping of microbial carbon flux distributions using a novel sensor reactor approach: Ii - c-13-labeling-based metabolic flux analysis and L-lysine production. *Metabolic Engineering*, 5(2):96–107, 2003.

H. Ebbighausen, B. Weil, and R. Kramer. Transport of branched-chain amino-acids in Corynebacterium glutamicum. *Archives of Microbiology*, 151(3):238–244, 1989.

I. Eggeling, C. Cordes, L. Eggeling, and H. Sahm. Regulation of acetohydroxy acid synthase in Corynebacterium glutamicum during fermentation of alpha-ketobutyrate to L-isoleucine. *Applied Microbiology and Biotechnology*, 25(4):346–351, 1987.

L. Eggeling, S. Morbach, and H. Sahm. The fruits of molecular physiology: Engineering the L-isoleucine biosynthesis pathway in Corynebacterium glutamicum. *Journal of Biotechnology*, 56:167–182, 1997.

L. Eggeling, W. Pfefferle, and H. Sahm. Amino acids. In C. Ratledge and B. Kristiansen, editors, *Basic Biotechnology*, volume 2nd edition, pages 281–303. Cambridge University Press, Cambridge, 2 edition, 2001.

J. Elf, O.G. Berg, and W. Ehrenberg. Comparison of repressor and transcriptional attenuator systems for control of amino acid biosynthetic operons. *Journal of Molecular Biology*, 313(5):941–954, 2001.

J. Enriquez. Green biotechnology and European competitiveness. *Trends in Biotechnology*, 19(4):135–139, 2001.

S. Ensari, J.H. Kim, and H.C. Lim. Unstructured model for L-lysine fermentation under controlled dissolved oxygen. *Biotechnology Progress*, 19(4):1387–1390, 2003.

S. Ensari and H.C. Lim. Kinetics of L-lysine fermentation: a continuous culture model incorporating oxygen uptake rate. *Applied Microbiology and Biotechnology*, 62(1): 35–40, 2003.

A.A. Esener, J.A. Roels, and N.W.F. Kossen. Fed-batch culture - modeling and applications in the study of microbial energetics. *Biotechnology and Bioengineering*, 23(8): 1851–1871, 1981.

D. Espie and S. Macchietto. The optimal-design of dynamic experiments. *Aiche Journal*, 35(2):223–229, 1989.

D. Faller, U. Klingmuller, and J. Timmer. Simulation methods for optimal experimental design in systems biology. *Simulation-Transactions of the Society for Modeling and Simulation International*, 79(12):717–725, 2003.

V. Fedorov and V. Khabarov. Duality of optimal designs for model discrimination and parameter estimation. *Biometrika*, 73(1):183–190, 1986.

D.P. Filev, M.S. Kishimoto, S. Sengupta, T. Yoshida, and H. Taguchi. Application of the fuzzy theory to simulation of batch fermentation. *Journal of Fermentation Technology*, 63:545–553, 1985.

I. Ford, D.M. Titterington, and C.P. Kitsos. Recent advances in nonlinear experimental design. *Technometrics*, 31(1):49–60, 1989.

G. Frazzetto. White biotechnology - the application of biotechnology to industrial production holds many promises for sustainable development, but many products still have to pass the test of economic viability. *Embo Reports*, 4(9):835–837, 2003.

A.G. Fredrickson, R.D.I. McGee, and A.M. Tsuchiya. Mathematical models in fermentation processes. *Advances in Applied Microbiology*, 23:419–, 1970.

G.F. Froment. Model discrimination and parameter estimation in heterogeneous catalysis. *Aiche Journal*, 21(6):1041–1057, 1975.

G.F. Froment and R. Mezaki. Sequential discrimination and estimation procedures for rate modelling in heterogeneous catalysis. *Chemical Engineering Science*, 25:293–300, 1970.

C.E. Garcia, D.M. Prett, and M. Morari. Model predictive control - theory and practice - a survey. *Automatica*, 25(3):335–348, 1989.

A.N. Glazer and H. Nikaido. *Microbial Biotechnology.* Freeman, New York, 1995.

D.E. Goldberg. *Genetic Algorithms in Search, Optimization and Machine Learning.* Wiley Publishing Company, Addison, 1989.

I. Golobic, H. Gjerkes, I. Bajsic, and J. Malensek. Software sensor for biomass concentration monitoring during industrial fermentation. *Instrumentation Science & Technology*, 28(4):323–334, 2000.

L.R.B. Goncalves, R. Sousa, R. Fernandez-Lafuente, J.M. Guisan, R.L.C. Giordano, and R.C. Giordano. Enzymatic synthesis of amoxicillin - avoiding limitations of the mechanistic approach for reaction kinetics. *Biotechnology and Bioengineering*, 80(6): 622–631, 2002.

P. Gourdon, M. Raherimandimby, H. Dominguez, M. Cocaign-Bousquet, and N.D. Lindley. Osmotic stress, glucose transport capacity and consequences for glutamate overproduction in Corynebacterium glutamicum. *Journal of Biotechnology*, 104(1-3):77–85, 2003.

L.H.P. Harada, A.C. Da Costa, and R. Maciel. Hybrid neural modeling of bioprocesses using functional link networks. *Applied Biochemistry and Biotechnology*, 98:1009–1023, 2002.

R.H. Harms and G.B. Russell. Evaluation of valine requirement of the commercial layer using a corn-soybean meal basal diet. *Poultry Science*, 80(2):215–218, 2001.

M. Hayashi, H. Mizoguchi, N. Shiraishi, M. Obayashi, S. Nakagawa, J. Imai, S. Watanabe, T. Ota, and M. Ikeda. Transcriptome analysis of acetate metabolism in Corynebacterium glutamicum using a newly developed metabolic array. *Bioscience Biotechnology and Biochemistry*, 66(6):1337–1344, 2002.

E. Heinzle and U. Saner. Methodology for process control in research and development. In M. Pons, editor, *Bioprocess Monitoring and Control.* Hanser, Munich, 1991.

M.A. Henson. Nonlinear model predictive control: current status and future directions. *Computers & Chemical Engineering*, 23(2):187–202, 1998.

T. Hermann. Industrial production of amino acids by coryneform bacteria. *Journal of Biotechnology*, 104(1-3):155–172, 2003.

T. Hermann, W. Pfefferle, C. Baumann, E. Busker, S. Schaffer, M. Bott, H. Sahm, N. Dusch, J. Kalinowski, A. Puhler, A.K. Bendt, R. Kramer, and A. Burkovski. Proteome analysis of Corynebacterium glutamicum. *Electrophoresis*, 22(9):1712–1723, 2001.

C. Herwig and U. von Stockar. A small metabolic flux model to identify transient metabolic regulations in Saccharomyces cerevisiae. *Bioprocess and Biosystems Engineering*, 24(6):395–403, 2002.

T.M. Hess. Process optimization with dynamic modeling offers big benefits. *Instrumentation & Control Systems*, 73(8):43–48, 2000.

P.D.H. Hill. A review of experimental design procedures for regression model discrimination. *Technometrics*, 20(1):15–21, 1978.

W.J. Hill, W.G. Hunter, and D.W. Wichern. A joint design criterion for the dual problem of model discrimination and parameter estimation. *Technometrics*, 10:145–160, 1968.

D.B. Hodge and M.N. Karim. Modeling and advanced control of recombinant zymomonas mobilis fed-batch fermentation. *Biotechnology Progress*, 18(3):572–579, 2002.

A. Holmberg. On the practical identifiability of microbial growth models incorporating michaelis-menten type nonlinearities. *Mathematical Biosciences. An International Journal*, 62(1):23–43, 1982.

M. Hongo and M. Ueyeda. Studies on oxidation-reduction potentials(orp) of microbial cultures part ii. L-valine fermentation by Aerobacter aerogenes No. 505 and its conversion to lactic acid and alanine formation under anaerobic conditions. *Agr. Biol. Chem.*, 36(2):269–272, 1972.

J.I. Horiuchi, M. Kishimoto, and H. Momose. Hybrid simulation of microbial behavior combining a statistical procedure and fuzzy identification of culture phases. *Journal of Fermentation and Bioengineering*, 79(3):297–299, 1995.

T. Hsiang and P.M. Reilly. A practical method for discriminating amongst mechanistic models. *The Canadian Journal of Chemical Engineering*, 49:865–871, 1971.

T.C. Hsiang and P.M. Reilly. Use of uniform prior parameter distribution in model discrimination. *Canadian Journal of Chemical Engineering*, 52(6):830–833, 1974.

W.G. Hunter and A.M. Reiner. Designs for discriminating between two rival models. *Technometrics*, 7:307–323, 1965.

M. Ikeda and S. Nakagawa. The Corynebacterium glutamicum genome: features and impacts on biotechnological processes. *Applied Microbiology and Biotechnology*, 62 (2-3):99–109, 2003.

V. Jarlier and H. Nikaido. Permeability barrier to hydrophilic solutes in Mycobacterium chelonei. *Journal of Bacteriology*, 172(3):1418–1423, 1990.

J. Kalinowski, B. Bathe, D. Bartels, N. Bischoff, M. Bott, A. Burkovski, N. Dusch, L. Eggeling, B.J. Eikmanns, L. Gaigalat, A. Goesmann, M. Hartmann, K. Huthmacher, R. Kramer, B. Linke, A.C. McHardy, F. Meyer, B. Mockel, W. Pfefferle, A. Puhler, D.A. Rey, C. Ruckert, O. Rupp, H. Sahm, V.F. Wendisch, I. Wiegrabe, and A. Tauch. The complete Corynebacterium glutamicum ATCC 13032 genome sequence and its impact on the production of L-aspartate-derived amino acids and vitamins. *Journal of Biotechnology*, 104(1-3):5–25, 2003.

C. Keilhauer, L. Eggeling, and H. Sahm. Isoleucine synthesis in Corynebacterium glutamicum - molecular analysis of the ilvB-ilvN-ilvC operon. *Journal of Bacteriology*, 175(17):5595–5603, 1993.

R. Kelle. *Substratgeregelte Aminosäureproduktion mit Corynebacterium glutamicum.* PhD thesis, RWTH Aachen, 1996.

M.T. Kidd, B.J. Kerr, J.P. Allard, S.K. Rao, and J.T. Halley. Limiting amino acid responses in commercial broilers. *Journal of Applied Poultry Research*, 9(2):223–233, 2000.

E. Kimura. Triggering mechanism of L-glutamate overproduction by DtsR1 in coryneform bacteria. *Journal of Bioscience and Bioengineering*, 94(6):545–551, 2002.

S. Kinoshita, S. Udaka, and M. Shimono. Studies on the amino acid fermentation. part i. production of L-glutamic acid by various microorganisms. *Journal of General and Applied Microbiology*, 3:193–205, 1957.

H. Kitano. Computational systems biology. *Nature*, 420(6912):206–210, 2002.

A.R. Konak. Derivation of a generalized Monod equation and its application. *Journal of Applied Chemistry and Biotechnology*, 24(8):453–455, 1974.

R. Krämer. Secretion of amino-acids by bacteria - physiology and mechanism. *Fems Microbiology Reviews*, 13(1):75–93, 1994.

J.O. Krömer, O. Sorgenfrei, K. Klopprogge, E. Heinzle, and C. Wittmann. In-depth profiling of lysine-producing corynebacterium glutamicum by combined analysis of the transcriptome, metabolome, and fluxome. *Journal of Bacteriology*, 186(6):1769–1784, 2004.

C. Lange, D. Rittmann, V.F. Wendisch, M. Bott, and H. Sahm. Global expression profiling and physiological characterization of Corynebacterium glutamicum grown in the presence of L-valine. *Applied and Environmental Microbiology*, 69(5):2521–2532, 2003.

C.M.S. Lee. constrained optimal designs for regression models. *Communications in Statistics A. Theory and Methods*, 16(3):765–783, 1987.

J. Lee, S.Y. Lee, S. Park, and A.P.J. Middelberg. Control of fed-batch fermentations. *Biotechnology Advances*, 17(1):29–48, 1999.

J.H. Lee, J. Hong, and H.C. Lim. Experimental optimization of fed-batch culture for poly-beta-hydroxybutyric acid production. *Biotechnology and Bioengineering*, 56(6): 697–705, 1997.

D. Leyval, D. Uy, S. Delaunay, J.L. Goergen, and J.M. Engasser. Characterisation of the enzyme activities involved in the valine biosynthetic pathway in a valine-producing strain of Corynebacterium glutamicum. *Journal of Biotechnology*, 104(1-3):241–252, 2003.

W. Liebl, M. Ehrmann, W. Ludwig, and K.H. Schleifer. Transfer of Brevibacterium divaricatum DSM-20297t, Brevibacterium flavum DSM-20411, Brevibacterium lactofermentum DSM-20412 and DSM-1412, and Corynebacterium-Lilium Dsm-20137t to Corynebacterium glutamicum and their distinction by ribosomal-RNA gene restriction patterns. *International Journal of Systematic Bacteriology*, 41(2):255–260, 1991.

W. Liebl, R. Klamer, and K.H. Schleifer. Requirement of chelating compounds for the growth of Corynebacterium glutamicum in synthetic media. *Applied Microbiology and Biotechnology*, 32(2):205–210, 1989.

P. Lindroth and K. Mopper. High performance liquid chromatographic determination of subpicomole amounts of amino acids by precolum fluorescence derivatization with o-phtaldialdehyde. *Analytical Chemistry*, 51(11):1667–1674, 1979.

R. Luedeking and E.L. Piret. A kinetic study of the lactic acid fermentation - batch process at controlled pH. *Journal of Biochemical and Microbiological Technology and Engineering*, 1(4):393–412, 1959.

S.K. Mandal and S.K. Majumdar. Effects of minerals on production of valine by Aerobacter aerogenes. *Folia Microbiologica*, 18(6):463–466, 1973.

A.C. McHardy, A. Tauch, C. Ruckert, A. Puhler, and J. Kalinowski. Genome-based analysis of biosynthetic aminotransferase genes of Corynebacterium glutamicum. *Journal of Biotechnology*, 104(1-3):229–240, 2003.

D. Meeter, W. Pirie, and W. Blot. A comparison of 2 model-discrimination criteria. *Technometrics*, 12(3):457–, 1970.

L. Michaelis and M.L. Menten. Die kinetik der invertinwirkung. *Biochemisches Zeitschrift*, 49:333–369, 1913.

J. Monod. *Recherches sur la croissance des cultures bacteriennes.*, volume 911 of *Actualites scientifiques et industrielles*. Hermann & cie, Paris, 1942.

G. Montepiedra and A.-B. Yeh. A two-stage strategy for the construction of D-optimal experimental designs. *Communications in Statistics.- Simulation and Computation*, 27(2):377–401, 1998.

A. Moore. Improving the image of biotechnology the European way. *Lancet*, 358(9294): 1664–1664, 2001.

S. Morbach, C. Junger, H. Sahm, and L. Eggeling. Attenuation control of ilvbnc in Corynebacterium glutamicum: Evidence of leader peptide formation without the presence of a ribosome binding site. *Journal of Bioscience and Bioengineering*, 90(5): 501–507, 2000.

S. Morbach, R. Kelle, S. Winkels, H. Sahm, and L. Eggeling. Engineering the homoserine dehydrogenase and threonine dehydratase control points to analyse flux towards L-isoleucine in Corynebacterium glutamicum. *Applied Microbiology and Biotechnology*, 45(5):612–620, 1996.

A. Muffler, S. Bettermann, M. Haushalter, A. Horlein, U. Neveling, M. Schramm, and O. Sorgenfrei. Genome-wide transcription profiling of Corynebacterium glutamicum after heat shock and during growth on acetate and glucose. *Journal of Biotechnology*, 98(2-3):255–268, 2002.

A. Munack. Optimal feeding strategy for identification of monod-type models by fed-batch experiments. In N.M. Fish, editor, *Computer Applications in Fermentation Technology: Modelling and Control of Biotechnological Processes*, International Conference on Computer Applications in Fermentation Technology, pages 195–204. SCI Elsevier applied science Publ., 4 edition, 1989.

K. Nakayama, S. Kinoshita, and S. Kitada. L-Valine production using microbial auxotroph. *Journal of General and Applied Microbiology*, 7(1):52–, 1961.

M. Nampoothiri and A. Pandey. Genetic tuning of coryneform bacteria for the overproduction of amino acids. *Process Biochemistry*, 33(2):147–161, 1998.

R. Neeleman, M. Joerink, C. Beuvery, and T. van Boxtel. Dual-substrate utilization by bordetella pertussis. *Applied Microbiology and Biotechnology*, 57(4):489–493, 2001.

J. Nielsen. Metabolic engineering. *Applied Microbiology and Biotechnology*, 55:263–283, 2001.

M. Nihtilä and J. Virkkunen. Practical identifiability of growth and substrate consumption models. *Biotechnology and Bioengineering*, 19(12):1831–1850, 1977.

M.A. Palaiomylitou, K.A. Matis, A.I. Zouboulis, and D.A. Kyriakidis. A kinetic model describing cell growth and production of highly active, recombinant ice nucleation protein in Escherichia coli. *Biotechnology and Bioengineering*, 78(3):321–332, 2002.

S.M. Park, A.J. Sinskey, and G. Stephanopoulos. Metabolic and physiological studies of Corynebacterium glutamicum mutants. *Biotechnology and Bioengineering*, 55(6): 864–879, 1997.

J. Pirt. *Principles of Microbe and Cell Cultivation,*. Blackwell Scientific Publications, Oxford, 1975.

I.E. Pownall. An international political economic view of the biotechnology industry. *Electronic Journal of Biotechnology*, 3(2):120–139, 2000.

K. Preuss, M.V. Le Lann, J. Proth, and H. Pingaud. Modelling and predictive control of fed-batch yeast growth on industrial pilot plant scale. *Chemical Engineering Journal*, 78(1):53–59, 2000.

D.J. Pritchar and D.W. Bacon. Potential pitfalls in model discrimination. *Canadian Journal of Chemical Engineering*, 52(1):103–109, 1974.

L. Pronzato. Adaptive optimization and d-optimum experimental design. *Annals of Statistics*, 28(6):1743–1761, 2000.

A. Puhler and A. Tauch. A new era in Corynebacterium glutamicum biotechnology. *Journal of Biotechnology*, 104(1-3):1–3, 2003.

F. Pukelsheim and J.-L. Rosenberger. Experimental designs for model discrimination. *Journal of the American Statistical Association*, 88(422):642–649, 1993.

E. Radmacher. *Untersuchungen zur L-Valinbildung mit Corynebacterium glutamicum.* MSc thesis (Diplomarbeit), Heinrich-Heine-Universität Düsseldorf, 2001.

E. Radmacher, A. Vaitsikova, U. Burger, K. Krumbach, H. Sahm, and L. Eggeling. Linking central metabolism with increased pathway flux: L-valine accumulation by Corynebacterium glutamicum. *Applied and Environmental Microbiology*, 68(5):2246–2250, 2002.

P.M. Reilly. Statistical methods in model discrimination. *The Canadian Journal of Chemical Engineering*, 48:168–173, 1970.

K.v.t. Riet and J. Tramper. *Basic Bioreactor Design.* Marcel Dekker, Inc., New York, 1991.

J.A. Roels. *Energetics and Kinetics in Biotechnology.* Elsevier Biomedical Press, Amsterdam, New York, Oxford, 1983.

H. Rönsch, R. Krämer, and S. Morbach. Impact of osmotic stress on volume regulation, cytoplasmic solute composition and lysine production in Corynebacterium glutamicum MH20-22B. *Journal of Biotechnology*, 104(1-3):87–97, 2003.

J.A. Roubos. *Bioprocess Modeling and Optimization - Fed-batch clavulanic acid production by Streptomyces clavuligerus.* PhD thesis, Technische Universiteit Delft, 2002.

H. Sahm, L. Eggeling, and A.A. de Graaf. Pathway analysis and metabolic engineering in Corynebacterium glutamicum. *Biological Chemistry*, 381(9-10):899–910, 2000.

J. Schubert, R. Simutis, M. Dors, I. Havlik, and A. Lübbert. Hybrid modeling of yeast production processes - combination of a-priori knowledge on different levels of sophistication. *Chemical Engineering & Technology*, 17(1):10–20, 1994.

K. Schügerl. Progress in monitoring, modeling and control of bioprocesses during the last 20 years. *Journal of Biotechnology*, 85(2):149–173, 2001.

C.E. Shannon. A mathematical theory of communication. *Bell System Technical Journal*, 27(4):623–656, 1948.

I. Shiio, S. Otsuka, and M. Takahashi. Effect of biotin on the bacterial fomation o glutamic acid. i. glutamate formation and cellular permeability of amino acids. *Journal of Biochemistry*, 51:56–62, 1962.

H. Shimizu. A tutorial review on bioprocess engineering systems. *Computers & Chemical Engineering*, 20:915–941, 1996.

R.M. Siewe, B. Weil, A. Burkovski, L. Eggeling, R. Kramer, and T. Jahns. Urea uptake and urease activity in Corynebacterium glutamicum. *Archives of Microbiology*, 169 (5):411–416, 1998.

B. Sonnleitner. Dynamic adaptation of microbes. *Journal of Biotechnology*, 65:47–60, 1998.

F. Spezzaferri. Nonsequential designs for model discrimination and parameter estimation. *Bayesian Statistics*, 3:777–783, 1988.

W.E. Stewart, T.L. Henson, and G.E.P. Box. Model discrimination and criticism with single-response data. *Aiche Journal*, 42(11):3055–3062, 1996.

W.E. Stewart, Y. Shon, and G.E.P. Box. Discrimination and goodness of fit of multiresponse mechanistic models. *Aiche Journal*, 44(6):1404–1412, 1998.

R. Takors, W. Wiechert, and D. Weuster-Botz. Experimental-design for the identification of macrokinetic models and model discrimination. *Biotechnology and Bioengineering*, 56(5):564–576, 1997.

J.R. Taylor. *An introduction to Error Analysis.* University Science Books, Mill-Valley, CA, 1982.

M. Terasawa, M. Inui, M. Goto, K. Shikata, M. Imanari, and H. Yukawa. Living cell reaction process for L-isoleucine and L-valine production. *Journal of Industrial Microbiology*, 5(5):289–293, 1990.

O. Tosaka, Y. Yoshihara, S. Ikeda, and K. Takinami. Biosynthesis of L-lysine and L-threonine in Brevibacterium .9. production of L-lysine by fluoropyruvate-sensitive mutants of Brevibacterium lactofermentum. *Agricultural and Biological Chemistry*, 49(5):1305–1312, 1985.

G.T. Tsao and T.P. Hanson. Extended Monod equation for batch cultures with multiple exponential phases. *Biotechnology and Bioengineering*, 17(11):1591–1598, 1975.

T. Turányi. Sensitivity analysis of complex kinetic systems. tools and applications. *Journal of Mathematical Chemistry*, 5:203–248, 1990.

K. Uosaki and T. Hatanaka. Optimal input for autoregressive model discrimination based on the Kullback's divergence. In *System modelling and optimization, IFIP conference 13th Tokyo 1987*, pages 101–108. Berlin: Springer 1988, Tokyo, 1988.

J.J. Vallino and G. Stephanopoulos. Metabolic flux distributions in Corynebacterium glutamicum during growth and lysine overproduction. *Biotechnology and Bioengineering*, 41(6):633–646, 1993.

C. Varela, E. Agosin, M. Baez, M. Klapa, and G. Stephanopoulos. Metabolic flux redistribution in Corynebacterium glutamicum in response to osmotic stress. *Applied Microbiology and Biotechnology*, 60(5):547–555, 2003.

K.J. Versyck, J.E. Claes, and J.F. Van Impe. Practical identification of unstructured growth-kinetics by application of optimal experimental-design. *Biotechnology Progress*, 13(5):524–531, 1997.

E. Walter and L. Pronzato. Qualitative and quantitativae experiment design for phenomenological models- a survey. *Automatica*, 26(2):195–213, 1990.

V.F. Wendisch. Genome-wide expression analysis in Corynebacterium glutamicum using DNA microarrays. *Journal of Biotechnology*, 104(1-3):273–285, 2003.

D. WeusterBotz, R. Kelle, M. Frantzen, and C. Wandrey. Substrate controlled fed-batch production of L-lysine with Corynebacterium glutamicum. *Biotechnology Progress*, 13 (4):387–393, 1997.

W. Wiechert. *Interactive Datenanalyse bei biotechnischen Prozessdaten*. PhD thesis, Universität Bonn, 1990.

J.A. Williams. Keys to bioreactor selections. *Chemical Engineering Progress*, 98(3): 34–41, 2002.

K.W. Wirtz. A generic model for changes in microbial kinetic coefficients. *Journal of Biotechnology*, 97(2):147–162, 2002.

C. Wittmann and E. Heinzle. Application of MALDI-TOF MS to lysine-producing Corynebacterium glutamicum - a novel approach for metabolic flux analysis. *European Journal of Biochemistry*, 268(8):2441–2455, 2001.

C. Wittmann, H.M. Kim, G. John, and E. Heinzle. Characterization and application of an optical sensor for quantification of dissolved O_2 in shake-flasks. *Biotechnology Letters*, 25(5):377–380, 2003.

C. Wittmann, T. Yang, I. Kochems, and E. Heinzle. Dynamic respiratory measurements of Corynebacterium glutamicum using membrane mass spectrometry. *Journal of Microbiology and Biotechnology*, 11(1):40–49, 2001.

W.S. Yip and T.E. Marlin. The effect of model fidelity on real-time optimization performance. *Computers & Chemical Engineering*, 28(1-2):267–280, 2004.

J.Q. Yuan, S.R. Guo, K. Schügerl, and K.H. Bellgardt. Profit optimization for mycelia fed-batch cultivation. *Journal of Biotechnology*, 54(3):175–193, 1997.

Y.H. Zhu, T. Rajalahti, and S. Linko. Application of neural networks to lysine production. *Chemical Engineering Journal*, 62:207–214, 1996.

Schriften des Forschungszentrums Jülich
Reihe Lebenswissenschaften / Life Sciences

1. **Toxizitätsprüfungen in Zellkulturen für eine Vorhersage der akuten Toxizität (LD50) zur Einsparung von Tierversuchen**
   von W. Halle (1998), 92 Seiten
   ISBN: 3-89336-221-5

2. **Die Rolle der Reaktionstechnik in der mikrobiellen Verfahrensentwicklung**
   von D. Weuster-Botz (1999), II, 320 Seiten
   ISBN: 3-89336-245-2

3. **Cell Culture Models as Alternatives to Animal Experimentation for the Testing of Neuroprotective Compounds in Stroke Research**
   Practical Handbook of Methods
   edited by A. J. Carter, H. Kettenmann (1999), 144 pages
   ISBN: 3-89336-250-9

4. **Action and Visuo-Spatial Attention**
   Neurobiological Bases and Disorders
   Book of Abstracts
   collected by P. H. Weiss (2000), XIV, 56 pages
   ISBN: 3-89336-272-X

5. **Genomweite Genexpressionsanalysen mit DNA-Chips zur Charakterisierung des Glucose-Überflussmetabolismus von *Escherichia coli***
   von T. Polen (2003), 100 Seiten
   ISBN: 3-89336-337-8

6. **Auslegung des Detektorsystems für einen hochauflösenden Positronen-Emissions-Tomographen mit hoher Sensitivität**
   von U. Heinrichs (2003), IV, 238 Seiten
   ISBN: 3-89336-340-8

7. **Biological Principles Applied to Technical Asymmetric Catalysis**
   by A. Liese (2003), VI, 206 pages
   ISBN: 3-89336-344-0

8. **Designstudie eines µCT-Zusatzes für einen hochauflösenden Positronen-Emissions-Tomographen: Beispiel für ein multimodales bildgebendes System**
   von M. Khodaverdi (2004), III, 162 Seiten
   ISBN: 3-89336-360-2

9. **Bioprocess Development for the Generation of Monocyte-Derived Dendritic Cells: Applicability in Breast Cancer Immunotherapy**
   by H.R. Bohnenkamp (2004), XLII, 128 pages
   ISBN: 3-89336-364-5

10. **Regulation der *clp*-Genexpression durch ClgR und Definition des ClgR-Regulons aus *Corynebacterium glutamicum***
    by S. Engels (2004), V, 125 pages
    ISBN: 3-89336-379-3

11. **Metabolomanalyse zur Untersuchung der Dynamik im Aromatenbiosyntheseweg in L–Phenylalanin Produzenten von *Escherichia coli***
    by M. Oldiges (2005), XVI, 181 pages
    ISBN: 3-89336-380-7

12. **Identifizierung und Charakterisierung eines Transkriptionsregulators der Aconitase von *Corynebacterium glutamicum***
    by A. Krug (2005), VI, 122 pages
    ISBN: 3-89336-382-3

13. **Prozessentwicklung der elektroenzymatischen Sulfoxidation mit Chloroperoxidase**
    by S. Lütz (2005), XIV, 178 pages
    ISBN: 3-89336-387-4

14. **Export von Proteinen mit Zwillingsarginin-Signalsequenzen über den Tat-Weg in *Escherichia coli***
    by P. J. Kreutzenbeck (2005), 118 pages
    ISBN: 3-89336-388-2

15. **Untersuchungen zur Fettsäure- und Zellwandsynthese sowie zur Glutamatbildung mit *Corynebacterium glutamicum***
    by E. Radmacher (2005), 130 pages
    ISBN: 3-89336-389-0

16. **Monomodale und multimodale Registrierung von autoradiographischen und histologischen Bilddaten**
    by A. Vieten (2005), 116 pages
    ISBN: 3-89336-390-4

17. **Biosynthese von Phosphonaten: Charakterisierung des rekombinanten Enzyms Phosphonopyruvat-Decarboxylase aus *Streptomyces viridochromogenes* Tü494**
    von S. Johnen (2005), 128 Seiten
    ISBN: 3-89336-400-5

18. **Ex-vivo Generierung von neutrophilen Zellen zur Prävention und Therapie der Sepsis**
    von R. Herbold (2005), 202 Seiten
    ISBN: 3-89336-407-2

Schriften des Forschungszentrums Jülich
Reihe Lebenswissenschaften / Life Sciences

19. **Entwicklung eines Donor/Akzeptor-Konzeptes für die asymmetrische Synthese unsymmetrischer Benzoine mit Hilfe ThDP-abhängiger Enzyme**
von P. Dünkelmann (2005), 222 Seiten
ISBN: 3-89336-408-0

20. **Analyse der Bindungsspezifität der humanen Lck-SH3-Domäne anhand artifizieller und physiologischer Peptid-Liganden und strukturelle Charakterisierung dieser Peptide im Komplex mit SH3-Domänen**
von T. T. Tran (2005), 155 Seiten
ISBN: 3-89336-412-9

21. **Modeling Based Process Development of Fed-Batch Bioprocesses: L-Valine Production by *Corynebacterium glutamicum***
by M. Brik Ternbach (2005), 202 Seiten
ISBN: 3-89336-413-7

Forschungszentrum Jülich
in der Helmholtz-Gemeinschaft

Band / Volume 21
ISBN 3-89336-413-7

Lebenswissenschaften
Life Sciences